MODELING LIVER METABOLISM FOR DRUG DEVELOPMENT

By

CARRIE L. GERMAN

Bachelor of Science in Secondary Education

Oklahoma State University

Stillwater, Oklahoma

2006

Submitted to the Faculty of the
Graduate College of the
Oklahoma State University
in partial fulfillment of
the requirements for
the Degree of
MASTER OF SCIENCE
July, 2014

MODELING LIVER METABOLISM FOR DRUG

DEVELOPMENT

Thesis Approved:

Dr. Sundar Madihally

Thesis Advisor

Dr. Gary Foutch

Dr. AJ Johannes

Name: Carrie L. German

Date of Degree: July 2014

Title of Study: MODELING LIVER METABOLISM FOR DRUG DEVELOPMENT

Major Field: Chemical Engineering

The objective of this study was to evaluate scaffold culture conditions using computational fluid dynamics (CFD) and experimentation for supporting three-dimensional (3D) hepatocyte cultures. I used a CFD software to simulate 3D static bioreactors and two different designs of axial-flow bioreactors to assess the effect of scaffold thickness (0.25mm to 2mm), location within the culture (zero to 1mm), and scaffold porosity (0.25 and 0.85) and compare with experimental results obtained using HepG-2 cells. A 14mm diameter chitosan-gelatin (CG) scaffold (0.85 porosity) prepared by freeze drying of various thicknesses to be placed in a six-well plate was simulated. Simulations were performed at constant cell density and exponential growth in each scaffold thickness. Axial-flow bioreactors were constructed in-house according to the simulated dimensions. Changes in the concentration of three components (oxygen, estrogen and urea) were evaluated using rate constants from literature. Static bioreactors were simulated for 48 h (typical media culture duration) and axial-flow bioreactors were simulated at steady state flow rates ranging from 0.1mL/min to 10 mL/min. Concentrations of all three molecules were affected by placement of the scaffold at 0mm as molecules could not diffuse into the scaffold through the bottom. These results showed that scaffolds thicker than 0.5mm scaffolds in static bioreactors were not capable of supporting three-dimensional liver tissue cultures due to oxygen diffusion limitations. Only oxygen concentration profiles were affected by a further increase in elevation as the static bioreactor was open to the atmosphere and oxygen could diffuse into the media from the air. Simulation results were validated by measuring oxygen consumption and urea production.

Table of Contents

List of Tables

Table Page

List of Figures

Figure Page

CHAPTER I

INTRODUCTION

Approximately 2 billion prescriptions are filled each year in the United States; however, few fully understand the amount of time, money, resources, and man power necessary to develop a new medication. An assortment of scientists, chemists, physiologists, pharmacologists, molecular biologists, toxicologists, and statisticians must work together to gather data and give input for the development of a single drug. A company can plan to spend an average of 12 years and $350 million on the process of evolving a medication from a project in a research laboratory to a product at the pharmacy counter [7]. The high price tag is a result of company investment in drugs that fail. Despite the time, money, and effort input by numerous professionals, approximately 95% of drugs studied in humans fail to be effective and safe [13]. Efforts are constantly being made to try to improve the efficiency of the drug development process.

The liver is the metabolic hub of the body, where substances (i.e. drugs) are broken down to form by-products. In some cases, the body is incapable of excreting a sufficient amount of toxic by-products, and the liver becomes damaged. Drug-induced liver injury, termed hepatotoxicity, is the most common reason for the after-market withdrawal of a drug, despite effectiveness in treating a disease [20]. Evaluating hepatotoxicity at the whole body level is expensive. Hence,

numerous, less complex hepatocyte culture systems have been investigated [2, 10, 34]. Issues with incubation periods, diffusion limitations, and nutrient distribution have been reported in many systems, as hepatocytes have a significantly higher level of function relative to other cell types. Oxygen deficiency has most commonly been reported as a limiting factor in the investigation of highly metabolically active hepatocyte cultures. Being able to visualize and better understand nutrient distribution in these systems would allow for system optimization and more accurate results when nutrient/toxin distribution is uniform relative to all cells.

Computational fluid dynamics (CFD) is a powerful modeling tool used in many areas of chemical engineering and biomedical engineering to simulate flows of gases and liquids, heat and mass transfer, moving bodies, multiphase physics, and chemical reactions. Simulation of cell culture systems using CFD allows for system optimization via parameter variation. These simulations would provide a better understanding of nutrient/toxin distribution throughout systems, allowing for more accurate signaling results for application in toxicity testing.

Based on this concept, this study focused on modeling the hepatocyte cultures in static cultures and bioreactors, and validating these with experimental results. I utilized three different components in my analysis: i) consumption of oxygen which is necessary for the survival and function of hepatocytes; ii) production of metabolic product, urea, which is unique to the liver, and iii) estrogen, a hormone known to play a significant role in metabolic function of the liver. Initial concentrations were either based on solubility or physiological level. I used commercially available CFD software (Comsol Multiphysics 4.3b) to assess the effect of a 14mm diameter scaffold with various thicknesses, elevations, porosities, and constant vs. increasing cell density. Michaelis–Menten rate constants from literature were used for oxygen and estrogen. For urea production, a zero order reaction was used.

The objectives of the study are to

i) To understand the limitations of the static bioreactor via CFD Simulation.

A 3D static culture of various scaffold thicknesses to be placed in a six-well plate was simulated. In static cultures, changes in the concentration of oxygen, estrogen and urea were evaluated over a 48 h time period (typical media culture duration). Fluid properties were that of water, and effective diffusivities were based on the Mackie-Meares relationship. Overall concentrations in the static culture were determined through multiple point analysis of Fick's Law and rate laws at nodes throughout the three dimensional structure. Model concentration distributions were tracked as scaffold thickness, porosity, cell count, and elevation were varied. Time-dependent concentration profiles were analyzed for 1mm, 0.75mm, 0.5mm, and 0.25mm thick scaffolds of 0.85 and 0.25 porosities for a constant and increasing cell count in order to determine limitations. These results showed that scaffolds 0.5mm and thicker were not capable of supporting three-dimensional liver tissue cultures due to oxygen diffusion limitations. I questioned whether it would be beneficial to change the location of the scaffold within the growth medium. Increasing the elevation was shown to reduce the effective thickness for oxygen transport while altering the concentration of nutrients dissolved in the medium. Scaffold elevations of 0mm, 0.5mm, and 1mm with respect to the bottom of the bioreactor were examined. Concentrations of all three molecules were affected by placement of the scaffold at 0mm as molecules could not diffuse into the scaffold through the bottom. Only oxygen concentration profiles were affected by a further increase in elevation as the static bioreactor was open to the atmosphere allowing oxygen to diffuse into the media from air.

ii) To develop an axial-flow bioreactor via CFD Simulation.

Due to scaffold thickness limitations in the static bioreactor, an axial-flow bioreactor of identical dimensions was simulated (referred as Case 1). A truncated version (referred as Case 2) of the axial-flow bioreactor to exactly fit the scaffold diameter was also investigated to optimize nutrient distribution through the scaffold region and to reduce bioreactor volume. Scaffolds of

1mm and 2mm thicknesses were investigated at 0.25 and 0.85 porosities. The shape of the bioreactor was initially optimized for uniform nutrient distribution. Then concentration profiles were determined at steady-state for each molecule, using similar rate kinetic parameters in a convective-diffusion equation. Scaffold elevation was set at 0.5mm from the bottom of the bioreactor. Toxicity due to build-up of urea was not a concern in the axial-flow bioreactors. Fluid flow rate was varied to test the effect on nutrient sufficiency and shear stresses experienced by cells. In the truncated version, uniform oxygen distributions were observed even at flow rates as low as 0.1 mL/min. These analyses led to the conclusion that Case 2 bioreactors should be constructed for experimental validation of the model.

iii): To validate the axial-flow bioreactor simulation with experimental results.

Axial-flow bioreactors were constructed in-house according to the simulated dimensions. Chitosan-gelatin scaffolds of 0.85 porosity were prepared by freeze drying technique. A residence time distribution (RTD) analysis was performed to determine nutrient distribution including the bioreactor and scaffold. Tracer was introduced as a step input at a volumetric flow rate of 0.1mL/min. Obtained mean residence time (t_m) was compared with the theoretical space time calculated from the volumetric flow rate and the volume of the bioreactor. These calculations showed distribution of nutrients in the entire region with less than 5% dead space. These regions are similar to those observed in simulation results. Then, experiments were performed using a hepatocarcinoma cell line (HepG-2 cells from ATCC) at the cell density used in all simulations. Oxygen consumption was measured using an in-line flow through electrode at the bioreactor outlet. Urea concentration was measured from the samples collected using a spectrophotometric assay. These results showed agreement with the simulation results.

These results show the possibility of using axial-flow bioreactors for use in testing hepatotoxicity. Using these conditions, one could develop multiple wells and bioreactors that could be used in rapid drug screening.

CHAPTER II

BACKGROUND

2.1. THE DRUG DEVELOPMENT PROCESS

New medicines and treatments are developed through a series of controlled trials in which the efficacy and toxicity of a drug are analyzed. A drug must pass through several phases of the process before even being considered for Federal Drug Administration approval (Figure 2.1). An enormous amount of research is performed before laboratory tests begin. During the preclinical phase, laboratory and animal tests are performed to assess drug safety and biological activity. In phase 1 of clinical trials, tests are performed on healthy, human volunteers in order to assess drug safety and determine dosage. Phase 2 of clinical trials evaluates drug efficacy and side effects in patient volunteers. Finally, in phase 3 of clinical trials, tests are performed to verify drug efficacy and monitor adverse, long-term side effects [36].

Table 2.1: Phases of the drug approval process.
www.medscape.com

	Preclinical Testing	Phase 1	Phase 2	Phase 3
Subjects	Laboratory & Animal Studies	20 – 100 Healthy Volunteers	100 – 300 Patient Volunteers	1,000 – 3,000 Patient Volunteers
Purpose	Assess safety & biological activity	Determine safety & dosage	Evaluate effectiveness & side effects	Verify effectiveness & monitor adverse long-term use
Time	Year 1 - 2	Year 3	Year 4 - 5	Year 6 - 8
New Drugs Passed	100%	70%	33%	27%

2.2. DRUG DEVELOPMENT AND THE LIVER

The liver is a multifunctional organ involved in the metabolism, detoxification, and excretion of many substances essential for homeostasis. Thus, the liver is known as the metabolic hub of the body, the location where nutrients and toxins alike travel, are broken down, and are either circulated to the rest of the body or excreted. Liver tissue cultures are used in the preclinical stage of drug development due to the liver's vital role in the detoxification of the body. More specifically hepatocyte cultures are used, as these cells comprise 80% of the liver. Many *in vitro* culture techniques using HepG2 cells, a hepatocyte derived cell line from the liver, have been explored [2, 10, 34]. Although primary hepatocytes serve as an excellent *in vitro* model for drug metabolism in the body, difficulties are encountered in finding supplies of disease-free cells (in many cases cirrhotic), that are steadily available. Thus, HepG2 cells, which are considerably easier to handle and cheaper have been used extensively in the evaluation of drug toxicity for a number of years [35].

2.4. CURRENT HEPATOCYTE CULTURING SYSTEMS

Numerous *in vitro*, hepatic cell culturing systems, such as cell suspension, co-culture systems, aggregate systems, and bioreactors, have been investigated.

Two-dimensional cell culturing techniques have had success in maintaining cell proliferation. However, cell growth is restricted to a flat, tissue-culture treated surface which reduces the number of cells that could be cultured in a given volume of growth medium. Also, 2D cultures are typically mono-cultures, consisting of only one cell type, and lack extracellular matrix or interstitial fluid. Drugs to be tested in two-dimensional systems are exposed to only part of the cell surface, as the other side is exposed to the tissue culture surface material.

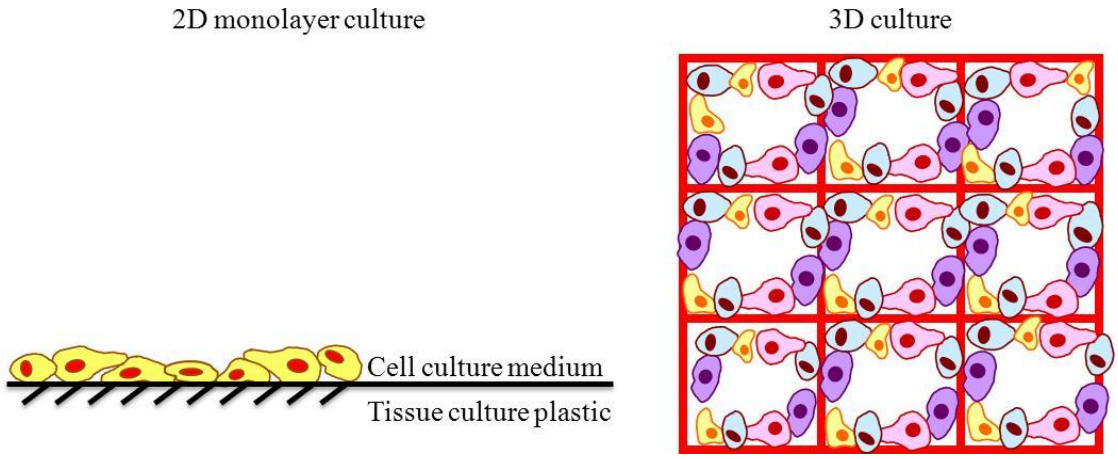

Figure 2.1: Structural comparison of 2D and 3D cell culture.

Though these culturing systems are easy to set up and maintain, while still providing good cell viability; two-dimensional cell cultures are poor approximations of tissue *in vivo*. Two-dimensional cell cultures lack necessary architectural structure and face significant transport limitations, causing major limitations for the application of such culturing systems in drug toxicity testing [7].

Cell suspension systems on the other hand, are not restricted to a flat surface, nor must they be maintained in culture flasks that are tissue-culture treated. While this system allows for an increase in cell count and a non-tissue-culture treated environment, many drawbacks still exist. The anchor-dependent nature of the majority of vertebrate cells requires a specifically treated surface to promote cell adhesion and spreading. Another issue encountered in cells suspension culturing systems is that as the culture volume to surface area ratio is increased beyond which adequate gas exchange is hindered (usually 0.2–0.5 mL/cm^2), the medium requires agitation to adequately distribute nutrients throughout the system. Agitation can also be a concern in systems, as convection in the system can cause shear stress issues that could result in cell death [11].

Three-dimensional (3D) cell culture systems are preferred to two-dimensional culture systems because 3D cultures require less area to seed more cells [34]. With the introduction of 3D culture techniques as early as 1912 [4], the most simple one being the aggregate or spheroid culture (Figure 2.2), scientists have noticed that organotypic cell cultures are more readily developed in higher density cultures.

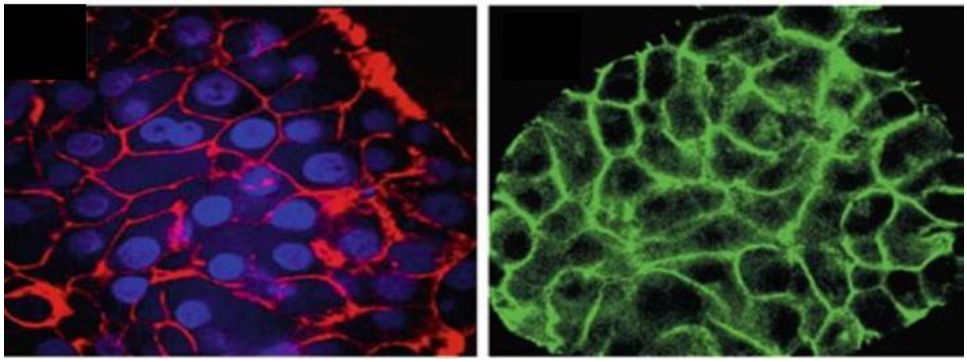

Figure 2.2: Hepatocyte Spheroids (Tissue Engineering in Regenerative Medicine; Bao et al. Chapter 17).

A higher cell count improves sensitivity in toxicity measurements. However, aggregate systems or spheroids have issues with uniform distribution of nutrients. As distance from the surface of the cell aggregate increases internally, nutrient concentration decreases, governed by diffusion.

Cells located closer to the center of the aggregate are deprived of the nutrient level necessary to survive.

With recent advances in tissue engineering and development of biodegradable porous structures, three-dimensional cell cultures have found increased popularity for the culturing of high density hepatocyte cultures. Porous structures from various sources have been developed to culture hepatocytes in 3D models, including Matrigel® obtained from a mouse sarcoma [28]. However, in static culture systems, diffusion is the primary driving force for nutrient transport throughout the porous structure, dictated by Fick's first law. Many static bioreactor investigations have reported issues with incubation periods due to reliance on diffusion alone as a means of nutrient distribution [10]. The frequency with which media must be changed to maintain adequate nutrient supply can become problematic.

2.3. HEAPTOTOXICITY TESTING

The creation of a new medicine or treatment requires the development of a drug that effectively treats injury or disease. However, effectiveness is not the only required quality in a new drug. It is vital that new drugs and treatments be both effective and safe. Hepatotoxicity testing is performed to analyze the toxicity and safety level of a drug. Hepatotoxicity testing involves the evaluation of changes in biomarkers. These changes include morphological changes, alteration of protein expression, mitochondrial respiration inhibition, and many more, depending on the biomarker of choice [14]. The presence of these markers at or above specific levels in hepatotoxicity analysis indicates toxic liver injury. Over 900 drugs, toxins, and herbs have been reported to cause liver injury. The most common cause for after-marketing withdrawal of a drug is drug-induced liver injury [20]. This indicates serious limitations in preclinical testing systems as well as large gaps in knowledge of drug-specific metabolism [1]. Understanding metabolism and distribution of nutrients and toxins alike are vital keys to creating an *in vitro* environment

capable of maintaining hepatocyte vitality while providing accurate readings of toxic signals from cells.

2.5. THE IMPORTANCE OF OXGEN CONSUMPTION ANALYSIS

As previously discussed, hepatocyte cultures are used in drug development analysis. Because hepatocytes are known for a higher level of metabolic rate relative to other cell types, one has to understand the distribution of various components in *in vitro* models [17, 23]. This knowledge is vital to the drug development process, as the uniformity of distribution of nutrients and toxins to cells affects the accuracy of signal results. Inadequate nutrient distribution leads to decreased cell viability, lowered growth rates and poor functionality and thereby leads to poor reliability of data [3, 21].

2.6. ESTROGEN AND THE LIVER

The ovarian sex hormone 17β-estradiol (MW=232.4 g/mol), commonly referred to as estrogen, is involved in metabolism apart from reproductive functions. The liver is a site for biosynthesis of estrogens, and the main site for further biotransformation. Once the estrogens are synthesized by aromatase in peripheral tissues including the liver, they are released to the circulation system. Figure 2.3 shows estrogen's metabolic pathway via the liver.

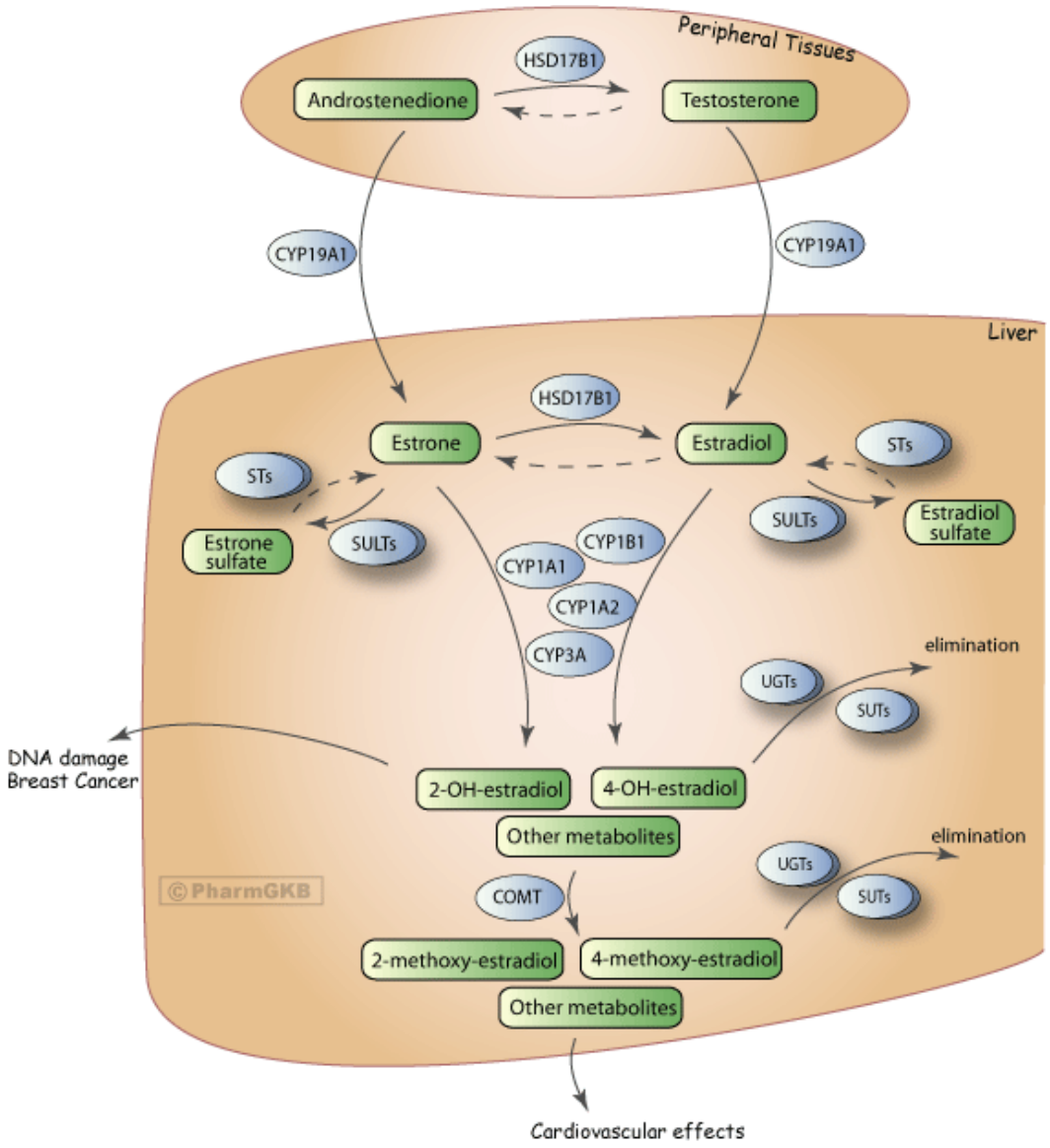

Figure 2.3: Estrogen metabolism in the liver.
Copyright: by PharmGKB. With permission from PharmGKB and Stanford University (https://www.pharmgkb.org/pathway/PA145011118)

Understanding how uptake of different molecules and diffusivities change is important to determine the usage of 3D cultures. I wanted to investigate the effect of increased molecule size on concentration distribution. As estrogen is a considerably large molecule (relative to urea and oxygen) that is metabolized in the liver, I decided to evaluate consumption characteristics.

2.7. UREA AND THE LIVER

The metabolic waste from nitrogenous by-products of amino acid break down in the liver are converted into urea, a polar molecule (MW= 60 g/mol) which readily dissolves in water, and in disposed of via the renal system.

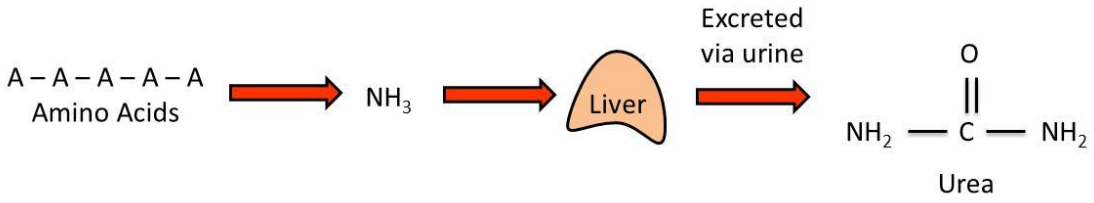

Figure 2.4: Basic process of urea production from amino acids.

The main chemical reactions for the synthesis of urea from ammonia (NH_3) according to the path shown in Figure 2.3 are as follows:

$$2NH_3 + CO_2 \rightleftharpoons H_2N\text{-}COONH_4$$

$$H_2N\text{-}COONH_4 \rightleftharpoons (NH_2)_2CO + H_2O$$

As amino acids are present in media supplied to cells to provide nutrients necessary for survival, urea is expected to be produced. Very high concentrations of urea are toxic to cells and could be necrotic. In the clinical setting, the normal level of urea in plasma is around 30mg/100mL and increase of this value to 50mg/100mL is considered high and a possible indication of improper liver functionality [37]. Understanding urea production and distribution in *in vitro* hepatic cell cultures is vital to ensuring that urea toxicity does not occur and in turn affect cell vitality or the accuracy of signaling results.

2.8. COMPUTATIONAL FLUID DYNAMICS AND MATHEMATICAL MODELING

The use of CFD programming to visualize and better understand nutrient distribution in hepatocyte culturing systems is vital to creating an optimized system. One of the greatest features of simulation is that parameter changes can easily be made. Some parameter changes to a constructed model, such as altering the diameter of a bioreactor, would require the construction of

multiple models, which can become expensive. CFD coupled with reaction kinetics can provide a better understanding of nutrient consumption and toxin production in cell culture systems. This improved knowledge base allows nutrient deficiency and toxicity issues to be addressed more efficiently, which can then be applied to experimental analysis.

Reaction kinetics differ according to the molecule being consumed or produced. Michaelis-Menten kinetic values can be readily obtained from literature for numerous molecules. These values (specific values discussed in chapter 3) were discovered in literature for both estrogen and oxygen. This is why the Michaelis-Menten equation was used to characterize the consumption rate of these two molecules. As Michaelis-Menten constants were not available for determining the rate of urea production, the production rate of urea was determined to be based on a zero order equation based on literature (specific details discussed in chapter 3). Cell density plays a big role in determining the rate at which a molecule is consumed or produced. Growth rate characteristics have not been previously considered when looking at long term incubation of cells. Considering the doubling time of cells would significantly impact molecular consumption/production rates.

Molecular transport must also be taken into consideration when simulating cell culture systems. Diffusion dominated transport of static cell culture systems is characterized by Fick's law for reacting systems. In a non-static system, like the flow-through bioreactor, molecular transport by convection is considered in addition to diffusional transport. Fluid flow in such systems is characterized by the Navier-Stokes equation (shown in chapter 4) in non-porous regions, and by the Brinkman or Darcy equation (shown in chapter 4) in porous regions. CFD programs combine the molecular transport and reaction kinetics equations, along with a number of defined initial conditions (i.e. concentration or velocity) to create a multitude of profiles, such as pressure gradients, velocity profiles, and concentration profiles. These profiles provide a wealth of knowledge pertaining to nutrient distribution throughout a system. Profile analysis can provide a

better understand better understanding of results, and can aide in determining accuracy of signaling results in toxicity testing.

2.9. BIOREACTORS

A way to improve the nutrient distribution is by constant mixing or applying flow systems where nutrient distribution is facilitated by convection. Bioreactors have been of particular interest due to the degree of control over system parameters. Successful culturing in bioreactors has resulted in the development of numerous bioreactor types in a variety of shapes and sizes. Although flow-through bioreactors can provide more uniform nutrient concentration distributions, shear stress exerted on cells must be considered. Hence, few different flow configurations have been explored. For example, axial-flow reactors flow vertically in an upward direction through the cell-seeded region, while parallel-flow reactors flow horizontally through or above the cell-seeded region. Figure 2.5 shows some examples of flow-through bioreactors that have been previously investigated.

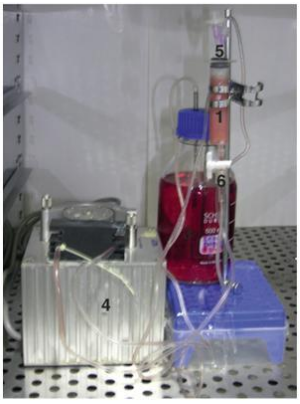

Axial-flow, cryogel bioreactor
Nature Protocols
Vol. 8 821–835 (2013)

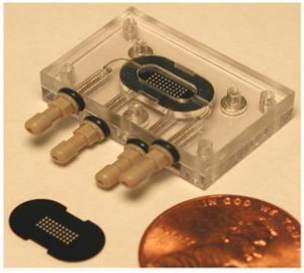

Microchip bioreactor
IEEE Eng Med Biol Soc. (2005;7:7490-2)

Parallel-flow bioreactor
J. of Biomedical Materials Research Part B (2013; Vol. 102, Num. 4)

Figure 2.5: Flow-through bioreactor examples.

Optimization of bioreactor shape has been investigated, showing that rounded reactors contain less dead volume than rectangular shaped reactors. Conical shaped inlets and outlets have

demonstrated increased uniformity of nutrient distribution [29]. While many of the systems discussed have been constructed and used for experimental analysis, little research has been done to model these systems.

CHAPTER III

STATIC BIOREACTOR 3-D SIMULATION

3.1. INTRODUCTION

Various approaches by others have been explored to colonize hepatocytes within porous scaffolds. One method is the transformation of the tissue culture plastic technique, where hepatocytes are populated in a batch culture on flat plates. Porous scaffolds containing hepatocytes are inserted into the tissue culture well and fed with the growth medium. Hepatocytes are supplied with nutrients by adding a certain amount of medium that is replenished frequently, typically at 48 hour intervals. This method has been successfully used to regenerate very thin structures. However, adapting the technique to a thicker structure is not well understood, particularly the limitations of these batch bioreactors in the distribution of nutrients and removal of metabolic products. In this study, I evaluated the static culture for the capability to support a three-dimensional hepatic culture. I examined nutrient and metabolic product concentration distributions throughout the cell-seeded scaffold. CFD simulation (COMSOL 4.3b) was used to examine hepatocyte consumption of oxygen and estrogen, as well as urea production. The scaffold thickness, porosity, constant versus increasing cell count, and elevation from the bottom of the tissue culture well were varied in order to determine their effect on concentration

distributions. For each analysis the oxygen, estrogen, and urea concentration distributions and volume-average concentrations were evaluated. These evaluations provided data for environment limitation analysis.

3.2. SIMULATION SETUP

3.2.1. Bioreactor Geometry

A discoid shape, static bioreactor with a height of 2.34mm and a 16.5mm radius was simulated (Figure 3.1). Dimensions were based on those of a six-well plate available commercially. The scaffold region had a radius of 7mm and was placed concentrically to the bioreactor.

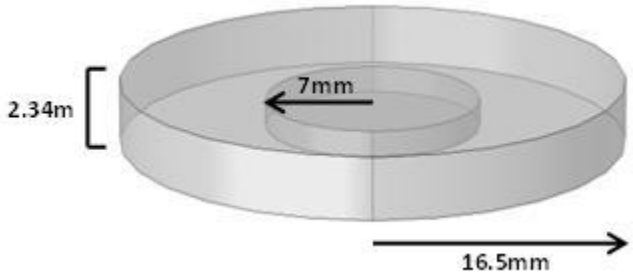

Figure 3.1: Static bioreactor dimensions.
(picture from COMSOL 4.3a simulation)

The height of the scaffold was varied from 0.25mm to 1mm. A constant cell density of 1.29×10^{12} cells/m^3 was used in simulation. For each scaffold height, scaffold volume was calculated (Table 3.1) and the number of Hep-G2 cells (hepatocarcinoma cell line used in experiments) seeded inside of the scaffold was determined. A detailed example of the input of static bioreactor geometry is in Appendix D.

Table 3.1: Cell count table based on a cell density of 1.29×10^{12} cells/m^3.

Scaffold Thickness (mm)	Scaffold Volume (mm^3)	Number of cells
1	153.94	200,000
0.75	115.45	150,000
0.5	76.97	100,000
0.25	38.5	50,000

3.2.2. Governing Equations and Boundary Conditions

Some initial assumptions were made in determining boundary conditions and properties to be used. These assumptions are as follows:

- The media properties were equivalent to those of water at 37°C.
- The exposed top surface was saturated with oxygen at any given time, supplying a constant concentration similar to experimental culture methodology.
- The diffusion values remained constant and isotropic.
- There was no flux at any exterior boundaries.

Media's initial oxygen concentration of 0.225 mol/m^3 was calculated at 37°C using Henry's Law. The initial estrogen concentration to be added to the media was calculated based on the physiological concentration of estrogen in the body. Lastly, the initial nitrogen concentration in media was determined using the nitrogen content of proteins [31] and the summation of the specific volume of amino acids, a byproduct of protein digestion, in the media used (Eagle's Minimum Essential Medium, a product of ATCC). Detailed calculations for oxygen, estrogen and urea can be found in Appendix A, Appendix B and Appendix C, respectively.

The physics module, *Transport of a Diluted Species*, was chosen based on governing equations for mass transport. Mass transport through the scaffold region was assumed to follow Fick's Law for reacting systems,

$$\frac{\partial C_i}{\partial t} = D_i \nabla^2 C_i + r_i \tag{3.1}$$

where $\frac{\partial C_i}{\partial t}$ is the change in concentration of molecule *i* over time, D is the diffusivity constant for molecule *i* in water, $\nabla^2 C_i$ is the second order gradients along each of the major dimensions in the system, and r_i is the rate of consumption or production depending on the molecule, *i*, being evaluated. In the scaffold region the effective diffusivity constant was used in Fick's Law. Effective diffusivity constants were calculated using the Mackie-Meares relation [22],

$$D_{eff} = D_{\infty}\left(\frac{\varepsilon_p}{2-\varepsilon_p}\right)^2 \tag{3.2}$$

where D_{eff} is the effective diffusivity, D_{∞} is the free diffusivity of the molecule in water, and ε_p is the porosity of the scaffold. Calculated effective diffusivity values are shown in Table 3.2. Detailed diffusivity calculations for oxygen, estrogen, and urea are in Appendices A, B, and C respectively.

Table 3.2: Free diffusivity and calculated effective diffusivity values.

Molecule	Free Diffusivity (m^2/s)	Effective Diffusivity (m^2/s) Porosity = 0.85	Effective Diffusivity (m^2/s) Porosity = 0.25	Molecular Weight (g/mol)
Oxygen[32]	3.00E-09	1.64E-09	6.12E-11	32
Urea [5]	9.25E-08	5.05E-08	1.03E-09	60
Estrogen[33]	4.00E-10	2.19E-10	8.16E-12	232.4

The uptake rate equation (r_i) for both oxygen and estrogen was assumed to follow Michaelis-Menten kinetics,

$$-r_i = \frac{V_m C_i}{K_m + C_i} \tag{3.3}$$

where V_m is the maximum uptake rate of molecule *i*, C_i is the concentration of the molecule at any time, and K_m is the Michaelis-Menten constant for molecule *i*. The Michaelis-Menten kinetic parameters used in this study for estrogen [8] and oxygen[6] are shown in Table 3.3.

To account for cell growth, it was assumed that the doubling time for cells was 24 h. The following differential equation was used to determine the change in the number of cells, ∂N, in the scaffold over time,

$$\frac{\partial N}{\partial t} = \mu N_0 \tag{3.4}$$

where μ represents the specific growth rate constant and N_0 represents the initial number of cells seeded in the scaffold. An analytic function was input to simulation to vary the kinetic constant, V_m, over time. Details of these calculations for oxygen and estrogen are in Appendix A and B, respectively.

An zero order rate law was assumed for determining the rate of urea production (r_{Urea}),

$$r_{Urea} = k \tag{3.5}$$

where *k* is the rate constant. The urea rate constant is based on the number of cells and thus increases as the number of cells increase. The urea rate constants for each scaffold thickness can be seen in Table 3.3.

Table 3.3: Rate law kinetics for oxygen, estrogen, and urea.

Rate Law Kinetics				
	Oxygen	**Estrogen**	**Urea**	
Km (mol/m^3)	0.0283	0.006	**Scaffold Thickness (mm)**	**k (μmol/m^3/s)**
Vm (mol/m^3*s)	4.42E-5	9.53E-09	2.00	16.8
			1.00	8.41
			0.75	6.31
			0.50	4.21
			0.25	2.10

Calculations for urea rate constants can be seen in Appendix C. Detailed procedures for the input of boundary conditions and equations are provided in Appendix D.

3.2.3. Meshing

Meshing of simulations was done using a free tetrahedral mesh for all geometry with a maximum element size of 0.5mm and a minimum element size of 0.2mm. The number of nodes used for this simulation was 260,731. A grid test was performed decreasing the maximum element size to 0.4mm and increasing the number of nodes to 514,021. The percent difference in the volume average concentration was 0.016%, which indicated that the mesh quality had been refined enough so as to not affect results.

3.2.4. Evaluation

All simulations were performed for a 48 h duration, mimicking that of experimental conditions. Concentration profiles were created by simultaneously solving Equation (1) at mesh nodes throughout the three-dimensional static bioreactor. The volume-average concentration was evaluated to mimic that obtained from experimental conditions and for use in the grid check

evaluation. The procedure for obtaining concentration profiles for desired molecules and volume average concentrations are described in Appendix D.

3.3. RESULTS

3.3.1. Oxygen Consumption Characteristics

Typically when cells are cultured, growth medium is changed every alternate day. It is expected that cells are exposed to the lowest amount of nutrients at the end of 48 h. Hence, nutrient distribution at 48 h was analyzed. Results from the simulation for oxygen consumption were analyzed for various scaffold thicknesses. As scaffold thickness increased (Figure 3.2) and thus cell count increased, so did oxygen consumption.

3.3.2. Influence of Porosity on Oxygen Transport

Characteristics of the porous scaffold change during tissue regeneration, i.e., permeability of the matrix to nutrient distribution decreases due to decreased pore size. In order to simulate this condition, the effect of change of porosity from 85% to 25% on oxygen distribution was investigated. Decreased porosity decreased the value of effective diffusivity input to the simulation (Appendix A). Oxygen distribution at 48 h was tested in scaffolds of different thicknesses and assuming a constant cell density of 1.29×10^{12} for the two different porosities discussed. Decreased porosity (Figure 3.2) decreased the overall scaffold oxygen concentration for all four scaffold thicknesses. Oxygen deficient areas were not present in any of the 85% porosity scaffold thicknesses analyzed. However, oxygen deficiencies were seen in the 1mm and 0.75mm thick scaffold simulations at 25% porosity. These deficiencies existed despite the abundance of oxygen outside of the scaffold, indicating that the effective diffusivity limited oxygen transport into the scaffold region. As effective diffusivity is directly related to porosity, it was determined that scaffold porosity was a limiting factor for the static bioreactor at lower porosities for scaffolds 0.75mm and thicker.

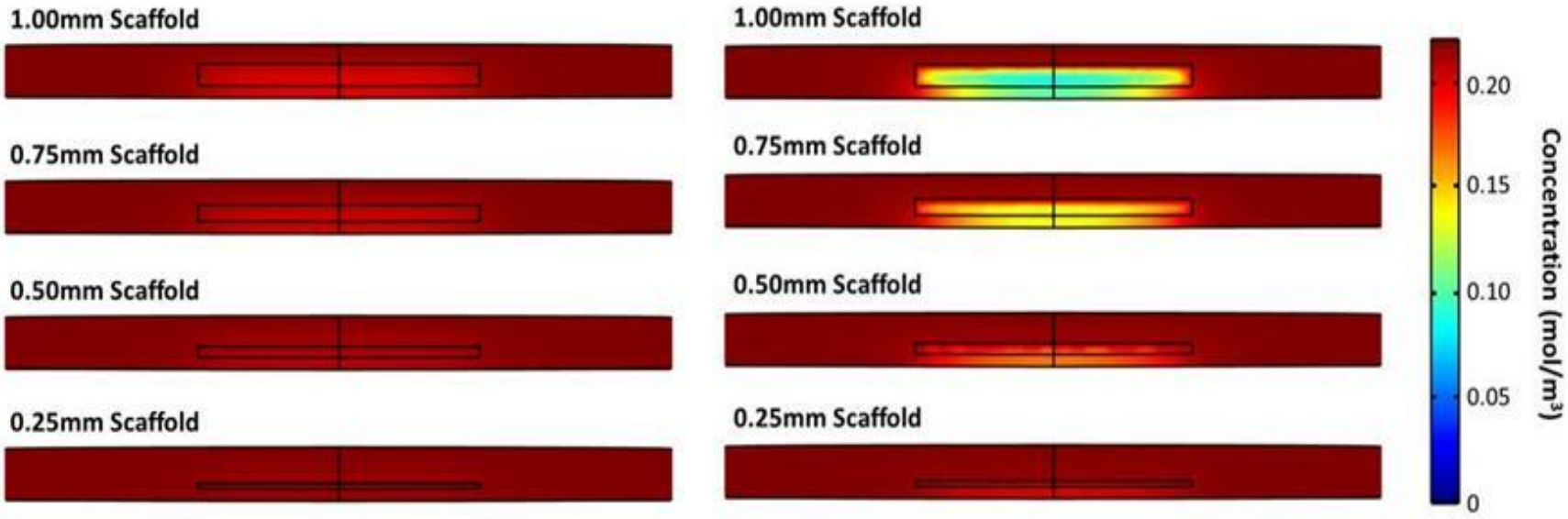

Figure 3.2: Effect of porosity on oxygen consumption at 48 h for 85% porosity (left) and 25% porosity (right). Shown are the cross-section views of the entire static bioreactor.

3.3.3. Influence of Cell Density on Oxygen Concentration Distribution

The initial investigation assumed a constant cell density over the 48 h time period. In a static cell culture it is important to consider cell growth in addition to scaffold porosity changes in order to account for accompanying variability in the reaction rate over time. When cell growth was incorporated into the simulation, increased cell density (Figure 3.3) decreased the oxygen concentration in the scaffold region for all scaffold thicknesses when compared with those profiles at a constant cell density. Increased cell density decreased oxygen concentration distribution uniformity in all scaffold thicknesses and at both porosities discussed. The oxygen concentration profiles at 25% porosity after 48 h showed areas of severe oxygen deficiency, concentration near zero, in the scaffold region of the 0.75mm and 1mm thick scaffold simulations. Though less severe, even the 0.5mm thick scaffold showed oxygen deficiency in the scaffold region at the same porosity and time elapsed.

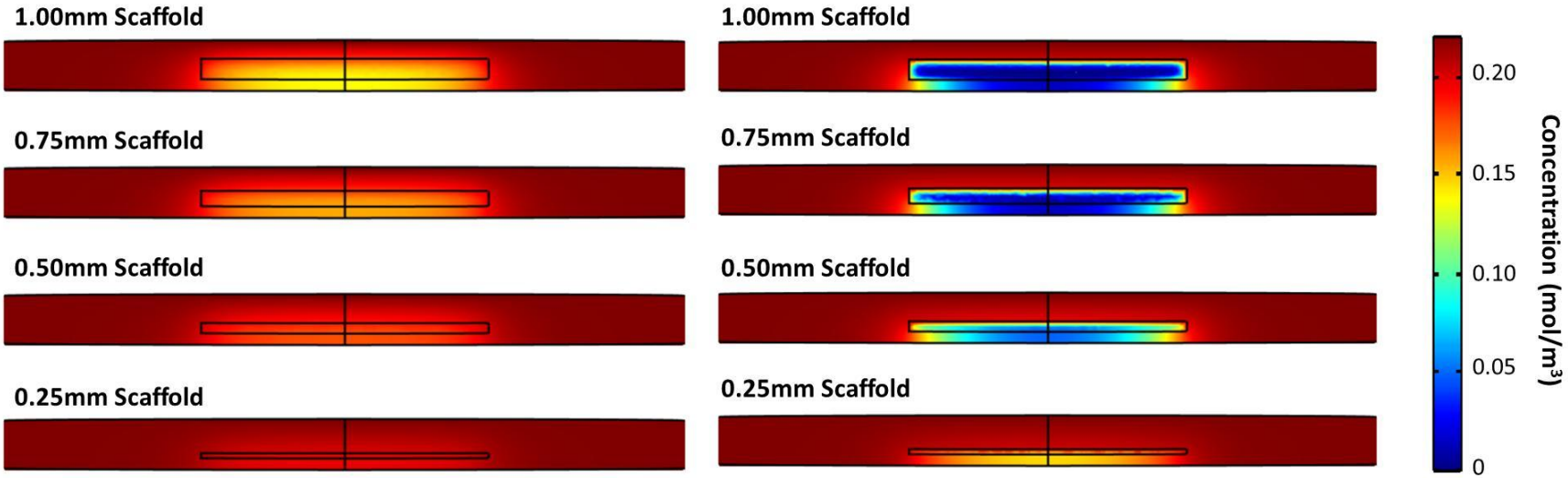

Figure 3.3: Oxygen consumption with increasing cell density at 48 h for 85% porosity (left) and 25% porosity (right). Shown are the cross-section views of the entire static bioreactor.

In order to better understand the consumption profile, change in concentration of oxygen as a function of time was plotted for tested thicknesses at the discussed porosities for both a constant cell density and an increasing cell density. These results (Figure 3.4) showed maximum decline within the first half hour for all simulations. As scaffold thickness increased, overall oxygen concentration for the bioreactor decreased. Decreased porosity led to further oxygen concentration decrease for all scaffold thicknesses.

At 85% porosity, the overall oxygen concentration increased through the second half hour for all scaffold thicknesses. This is attributed to the initial increase in consumption which created a concentration gradient. Oxygen diffusion from the top surface is promoted due to the newly developed concentration gradient. Steady state was reached by the end of the first hour when a constant cell density at 85% porosity was assumed. On the other hand, when increased cell density as a function of time was considered, the oxygen concentration decreased exponentially beginning at the end of the first hour. An exponential increase in the rate of consumption while maintaining the same rate of oxygen diffusion into and through the system explains the exponential decay in the overall oxygen concentration of the bioreactor.

At 25% porosity, only the 0.25mm and 0.5mm thick scaffolds showed any increase in overall oxygen concentration. Simulation for all four scaffold thicknesses, where a constant cell density was assumed, reached steady state even at 25% porosity. However, the time period necessary to reach steady state increased as scaffold thickness increased. This trend was not seen in the 85% porosity simulations. This difference is attributed to the significant difference in effective diffusivity of oxygen through the scaffold region at the two different porosities, as well as the rate of diffusion of oxygen into the system from the atmosphere. The rates of oxygen diffusion into the scaffold region and into the system from the atmosphere are much smaller than the rate of oxygen consumption by cells.

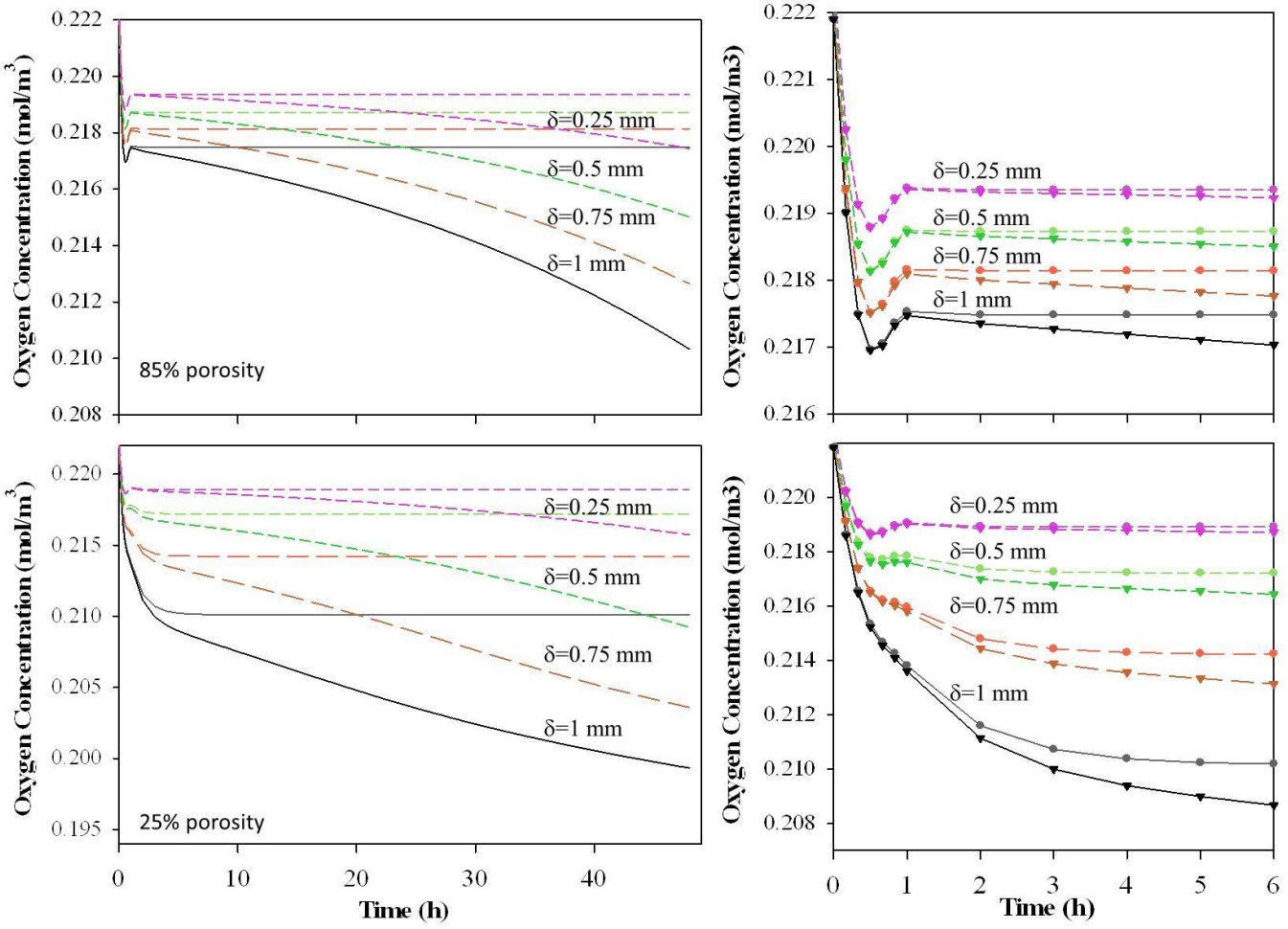

Figure 3.4: Oxygen concentration in the media over time plot.

Plots to the right are a closer view of the plots to the left. Circles correspond to constant cell number simulation. Inverted triangles correspond to simulation with exponential growth of cells.

The 25% porosity volume average concentration was lower after 48 hours when compared to the volume average concentration of the same scaffold thickness at 85% porosity. The difference in volume average concentration at the two different porosities became more pronounced as scaffold thickness increased.

3.3.4 Influence of Elevation on Oxygen Consumption

Increased thickness and cell density, along with a decreased scaffold porosity showed significant deficiency of oxygen, particularly near the bottom of the static bioreactor. Since there was sufficient oxygen at other areas except scaffolds, I questioned what would happen if the elevation of the scaffold was altered. For this purpose, the elevation of the 1mm thick, 25% porosity scaffold with an exponentially increasing cell density was increased from 0mm to 0.5mm and 1mm, progressively. Analysis of oxygen distribution at 48 h showed (Figure 3.5) similar distribution profiles for all elevations.

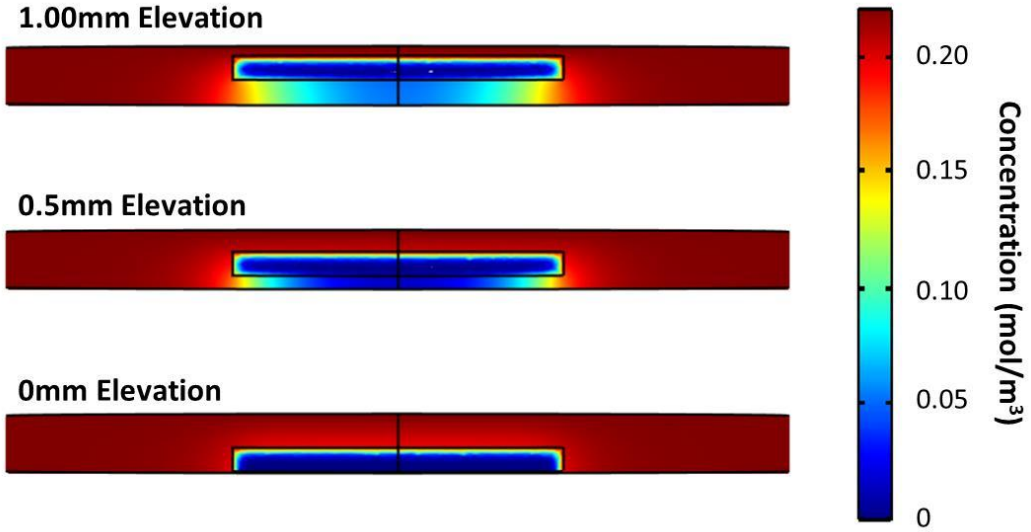

Figure 3.5: Elevation effect on oxygen consumption at 48h in 1 mm thick scaffolds at 25% porosity, with increasing cell density.

To better understand the effect of elevation, average concentration in the media at 48 h was determined. The volume average concentration over time (Figure 3.6) indicated that when the

scaffold was placed at 0mm, directly on the bioreactor bottom, volume average concentration in the media was higher. This could be due to the cells along the bottom of the scaffold receiving little to no oxygen, resulting in less consumption and increasing the volume average concentration in the media. As the elevation of the scaffold increased, the volume average concentration in the media decreased. This demonstrated that hepatocytes consumed more oxygen as the scaffold approached an oxygen source. However, a large portion of the scaffolds were still deficient in oxygen.

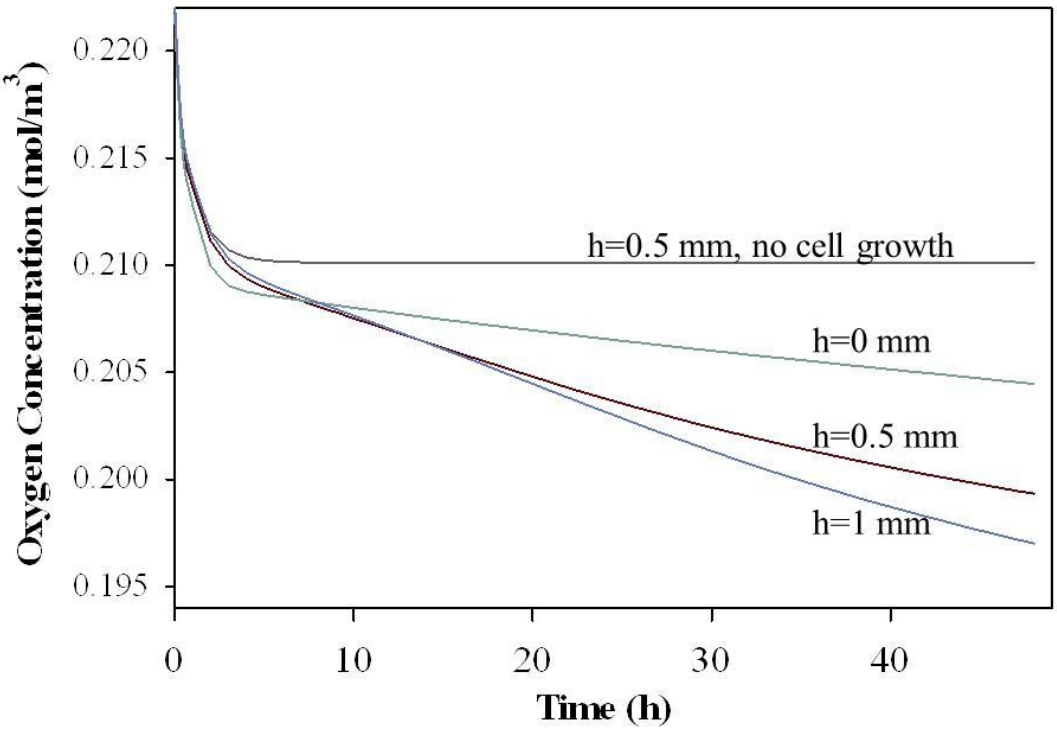

Figure 3.6: Effect of scaffold elevation on oxygen concentration for 1mm thick scaffolds at 25% porosity.

***h = 0, 0.5, and 1 are simulations with increasing cell density over time.**

3.3.5. Changes on Estrogen Distribution

Understanding how uptake of molecules and diffusivities change with different molecules is important to determine the effect on nutrient distribution. The ovarian sex hormone 17β-estradiol

(MW=232.4 g/mol), commonly referred as estrogen and its receptors, estrogen receptor-α and estrogen receptor-β, are involved in metabolism apart from reproductive functions [12]. Hence, I evaluated estrogen consumption in the simulation involving the four scaffold thicknesses previously discussed.

3.3.6 Scaffold Thickness and Porosity Influence on Estrogen Consumption

Similar to oxygen, the effects of scaffold thickness and porosity on estrogen concentration distribution were analyzed. For this analysis, a constant cell density was assumed. These results showed (Figure 3.7) that estrogen consumption increased with scaffold thickness, due to the increased cell number. Like oxygen, decreased porosity from 85% to 25% had a direct effect on the estrogen concentration distribution. Note that the maximum and minimum values of the estrogen concentration color scales are succinct. Overall, estrogen concentration was non-uniformly distributed, yet no deficient regions were observed.

3.3.7 Effect of Cell Density Change on Estrogen Concentration Distribution

Similar to oxygen, the effect that increasing cell density over time, due to cell proliferation, would have on estrogen concentration distribution was examined. The results showed (Figure 3.8) that increased cell density increased estrogen consumption for both porosities and all scaffold thickness simulated. This was attributed to the increased cell number. Even the most diverse estrogen concentration profile, the 1mm thick, 25% porosity scaffold, with an increasing cell density, did not show estrogen deficient areas. This analysis showed that estrogen concentration distribution was not a limiting factor for the static bioreactor

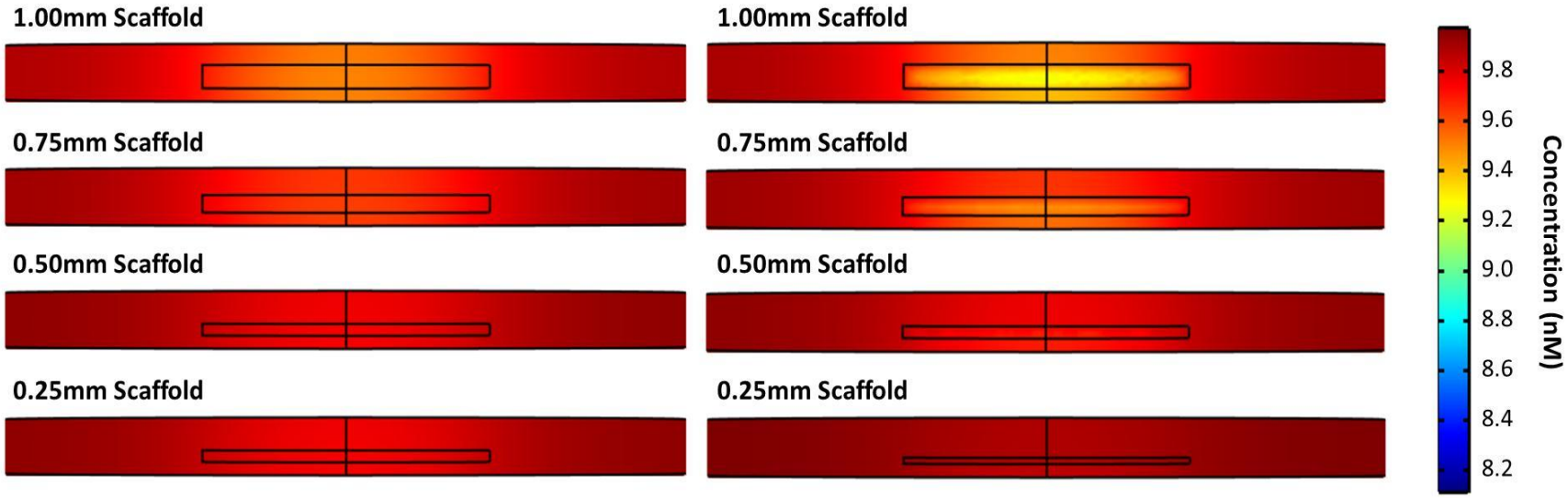

Figure 3.7: Effect of porosity on estrogen consumption at 48 h for 85% porosity (left) and 25% porosity (right). Shown are the cross-section views of the entire static bioreactor.

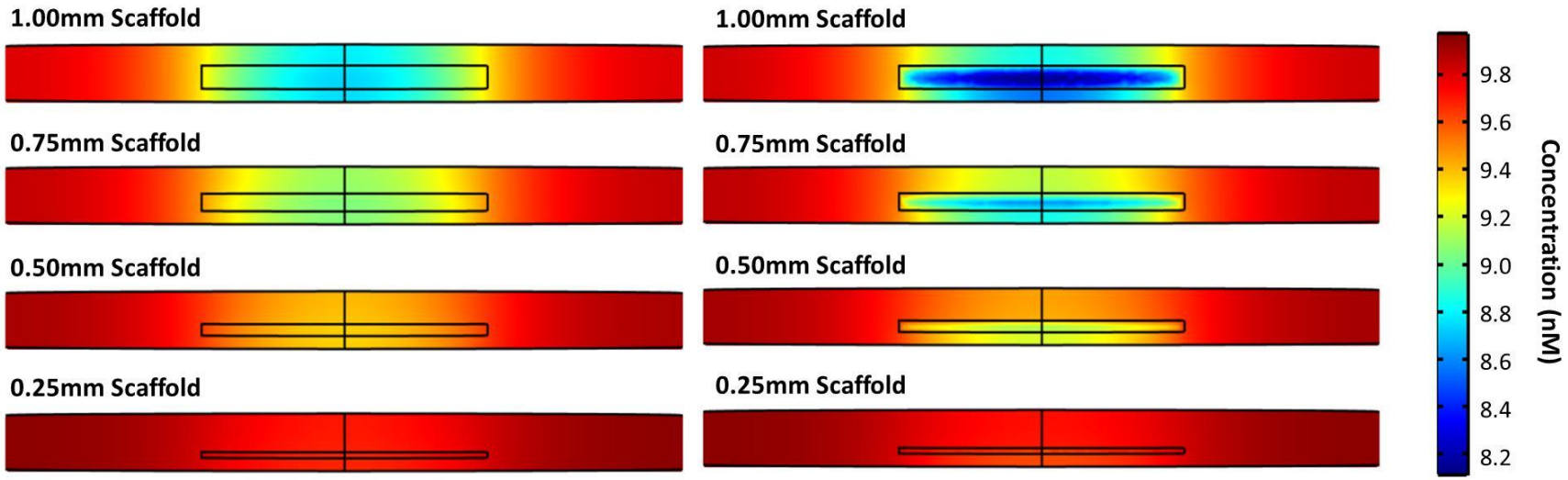

Figure 3.8: Estrogen concentration distribution with increasing cell density at 48 h for 85% porosity (left) and 25% porosity (right). Shown are the cross-section views of the entire static bioreactor.

Similar to oxygen, the change in the volume average concentration of estrogen was plotted for the tested duration of 48 h. These results showed (Figure 3.9) sequential decrease in estrogen value with increase in scaffold thicknesses. Also, this decrease appeared linear when a constant cell density was assumed, most likely attributed to the slow uptake by cells. An exponential decrease in volume average estrogen concentration appeared when an increasing cell density was assumed. This was attributed to the exponential increase in the cell number over time. The difference in concentration between the 25% and 85% porosity plots is unperceivable, further supporting the assumption that concentration differences observed in the estrogen consumption profiles are negligible and that the estrogen concentration profiles are uniformly distributed.

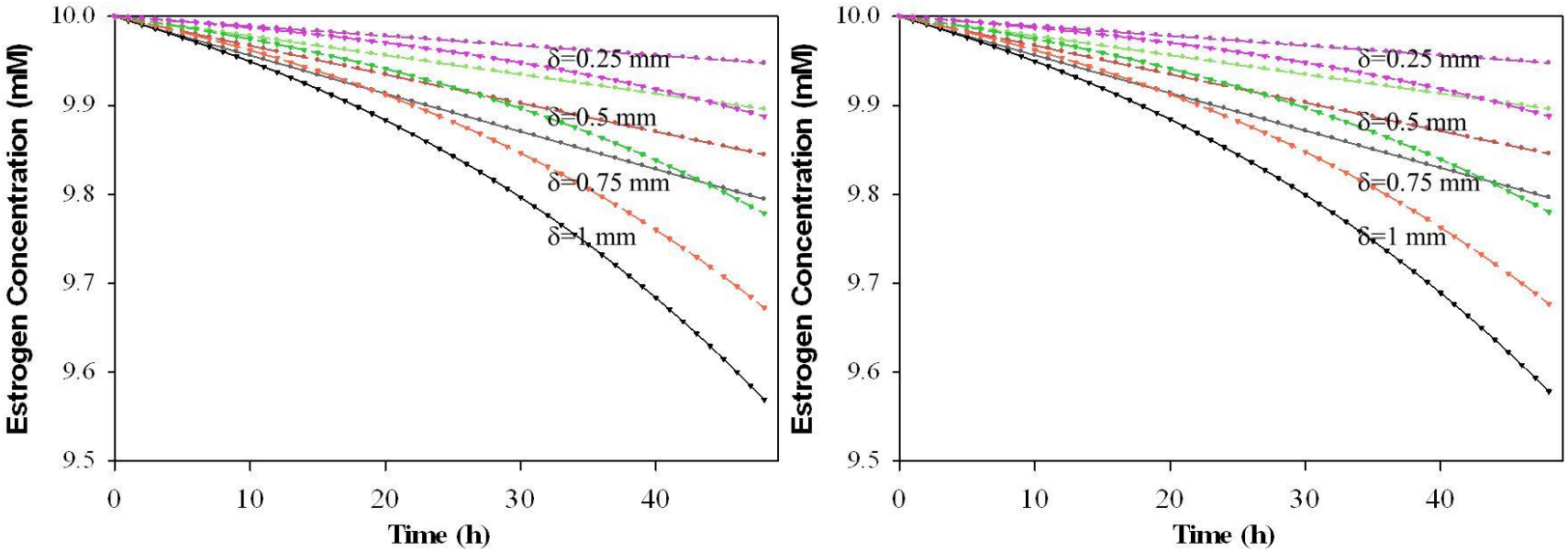

Figure 3.9: Estrogen concentration in the media over time plot.

3.3.5. Urea Production

Metabolic waste from the nitrogenous products are converted into urea and disposed via the renal system. Urea is a polar molecule (MW= 60 g/mol) and readily dissolves in water. In order to understand the productivity of urea and distribution in the scaffold, simulations were performed using the same four scaffold thicknesses discussed previously.

3.3.6. Effect of Scaffold Thickness and Porosity on Urea Concentration Distribution

Similar to previous analysis for oxygen and estrogen, the influence of scaffold thickness and scaffold porosity were investigated for the production of urea, first assuming a constant cell density, and again assuming that cell density increased with time. An increase in urea was observed (Figure 3.10) with an increase in scaffold thickness and cell number. Both scaffold region and medium appeared to be of the same concentration at the end of 48-h. This could be explained by the fact the urea production is limited by the diffusion of nitrogen into the scaffold where the reactions takes place. Urea diffusion constants both inside and outside of the scaffold are larger than those of nitrogen. This results in uniform distribution of urea throughout the bioreactor. A decrease in porosity lowered the effective diffusivity values for both nitrogen and urea. However, simulation showed that porosity had no effect on urea concentration profiles.

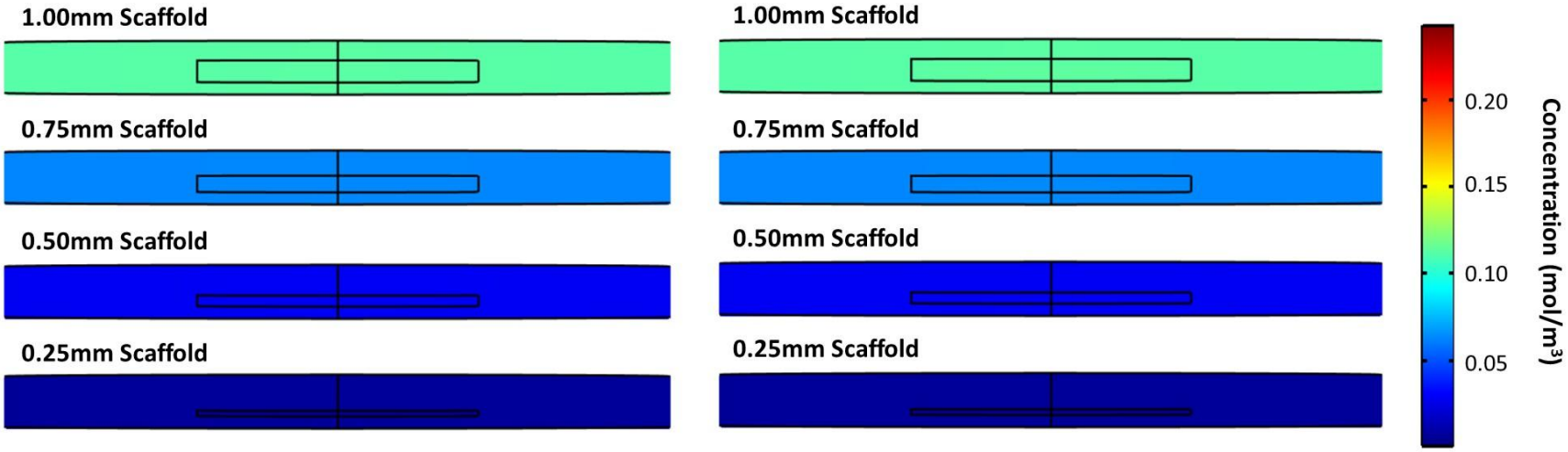

Figure 3.10: Scaffold thickness effect on urea production for 85% porosity (left) and 25% porosity (right). Shown are the cross-section views of the entire static bioreactor.

3.3.7. Influence of Cell Density on Urea Production

Analysis of the influence of cell density on urea concentration distribution was performed, similar to that for oxygen and estrogen. The urea concentration profiles (Figure 3.11) showed that an increasing cell density over time increased urea concentration for all scaffold thicknesses. This was attributed to the increased cell number. Also, as scaffold thickness increased, the difference in concentration between the constant cell count and increasing cell count simulations became more apparent. Even when an increasing cell density was assumed, porosity had no effect on urea concentration profiles.

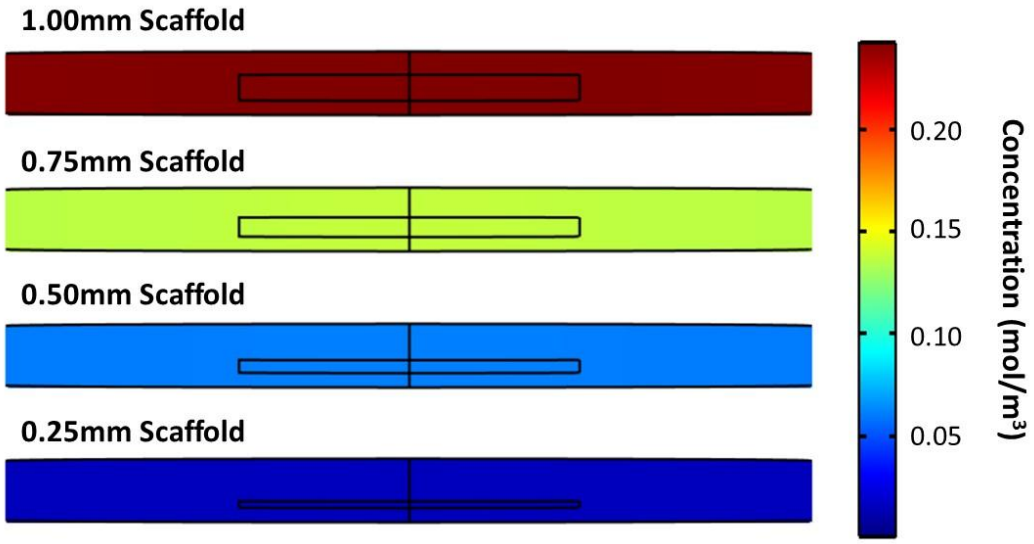

Figure 3.11: Effect of increasing cell density on urea concentration distribution for 85% porosity at 48 h.

Shown are the cross-section views of the entire static bioreactor.

The volume average concentration over time was plotted for all simulations. The plots (Figure 3.12) showed that the urea concentration in all four scaffolds increased constantly over time, when a constant cell density was assumed. In the case of increasing cell density, an exponential increase in urea concentration over time was observed. This was attributed to the exponential increase in cell number over time.

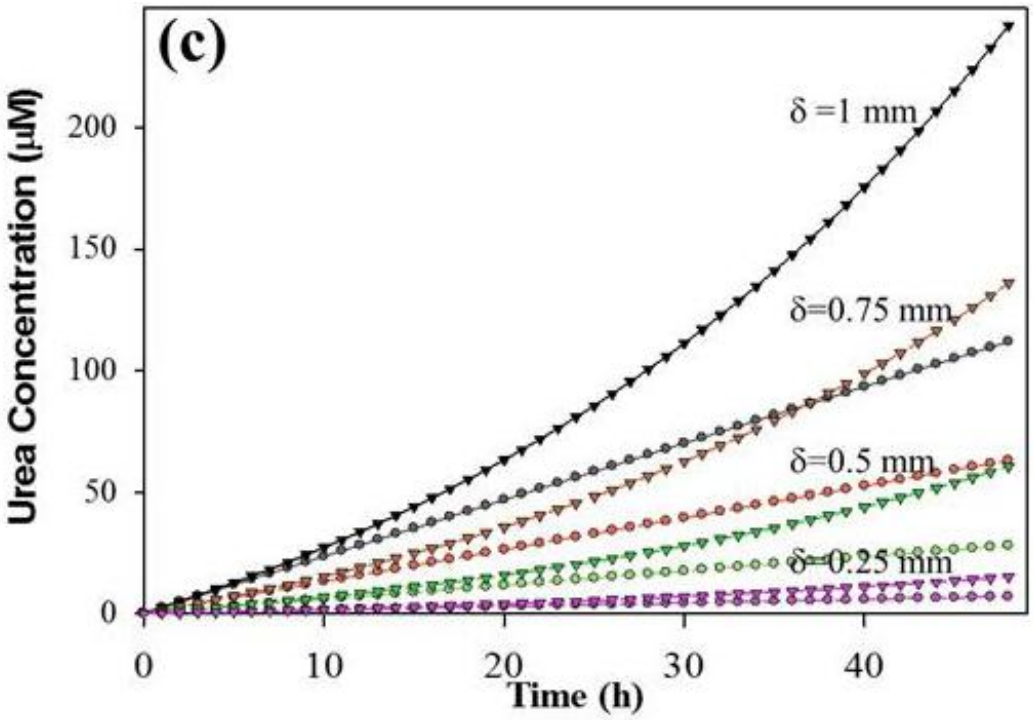

Figure 3.12: Urea concentration in the media over time plot at 25% porosity.

Very high concentrations of urea are toxic to the body and could be necrotic. In the clinical setting, the normal level of urea in plasma is around 30mg/100mL and increase of this value to 50mg/100mL is considered high and a possible indication of improper liver functionality. The highest value, 240μmol/m^3,was observed in the static bioreactor with 1mm thick scaffold when an increasing cell density over time was assumed, which corresponds to 1.44mg/100mL. This would indicate that urea concentration would not be near the toxic condition at the end of 48-h.

3.4 SUMMARY

In summary, the effect of scaffold thickness, porosity, cell density, and elevation on oxygen, estrogen, and urea concentrations in a static cell culture environment were investigated via simulation. Concentration profiles revealed that all varied parameters discussed had a direct effect on the uniformity of oxygen and estrogen concentration distributions. As scaffold thickness increased, oxygen deficiency and urea toxicity issues increased. Simulation showed that placement of the scaffold on the bottom of the bioreactor inhibited diffusion of oxygen into

cells along the bottom of the scaffold. Decreased porosity coupled with an increasing cell density over time, led to oxygen deficiency issues in all scaffold thicknesses. It was concluded that the static bioreactor was not capable of supporting three-dimensional hepatic cell cultures for the necessary 48 h time period investigated.

CHAPTER IV

FLOW-THROUGH BIOREACTOR 3-D SIMULATION

4.1 INTRODUCTION

Mass transfer in the static bioreactor was diffusion limited, causing non-uniform oxygen distributions and oxygen deficiency issues. The objective of this study was to test an axial-flow bioreactor capable of supporting three-dimensional hepatocyte cultures of scaffolds at least 1mm thick, similar to that of the static bioreactor. Nutrient and metabolic product concentration distributions were examined throughout the scaffold region, similar to the static bioreactor. Computational fluid dynamics simulations were utilized to examine oxygen consumption and urea production. Scaffold thickness and flow rate were varied in order to determine their effect on concentration levels and distributions. Oxygen and urea concentrations, shear stress, and velocity profiles as well as pressure drop across the bioreactor were evaluated for each analysis. These evaluations suggested that axial-flow bioreactors can support even 2-mm thick scaffolds.

4.2 SIMULATION SETUP

4.2.1. Bioreactor Geometry

Case1. Based on converting the static reactor into a flow system, similar proportions of bioreactor size and scaffold size were selected. Since axial-flow configuration showed less deformation of the scaffold due to fluid flow, that configuration was selected [24]. The regions and geometry of the axial-flow bioreactor are shown in Figure 4.1. Scaffold elevation was set 0.5mm from the top of the inlet cylinder. The hold-up region height was 0.84mm to match the 2.34mm height of the static bioreactor. The frustum semi-angle used was obtained from Bhaskar, 2012. The height of the frustum was determined using triangular geometry. The outlet and inlet cylinders had a diameter of 6mm. Both the inlet and outlet were 2mm in height.

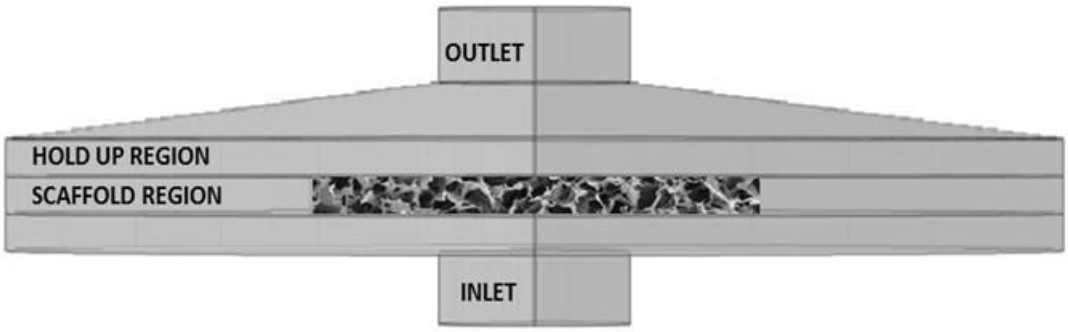

Figure 4.1: Design 1 axial-flow bioreactor regions.
(picture from COMSOL 4.3b simulation)

Case 2. Fluid naturally takes the path of least resistance, which would cause media in *Case 1* to flow-through open regions as opposed to directly through the scaffold. Also, the static bioreactor showed oxygen rich areas with limited use for hepatocytes due to diffusion limitations. This suggested the possibility of truncating the bioreactor to the scaffold size without compromising nutrient distribution. Additionally, a decrease in bioreactor volume would result in the use of less media, thus reducing operating costs. In order to force convection through the scaffold and

reduce bioreactor volume, area outside of the scaffold was eliminated from the design (Figure 4.2). The scaffold and bioreactor diameter were 14mm. The semi-angle of the bioreactor was changed due to reduced bioreactor diameter and my intent to maintain the same height from the bioreactor exit. Apart from 1 mm thick scaffolds, the possibility of using 2 mm thick scaffolds was tested as well.

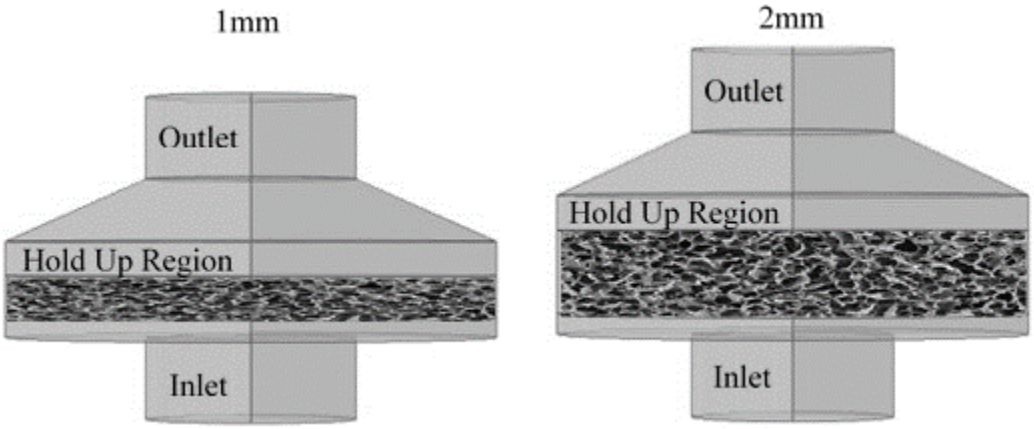

Figure 4.2: Design 2 axial-flow bioreactor regions.
(picture from COMSOL 4.3b simulation)

Both Case 1 and Case 2 bioreactor geometries were generated in COMSOL Multiphysics, version 4.3 (COMSOL, Inc., Burlington, MA), similar to previous publications [26]. In brief, three-dimensional (3D) bioreactor models were generated using the work plane settings option in the Geometry tab; this allows 2D drawings to be extruded to create 3D bioreactor models. Next, the sub-domain and boundary conditions are set in the Physics tab. The cell seeding density used in flow-through simulation was identical to that discussed in chapter two. The number of cells seeded in the 1mm and 2mm thick scaffolds for both Case 1 and Case 2 are seen in Table 4.1. Also, initial concentrations of nutrients in the growth medium are identical to that in the static bioreactor simulations.

Table 4.1: Cell count table based on a cell density of $1.29x10^{12}$ cells/m^3.

Cell Count		
Scaffold Thickness (mm)	**Scaffold Volume (mm^3)**	**Number of cells**
1	150	200,000
2	310	400,000

4.2.2. Assumptions

Assumptions used during flow simulation are listed below:

- Physical properties (density and viscosity) of the growth medium used for culturing cells are equivalent to those of water at 37°C.
- Effective diffusivity was constant, isotropic and is approximated using Mackie-Meares relationship similar to that in the static bioreactor.
- Porosity of the scaffold is constant either at 85% based on the chitosan-gelatin scaffolds to be used in the experiments) or 25% to assess the effect of reduced porosity
- No flux at all exterior boundaries other than the inlet and outlet
- Gravitation force was assumed to be negligible
- Bioreactor operates at steady state
- System is symmetric from the central axis
- Deformation in the scaffold due to fluid flow is negligible.

4.2.3. Governing Equations

Fluid behavior in non-porous regions was assumed to follow the Navier-Stokes equation,

$$-\nabla P + \eta \nabla^2 \upsilon = 0 \tag{4.1}$$

where *P* is the pressure, *v* is the velocity and η is the viscosity. Convective mass transport through the porous region was assumed to follow the Brinkman equation,

$$-\nabla P + \eta \nabla^2 v - \frac{\eta v}{k} = 0 \tag{4.2}$$

where P is the pressure, η is the media viscosity, v is the fluid velocity, and *k* is the permeability of the scaffold. The permeability of the scaffold was calculated using the equation

$$k = \frac{\pi}{128} n_A d^4 \tag{4.3}$$

where *d* is the pore diameter and n_A is the number of pores per unit area. Based on the characterization of chitosan-gelatin scaffolds [24], a pore diameter of 55 μm and pore number of 318 pores/mm^2 were used. The Brinkman equation was chosen because this equation takes into account the momentum transport by microscopic shear effects as well as pressure gradient forces involved in transport of the media from the free-flow region into the porous region.

Using the steady state values obtained for velocities in three directions, the concentration profiles of oxygen and urea were obtained by solving the convective-diffusive equation,

$$\nabla * (-D \nabla C_A) + u * \nabla C_A = r_A \tag{4.4}$$

where D is the effective diffusivity, C_A is the oxygen concentration at a given point, *u* is the fluid velocity and r_A is the reaction rate. Simulations were performed using the physics module *Reacting Flow, Diluted Species*, which was selected based on the module's governing equations for mass transport. The reaction rate was assumed to follow Michaelis-Menten kinetics for oxygen and zero order kinetics for urea production, as discussed in the static bioreactor simulations. The kinetic constants used in static bioreactor simulation were used for all axial-

flow bioreactors via proportioning based on the scaffold thickness. Both oxygen and urea reactions were solved simultaneously, similar to static bioreactor simulation.

Reynolds numbers were evaluated in order to assess the applicability of the Brinkman equation in the porous region. Both the average and maximum Reynolds numbers were calculated for the volume of the scaffold region using the equation,

$$\mathrm{Re} = \frac{\rho v_i}{\mu} \frac{\Phi_s D_p}{(1-\varepsilon_p)} \tag{4.5}$$

where ρ is the fluid density, υ_i is the fluid interstitial velocity (average or maximum, depending on the Reynolds number of interest), and μ is the fluid viscosity, Φ_s is the sphericity (approximately 1 for short cylinders), ε_p is the porosity, and D_p is the pore diameter.

The volumetric flow rate was varied for two reasons: i) to determine its effect on oxygen and urea concentration distributions and ii) to obtain a flow rate that would provide a measurable inlet to outlet concentration difference necessary for experimental validation. Volumetric flow rates tested, and each corresponding inlet velocity are shown in Table 4.2.

Table 4.2: Volumetric flow rate/inlet velocity equivalence.

Volumetric Flow Rate (mL/min)	Inlet Velocity (m/s) $\times 10^4$
0.1	0.593
1	5.93
10	59.3

4.2.4. Meshing

Meshing of all axial-flow bioreactor geometries were performed using a swept, mapped meshing, with a maximum element size of 0.28mm and a minimum element size of 0.0028mm. The mesh

was made finer throughout the scaffold region to obtain more precise results in this area of interest. The scaffold thickness was divided into 20 layers for 2mm thick scaffolds and 10 layers for 1mm thick scaffolds. Additionally, scaffold diameter was divided into 30 sections. The *Case 2* bioreactor, housing the 1mm thick scaffold contained a total of 91,890 nodes. A grid test was performed to ensure that mesh quality did not affect profile results. For grid test analysis, the maximum and minimum element sizes were changed to 0.25mm and 0.0025mm respectively, resulting in a total of 253,207 nodes throughout the case 2, 1mm thick scaffold bioreactor. Altering the node density changed the outlet oxygen concentration by 0.474%, which indicated that the mesh quality had been optimized at 91,890 nodes.

Average outlet concentration was evaluated for the purpose of experimental validation and use in grid test evaluation. The procedure for obtaining concentration profiles for axial-flow simulation is similar to that for static simulation. An example of how to obtain average outlet concentration is in Appendix D.

4.3. RESULTS

4.3.1. Applicability of Brinkman Equation to Predict Flow Through Porous Medium

Our group has extensively used Brinkman equation to evaluate flow-through porous medium in a variety of bioreactors [19, 25-27]. Based on those concepts, Brinkman equation was used in this study. To understand the utility of the Brinkman equation, the average and maximum interstitial velocities in the porous region were retrieved from simulation. Then the average and maximum Reynolds numbers were calculated (Table 4.3) for the highest flow rate tested (10mL/min). Detailed Reynolds number calculations for different flow rates are given in Appendix E. Both average and maximum Reynolds numbers were less than one at the highest flow rate.

Table 4.3: Average and maximum Reynolds numbers for Q = 10 mL/min.

	Case1	Case2 (1mm)	Case 2 (2mm)
Average Reynolds Number	0.0234	0.109	0.103
Maximum Reynolds Number	0.0787	0.139	0.136

Since Darcy's equation is generally used to evaluate flow through porous medium for Reynolds numbers less than one, simulation was also performed using the Darcy equation. Simulation using Darcy's equation showed no variance in output pressure drop compared to the simulation using the Brinkman equation. As previous studies pertaining to axial-flow bioreactors performed by my peers used the Brinkman equation to characterize fluid flow through porous regions, I used the Brinkman equation for comparison purposes.

4.3.2. Case 1: 1mm Thick Scaffold

4.3.2.1. Pressure Drop

Upon validation of using the Brinkman equation, the pressure distribution across the porous region where cells are grown was analysed. The average pressure drop across the bioreactor was calculated by calculating the difference between the inlet and outlet average pressure. Derived values, average surface evaluations were performed at the inlet and outlet to obtain the average pressure at each location. An example of how to obtain average values at a surface is shown in Appendix D. The average pressure drop across the reactor for each flow rate is shown in Table 4.4. Since these were based on Brinkman equation, the average pressure drop across the reactor increased as the flow rate increased.

Table 4.4: Case 1 average pressure drop at 25% porosity.

Volumetric Flow Rate (mL/min)	0.1	1	10
Average Pressure Drop (Pa)	0.03	0.21	5.21

4.3.2.2. Shear Stress Distribution

Flow rate directly dictates the sufficiency of nutrients necessary for cellular activity and local shear stresses experienced by cells. Very low flow rate could lead to nutrient deficiency and limited cell survivability. However, high flow rate leads to high shear stresses and the upper limit for the perfusion rate is set by the tolerance of cells to shear force induced by the flowing fluid. In particular, increasing the shear stress from a low range of 0.001 – 0.033 Pa to a higher range of 0.5 – 2.1 Pa, has been shown to decrease urea production to half the level [30]. Shear stress profiles of the scaffold region were developed to understand the shear stresses experienced by the cells at different volumetric flow rates (Figure 4.3). The maximum shear stress increased as the flow rate increased. Maximum shear stress was exhibited at the top of the inlet cylinder.

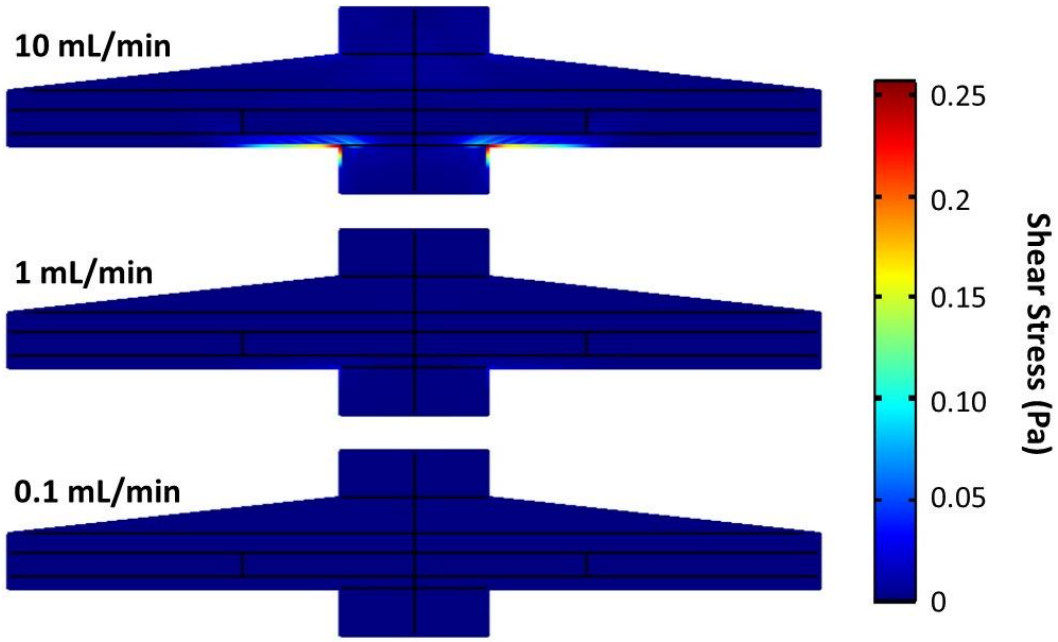

Figure 4.3: Effect of flow rate on shear stress at 25% porosity.

Shear stress profiles demonstrated that maximum shear stress was exerted near the top of the inlet cylinder. This was most evident at the maximum flow rate simulated, 10mL/min. Shear stress analysis of the scaffold region, where cells are housed and shear stress is of particular concern,

was then performed. The shear stress profile shown in Figure 4.4 revealed that the case 1 bioreactor exerted shear stress values near zero, particularly in the scaffold region, even at the highest flow rate and lowest porosity simulated.

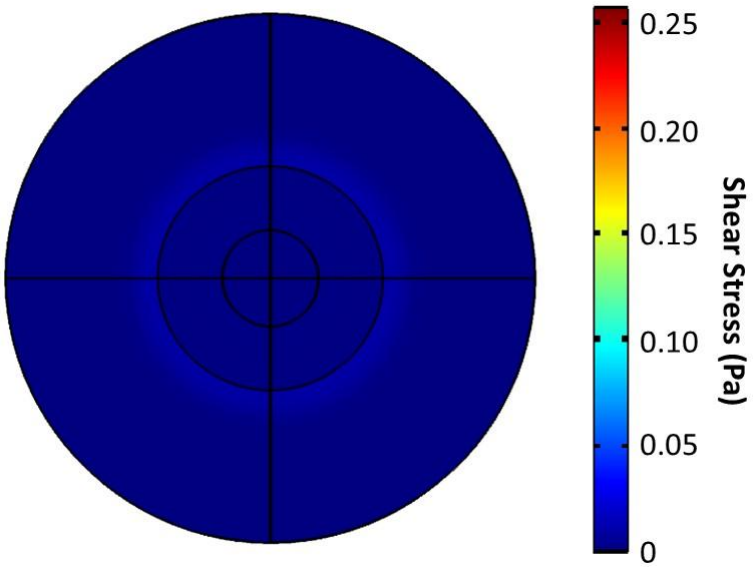

Figure 4.4: Shear stress profile for the bottom side of the scaffold at 10 mL/min and 25% porosity.

Maximum scaffold shear stress was also evaluated and determined using derived values, volume maximum evaluation. A maximum scaffold shear stress of 0.00195 Pa was experienced by cells in simulation when a flow rate of 10mL/min was simulated. Profiles showed that shear stress was uniformly distributed throughout the scaffold region of the case 1 bioreactor.

4.3.2.3. Oxygen Consumption Characteristics:

Simulations were performed with a defined rate law for oxygen to understand the nutrient distribution with consumption. The cell density (1.29×10^{12} cells/m^3) was the same as that used in the static bioreactors. Oxygen concentration profiles were examined at different flow rates to determine the effect of flow rate on oxygen concentration distribution. Oxygen concentration profiles associated with each flow rate are shown in Figure 4.5. As the flow rate increased, the

oxygen concentration became more uniformly distributed. The oxygen profiles showed that oxygen rich areas, similar to those seen in the static bioreactor simulations, still exist.

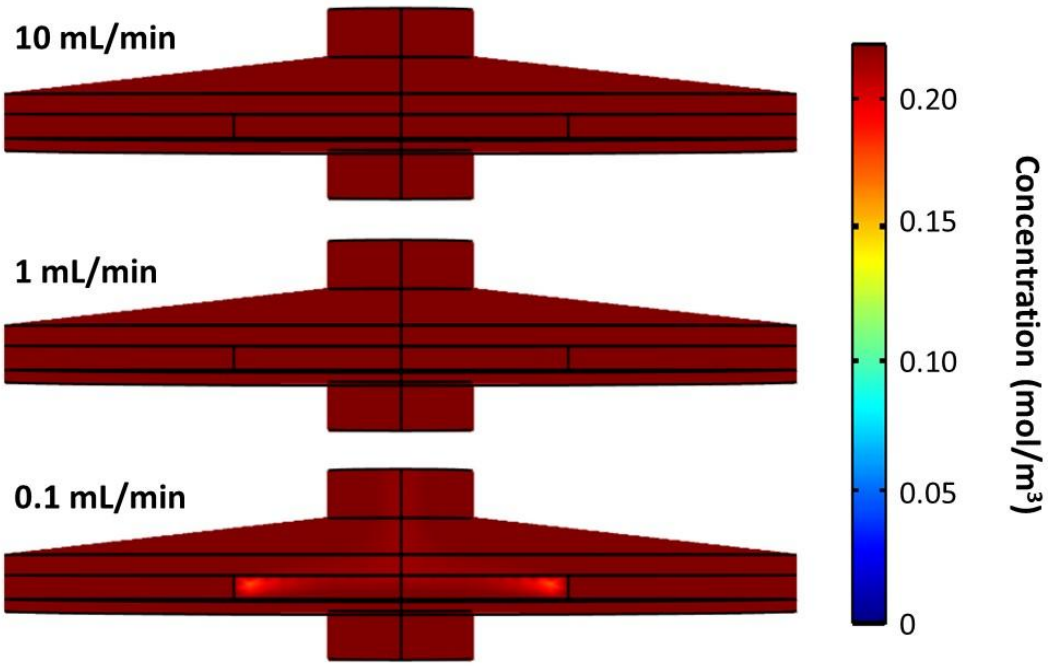

Figure 4.5: Effect of flow rate on oxygen concentration distribution at 25% porosity.

Oxygen concentration profiles demonstrated that oxygen was uniformly distributed throughout the case 1 bioreactor at flow rates as low as 1mL/min.

4.3.2.4. Urea Production:

Simulations for urea production were performed to determine the distribution of a metabolic product in the scaffold. These results showed (Figure 4.6) that urea was uniformly distributed for each of the three flow rates. The urea concentrations were significantly lower for all three flow rates in Case 1, relative to static bioreactors. In any case, urea toxicity was not a concern for the case 1, flow-through bioreactor system.

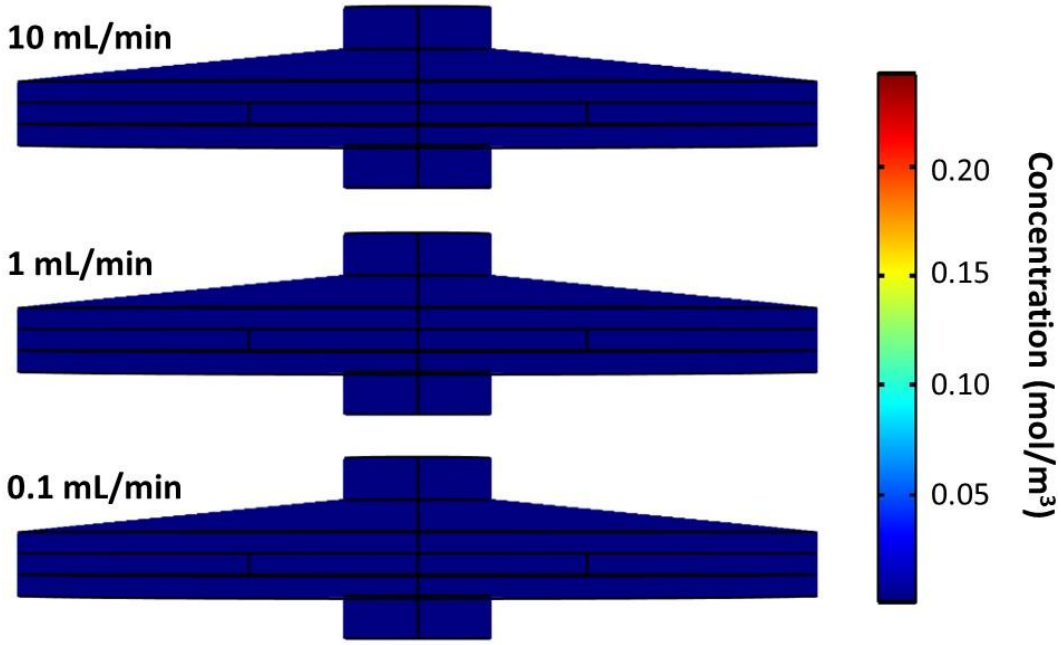

Figure 4.6: Effect of flow rate on urea concentration.

4.3.3. Case 2: 1mm thick scaffold

4.3.3.1. Pressure Drop

The average pressure drop for the case 2 reactor was obtained similar to Case 1 (Table 4.5). The average pressure drop increased compared to pressure drop at the same flow rate for Case 1. This suggests that truncating the bioreactor diameter to fit the scaffold size forced the fluid to pass through the scaffold, increasing the pressure drop.

Table 4.5: Average pressure drop with 1mm thick scaffold and 25% porosity.

Volumetric Flow Rate (mL/min)	0.1	1	10
Average Pressure Drop (Pa)	0.11	1.06	10.71

4.3.3.2. Shear Stress

Shear stress profiles shown in Figure 4.7, demonstrated that the case 2, 1mm thick scaffold bioreactor exerted shear stress values near zero, particularly in the scaffold region. The maximum shear stress in the scaffold region was 0.03162 Pa, at a volumetric flow rate of 10mL/min.

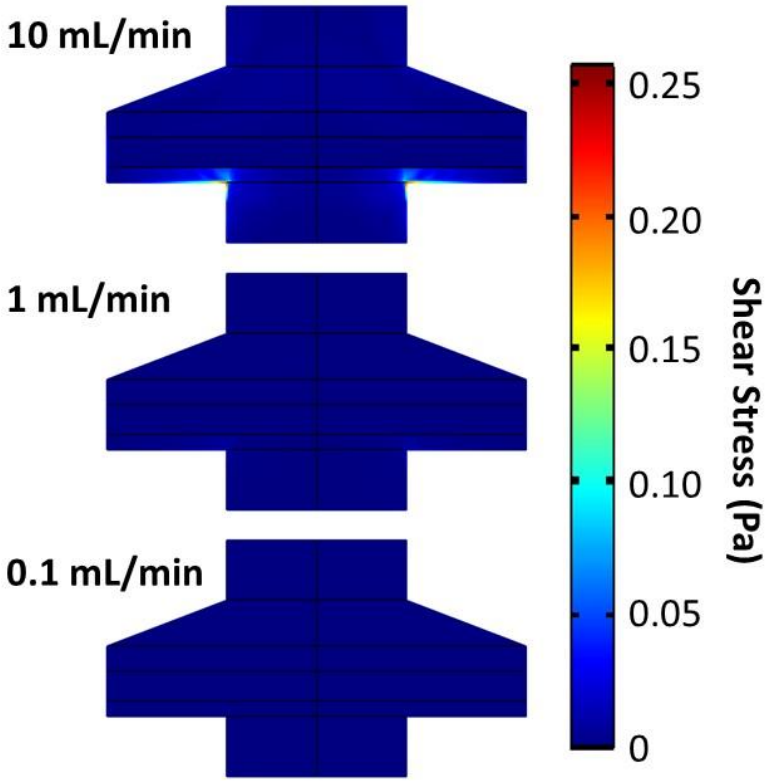

Figure 4.7: Effect of flow rate on shear stress in 1mm thick scaffold at 25% porosity.

4.3.3.3. Oxygen Consumption Characterization

Figure 4.8 shows the oxygen concentration profiles for three different flow rates over the range discussed. Truncation of the bioreactor showed uniform distribution of oxygen throughout the scaffold even at flow rates as low as 0.1mL/min.

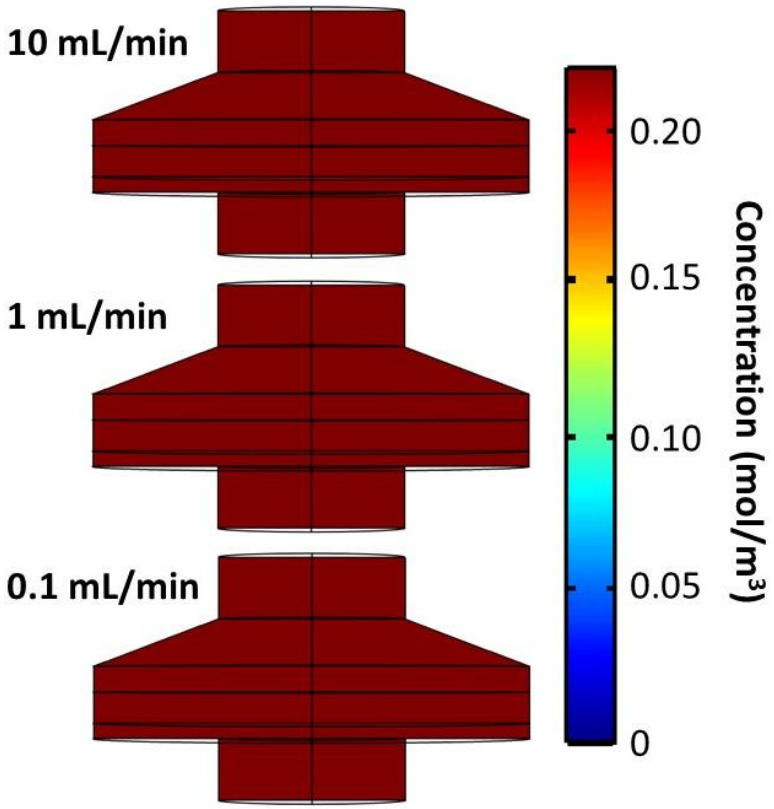

Figure 4.8: Effect of flow rate on oxygen concentration in 1mm thick scaffold at 25% porosity.

4.3.3.4. Urea Production

Simulations for urea production similar to those discussed for case 1 were performed. These results showed (Figure 4.9) that urea was uniformly distributed for each of the three flow rates.

The urea concentrations were again significantly lower for all three flow rates, relative to static bioreactors. Low urea concentrations discovered in both the case 1 and case 2 simulations led to the conclusion that urea toxicity was of no concern in the axial-flow bioreactor.

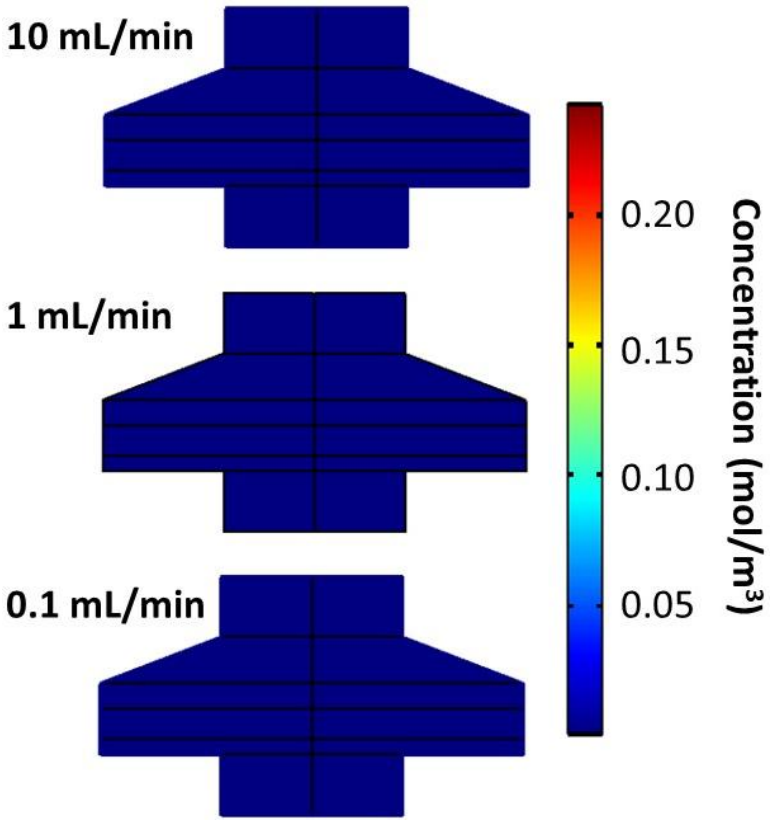

Figure 4.9: Effect of flow rate on urea concentration distribution at 25% porosity.

4.3.4. Case 2: 2mm Thick Scaffold

4.3.4.1. Pressure Drop

Similar to other cases, average pressure drop values were obtained. These results showed (Table 4.6) an increase in pressure drop compared to Case 1 as well as Case 2 1mm thick scaffolds. Increased thickness proportionally increased the pressure drop across the scaffold.

Table 4.6: Average pressure drop with 2mm thick scaffold and 25% porosity.

Volumetric Flow Rate (mL/min)	0.1	1	10
Average Pressure Drop (Pa)	0.20	2.02	19.85

The shown values for all three conditions were evaluated at 25% porosity which is used in permeability calculations. Since the pressure drop is inversely proportional to 1/k as predicted by

the Brinkman equation, increased permeability at 85% is expected to provide significantly less pressure drop across the bioreactor.

4.3.4.2. Shear Stress

Shear stress profiles were evaluated for flow rates of 10, 1, and 0.1 mL/min (Figure 4.10). A maximum shear stress of 0.3765 Pa was exerted in the scaffold region at the highest flow rate simulated. Profiles again demonstrated that exerted shear stress in the scaffold region of the case 2, 2mm thick scaffold were negligible.

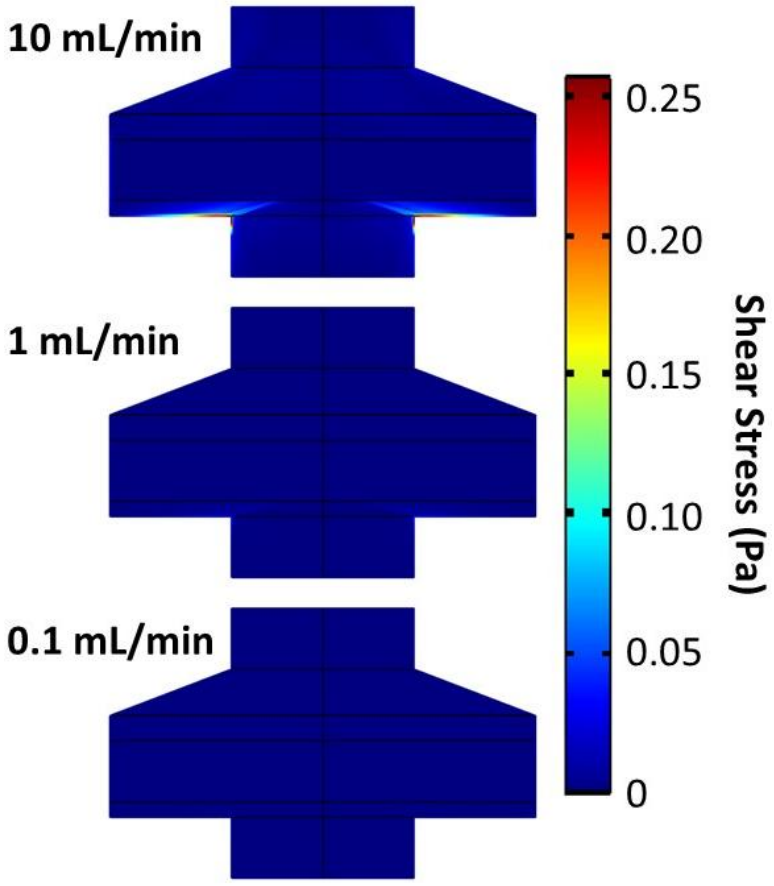

Figure 4.10: Effect of flow rate on shear stress in 2mm thick scaffold at 25% porosity.

4.3.4.1 Oxygen Consumption Characterization

Oxygen concentration profiles associated with three different flow rates over the range discussed are shown in Figure 4.11. Oxygen concentration was uniformly distributed at all flow rates similar to that of 1mm thick scaffolds. Since the simulations were performed at the same cell density (1.2×10^{12} cells/m^3), increased thickness increased the number of cells. Hence the consumption of oxygen proportionally increased relative to 1mm thick scaffolds.

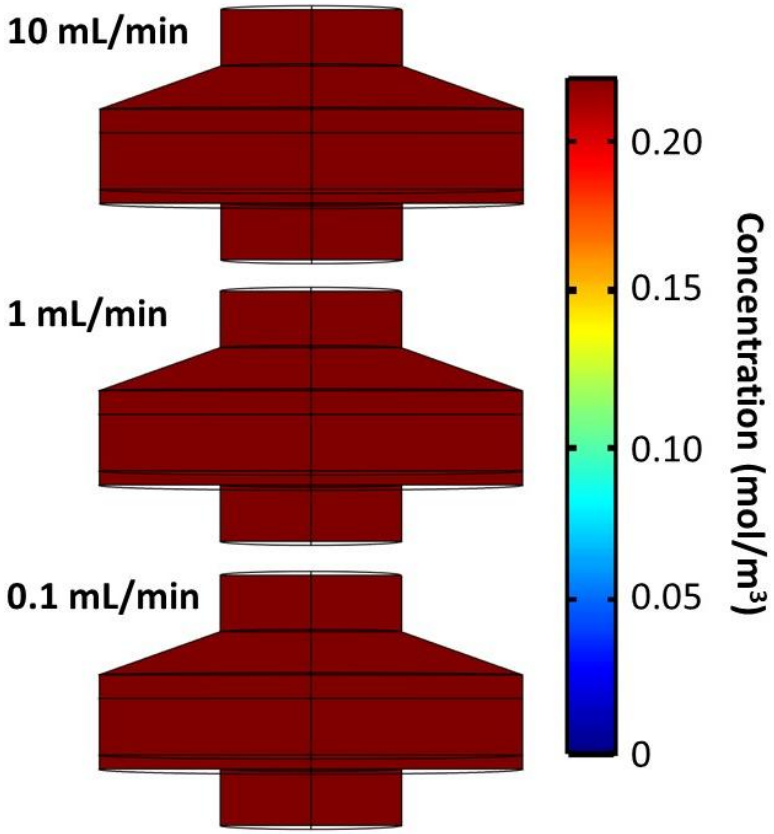

Figure 4.11: Effect of flow rate on oxygen concentration in 2mm thick scaffold at 25% porosity.

4.4. SUMMARY

Simulations were performed to determine the effects of bioreactor geometry and volumetric flow rate on oxygen and urea concentration distributions in an axial flow bioreactor. Truncating the

bioreactor to fit the exact scaffold diameter improved the uniformity of oxygen distributions when compared at the same volumetric flow rate. Urea toxicity was significantly decreased in all cases for axial-flow reactors, when compared with urea concentrations in the static reactor with the same scaffold thickness. Shear stress was also investigated due to concern for environmental condition concerns for cells. Shear stress increased as flow rate increased, but a level of shear stress at which cells would be damaged or die was not encountered in case 1 or case 2. It was concluded that the case 2 bioreactors should be constructed for experimental validation of the model, as oxygen was most uniformly distributed in case 2 simulations.

CHAPTER V

EXPERIMENTAL VALIDATION

Using various assumptions and governing equations, simulations were performed in CFD. In order to understand the utility of the simulation, experimental validation of nutrient distribution and consumption is necessary. A six-well plate, with the dimensions discussed in chapter 2, was used for static experimental studies. For flow-through experiments, an axial-flow bioreactor prototype was constructed with the dimensions discussed in chapter 3. Chitosan-gelatin scaffolds, prepared by freeze drying, were utilized in the experimentation due to extensive analyses previously performed on those scaffolds being available in the laboratory. Using the bioreactor and the scaffold, experiments were performed at the lowest flow rate discussed in simulation studies to measure nutrient distribution using residence time distribution analyses. Hepatocarcinoma cells (HepG2- cell line) were cultured and oxygen and urea concentration measurements were analyzed to validate model nutrient consumption and toxin production. Oxygen measurements were only performed on the flow-through system, as pinpointing an exact location for oxygen measurement in the scaffold inside of the static bioreactor scaffold would be impossible. Urea concentration measurements were obtained for both the static and flow-through systems, as urea was shown to be uniformly distributed in all cases. In addition, to understand the nutrient distribution in the bioreactor residence time distribution analysis using step input technique was performed.

5.1. METHODS AND MATERIALS

Chitosan (190-310kDa MW and 85% degree of deacetylation), Gelatin Type-A (Bloom 300) from porcine skin, and glacial acetic acid were obtained from Sigma Aldrich Chemical Co. (St. Louis, MO). Chloroform and Ethanol (200 proof) were obtained from Aaper Alcohol and Chemical Company (Shelbyville, KY). Urea assay kit was obtained from Sigma Aldrich Chemical Co. (St. Louis, MO).

5.1.1. Scaffold construction

Scaffolds of 1mm and 2mm thickness were prepared using a 10cm diameter circular mold on a Teflon sheet, following the procedure previously described [15]. In brief, 2%-2% (wt/v) chitosan gelatin solution was prepared in 0.5M acetic acid and 25mL of solution were poured into the molds. The solution was frozen at -80 °C overnight and then placed in a Virtis freeze dryer (Gardiner, NY) overnight. Obtained dry scaffolds were submerged in absolute ethanol to wash the acetic acid. Using a custom-made punch, 14mm diameter scaffolds were cut and used in all experiments. All scaffolds were washed in a phosphate buffered saline solution with a pH of 7.4 prior to experimentation.

5.1.2. Residence time distribution analysis

Experiments were performed to calculate mean residence time for both the 1mm thick scaffold bioreactor, using an open-loop flow system, similar to a previous publication [19] with some modifications. In brief, the axial-flow bioreactor was constructed in house to the specifications of the case 2 reactor as explained in simulation discussion in chapter 3. This bioreactor had a split design, where the top part had a conical structure leading to the outlet, and the bottom part provided the location for placement of the scaffold above the inlet. This bioreactor was connected to the flow loop designed to include two fluid reservoirs (Figure 5.1) pumped separately using two syringes placed in one syringe pump (74900 series, Cole-Parmer Instrument Company, Vernon Hills, IL); one syringe filled with deionized water and another syringe filled

with tracer. Tubes were attached to the end of each syringe and connected to a three-way stopcock (V1 and V3). The stopcocks diverted fluid either to another three-way stopcock (V2) or to a waste container. Stopcock V2 allowed either the tracer or deionized water to enter the tube leading to the bioreactor. Samples were collected from a tube connected to the bioreactor outlet.

Stopcocks V1 and V2 were initially set to divert tracer toward the bioreactor while stopcock V3 was set to divert deionized water toward the waste container. The syringe pump flow rate was set at 0.1mL/min. The tube path leading from the tracer syringe was filled with fluid and stopped once it reached stopcock V2. Stopcocks V3 and V2 were then set to divert deionized water to the bioreactor while stopcock V1 was set to divert tracer solution toward the waste container. Deionized water was run through the reactor until steady state was achieved. The tracer was then introduced by setting stopcock V3 to divert deionized water toward the waste container and setting stopcocks V3 and V2 to divert tracer solution toward the bioreactor. The experiment timer began once the tracer solution reached the bioreactor inlet. Samples at 0.2mL were taken every 15 minutes until the absorbance of the sample matched that of the initial tracer concentration in the syringe.

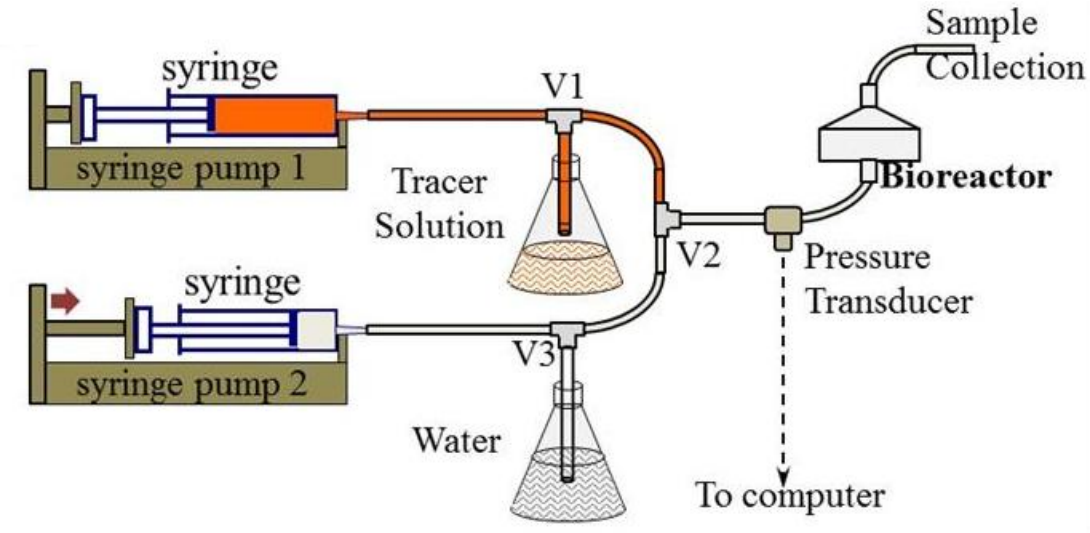

Figure 5.1: Schematic of RTD experiment setup.

Concentrations of tracer were determined using a spectrophotometer (Spectramax Emax spectrometer, Molecular Devices, Sunnyvale, CA) at 490 nm. The method discussed in Bhaskar, 2012, was used to determine the mean residence time. RTD data and calculations are in Appendix F.

5.1.3. Cell culture.

Human hepatocellular carcinoma cell line Hep G2 (ATCC® HB-8065™) was obtained from ATCC (Manassas,VA) and maintained in Eagle's Minimum Essential Medium (EMEM) following vendor's protocol. In brief, EMEM was supplemented with 10% fetal bovine serum (Invitrogen Corp.). Cells were incubated at 37°C, 5% CO2/95% air, and fed with fresh medium every other day. When cells were confluent, they were detached with 0.25% (w/v) Trypsin – 0.53mM EDTA obtained from Invitrogen Corp. (Carlsbad, CA), neutralized with the growth medium. Cells were centrifuged at 270g for 5 min and dispersed in growth medium.

As necessary, these cells were used in the experiments by counting viable cells using Trypan blue dye exclusion assay. An appropriate number of cells were seeded onto each sterile 1mm and 2mm thick chitosan-gelatin scaffold, and incubated overnight for cellular attachment.

5.1.4. Oxygen consumption validation.

Experimental setup was similar to the RTD analysis, with few changes to the mode of operation (Figure 5.2). Initially, all components (tubing and bioreactor) were dry steam sterilized at 134 °C for 45 min. The oxygen probe housing, oxygen probe, and bioreactor stands were disinfected with a 70% ethanol solution. The pressure transducer and syringes were obtained in sterile packaging. All surfaces, including the water bath and syringe pump were wiped down with the 70% ethanol solution. The entire flow loop (tubing, syringe, pressure transducer, bioreactor, and oxygen probe) was then assembled under a sterile hood.

The cell containing scaffold was placed inside of the bottom half of the bioreactor and saturated with media. The bioreactor was assembled and placed in an incubator at 37 °C overnight for cell attachment. The bioreactor was connected to the flow-loop in a sterile environment along with the oxygen probe and pressure transducer. Growth medium was loaded into a syringe and placed in the syringe pump. The tubing connecting the syringe and the bioreactor was passed through a water bath maintained at 37 ^{0}C. Based on the simulation studies explained in Chapter 3, the syringe pump was set to a flow rate of 0.1mL/min using the tubing diameter. A waste jar was set up to collect the growth medium exiting the bioreactor.

Timing of the experiment began once the first drop of media reached the bioreactor inlet. The experiment lasted 2 hours, similar to RTD analysis. Small samples (~0.2 mL) were collected every 30 minutes. Using the oxygen flow-through electrode (Microelectrodes, Inc., Bedford, NH), outlet oxygen concentration was monitored in real-time. After reaching steady state (~2 h based on four times the space time), oxygen reading was recorded for comparison with the simulation. Exiting medium collected during experimentation was used for urea analysis.

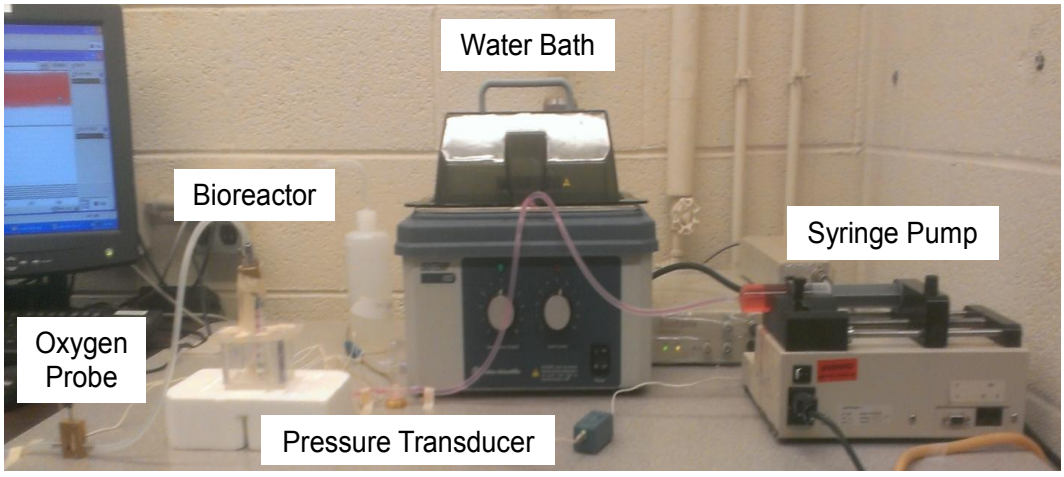

Figure 5.2: Oxygen consumption validation experimental setup.

5.1.5. Urea production validation

Urea concentration analysis was performed in both the static and axial-flow reactor settings. Axial-flow reactor samples were taken during the experiment described in the oxygen consumption validation section. The static bioreactor setup used a six-well plate and the 1mm chitosan-gelatin scaffolds discussed previously. A sterile six-well plate was opened under a sterile hood. Scaffolds for experimentation were prepared as discussed previously and placed into the middle of the six-plate. Mesh was used to hold the scaffolds in place and was sterilized using a 70% ethanol solution. The wells were then filled with media according to the dimensions of the simulated static reactor discussed in chapter 2, and taking into account displacement due to scaffold presence.

Static reactor experiments ran for 48h and 50h, due to uncertainties with the amount of time required for cell attachment. Samples were collected from each well at the end of the allotted experimentation period. A spectrophotometer was used to compare the absorbance of each sample to that of water and a diluted urea solution. These absorbance values were then used to calculate the urea concentration for each sample.

5.2. RESULTS

5.2.1. Residence time distribution

The non-ideal fluid distribution is characterized using the residence time distribution (RTD). The RTD measures the amount of time different molecules present in the fluid spend within the reactor [9, 18]. In other words, RTD is a measure of dispersal of a molecule in a flowing medium owing to the combined action of a velocity profile and molecular diffusion. To understand the distribution of nutrients, a C(t)/Co curve (Figure 5.3**)** was plotted from which mean residence time, t_m, was calculated. The methodology used for this calculation is in Appendix F. The t_m for the bioreactor with scaffold was 25.7 min. Multiplying this with the used flow rate of 0.1mL/min

gave the effective volume to be nearly 95% of the volume of the bioreactor. This confirmed uniform distribution of nutrients, similar to CFD profiles shown in Chapter 3.

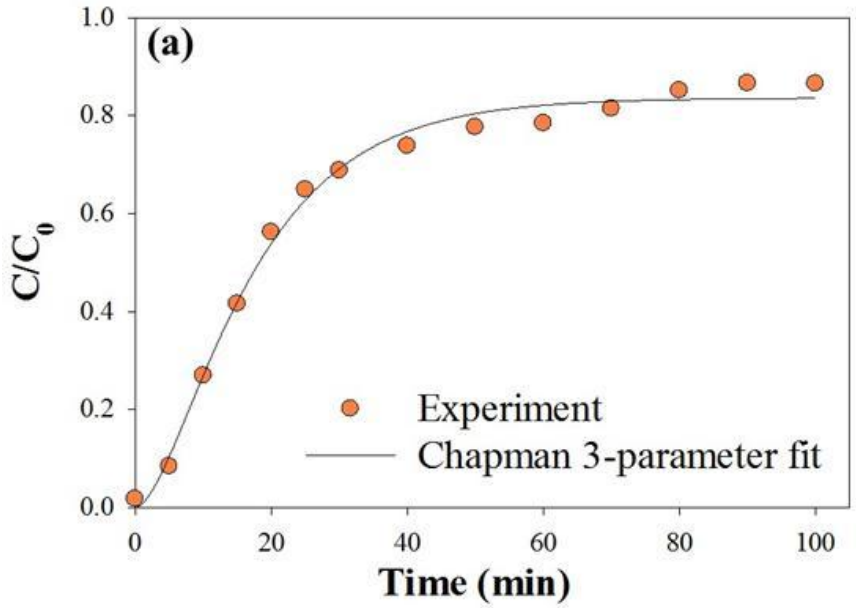

Figure 5.3: RTD concentration vs. time plot.

5.2.2. Oxygen concentration comparison

Non-ideal fluid flow patterns lead to non-uniform distribution of nutrients present in the fluid. The RTD analysis is independent of the metabolic reactions and hence nutrient consumption is not integrated into CFD modeling. To understand the implications of non-ideal fluid distribution on tissue regeneration, oxygen consumption characteristics were analyzed. The oxygen concentration collected by the oxygen probe was compared to the average outlet concentration obtained in simulation. Figure 5.4 shows the comparison of these results.

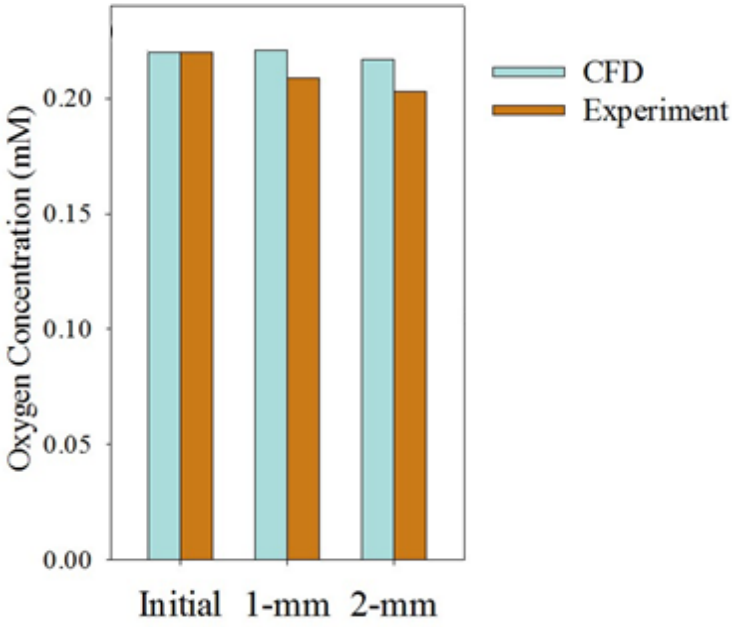

Figure 5.4: Comparison of outlet oxygen concentration.

5.2.3. Urea concentration comparison

In order to understand the implications of non-ideal fluid distribution on tissue regeneration, production characteristics of the toxin urea were analyzed. The urea concentration obtained by absorbance analysis was compared to the average urea concentration obtained in simulation. These comparissons were performed for both the static and axial-flow bioreactors (Figure 5.5).

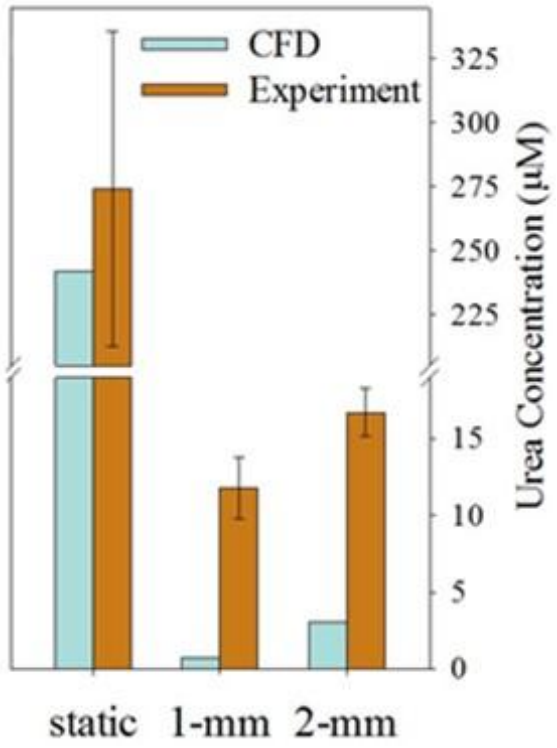

Figure 5.5: Comprison of urea concentration.

The experimental outlet urea concentrations generally agreed with predicted concentrations in static bioreactors. However, the model under predicted the outlet concentration compared to the experimental results from the axial-flow bioreactors. When accounting for cell number increase during the 12 h incubation, urea production in 2mm thick scaffolds increased to 4.6μM from 3.2 μM but was still significantly lower than experimental measurements.

5.3 SUMMARY

Experimentation was necessary for model validation. An RTD analysis was performed in order to determine the length of time the experiment should be run. Outlet oxygen concentration data was recorded during experimentation for comparison with simulation values. The model was able to predict outlet oxygen concentration with less than a ten percent difference. The model was able to predict urea production concentrations in static bioreactors with much more accuracy than in the axial-flow bioreactor.

CHAPTER VI

CONCLUSIONS AND RECOMENDATIONS

6.1 CONCLUSIONS

The axial-flow bioreactor developed showed improved nutrient distribution and possibility of culturing hepatocytes in 3D porous scaffolds. The following are the conclusions based on the three objectives

i) To understand the limitations of the static bioreactor via CFD Simulation.

As scaffold thickness increased, oxygen deficiency issues increased. Placement of the scaffold on the bottom of the bioreactor inhibited diffusion of oxygen into cells along the bottom of the scaffold. Decreased porosity led to oxygen deficiency issues in all scaffold thicknesses. Estrogen and urea concentration distributions posed no limitation on the static bioreactor setup.

The static bioreactor was not capable of supporting three-dimensional hepatic cell cultures due to oxygen deficiency issues encountered, particularly at decreased porosity due to proliferation.

ii) To develop an axial-flow bioreactor via CFD Simulation.

The elimination of excess area outside of the scaffold region, despite being oxygen rich, did not inhibit nutrient distribution throughout the scaffold region. Higher flow rates in the axial-flow bioreactor led to greater shear stresses inside of the scaffold region and larger pressure drops across the bioreactor. Uniform oxygen concentration distributions were observed even at low flow rates as low as 0.1 mL/min. Urea concentration was not a concern in these bioreactors.

The truncated, case 2 axial-flow reactors experienced shear stresses that were nearly one-fourth that of the case 1 axial flow bioreactor. The case 2 axial-flow bioreactor simulations demonstrated that nutrient distribution was more uniform when compared to the case 1 reactor at the same flow rate. It was concluded from simulation that the case 2 bioreactor was the optimal environment for experimental validation.

iii): To validate the axial-flow bioreactor simulation with experimental results

Obtained mean residence time (t_m) was compared with the theoretical space time calculated from the volumetric flow rate and the volume of the bioreactor. These calculations showed distribution of nutrients in the entire region with less than 5% dead space. These regions are similar to those observed in the simulation results. The model was able to closely predict outlet oxygen concentration

6.2 RECOMENDATIONS

1. Need for appropriate kinetic parameters. Kinetic constants obtained from 2D monolayer culture systems reported in literature were utilized in the simulation of cells on 3D porous scaffolds. However, many *in vitro* experiments show that cells respond differently in attachment, morphology, migration, and proliferation on 3D scaffolds unlike traditional 2D-tissue culture. Hence, it is expected that kinetic parameters could change based on the culture condition. Using kinetic parameters in simulation appropriate for the experimental condition could help improve

model predications. Hence performing experiments to determine the kinetic constants via experimentation is necessary. An experiment using the bioreactors constructed for this study or ones of similar geometry should be used to perform the experiment. The experiment should be conducted at four or more different flow rates.

2. Testing effect of drugs in the bioreactor. In this study, I used three components to test the simulation: oxygen, urea and estrogen. One has to extend these to testing drugs and assess the utility of the developed model in assessing hepatotoxicity.

REFERENCES

1. Bissell, D.M., et al., *Drug-induced liver injury: Mechanisms and test systems.* Hepatology, 2001. **33**(4): p. 1009-1013.
2. Bjork, J.W. and R.T. Tranquillo, *Transmural flow bioreactor for vascular tissue engineering.* Biotechnology and Bioengineering, 2009. **104**(6): p. 1197-1206.
3. Bursac, P.M., et al., *Mass transfer studies of tissue engineered cartilage.* Tissue Eng, 1996. **2**(2): p. 141-50.
4. Carrel, A., *On the Permanent Life of Tissue Outside of the Organism.* J. Exp. Med.,, 1912. **15**(3): p. 516–528.
5. Colton, C.K., et al., *Diffusion of urea in flowing blood.* AIChE Journal, 1971. **17**(4): p. 800-808.
6. Devarapalli, M., B.J. Lawrence, and S.V. Madihally, *Modeling Nutrient Consumptions in Large Flow-Through Bioreactors for Tissue Engineering.* Biotechnology and Bioengineering, 2009. **103**(5): p. 1003-1015.
7. ElectrospinningCompany. *Why 3D cell culture?* ; Available from: http://www.electrospinning.co.uk/why-3d-cell-culture/.
8. Fisher, M.B., et al., *In vitro glucuronidation using human liver microsomes and the pore-forming peptide alamethicin.* Drug Metabolism and Disposition, 2000. **28**(5): p. 560-566.
9. Fogler, H.S., *Elements of Chemical Reactor Engineering*. 4th ed. 2006, Upper Saddle River, NJ: Prentice Hall.
10. Gebhardt, R., et al., *New hepatocyte in vitro systems for drug metabolism: metabolic capacity and recommendations for application in basic research and drug development, standard operation procedures.* Drug Metab Rev, 2003. **35**(2-3): p. 145-213.
11. Gibco, i., *Cell culture basics*
12. Heine, P.A., et al., *Increased adipose tissue in male and female estrogen receptor-alpha knockout mice.* Proc Natl Acad Sci U S A, 2000. **97**(23): p. 12729-34.
13. Herper, M. *The Cost of Creating a New Drug Now $5 Billion, Pushing Big Pharma to Change*. Forbes, 2013. **2013**.
14. Horri, I., Yamada, H., *In vitro hepatotoxicity testing in the early phase of drug discovery.* Alternatives to Animal Testing and Experimentation, 2007. **14**(Special Issue): p. 437-441.
15. Huang, Y., et al., *In vitro characterization of chitosan-gelatin scaffolds for tissue engineering.* Biomaterials, 2005. **26**(36): p. 7616-27.
16. Katenz, E., et al., *Cryopreservation of primary human hepatocytes: the benefit of trehalose as an additional cryoprotective agent.* Liver Transpl, 2007. **13**(1): p. 38-45.
17. Kim, S.S., et al., *Dynamic seeding and in vitro culture of hepatocytes in a flow perfusion system.* Tissue Eng, 2000. **6**(1): p. 39-44.
18. Lawrence, B., et al., *Incorperating Nonideal Reactors in a Junior-Level Course using Computational Fluid Dynamics (CFD).* Chemical Engineering Education, 2004. **38**(2): p. 136-141.
19. Lawrence, B.J., M. Devarapalli, and S.V. Madihally, *Flow dynamics in bioreactors containing tissue engineering scaffolds.* Biotechnol Bioeng, 2009. **102**(3): p. 935-47.

20. Lee, W.M., *Drug-induced hepatotoxicity.* N Engl J Med, 2003. **349**(5): p. 474-85.
21. Lewis, M.C., et al., *Heterogeneous proliferation within engineered cartilaginous tissue: the role of oxygen tension.* Biotechnol Bioeng, 2005. **91**(5): p. 607-15.
22. Mackie, J.S. and P. Meares, *Diffusion in a cation exchanger resin II.* Proc. R. Soc, 1955. **232**(A): p. 495-505.
23. Mooney, D.J., et al., *Long-term engraftment of hepatocytes transplanted on biodegradable polymer sponges.* J Biomed Mater Res, 1997. **37**(3): p. 413-20.
24. Podichetty, J.T., *Effect of fluid flow on structural deformation of porous scaffolds*. Vol. 50. 2011.
25. Podichetty, J.T., D.V. Dhane, and S.V. Madihally, *Dynamics of diffusivity and pressure drop in flow-through and parallel-flow bioreactors during tissue regeneration.* Biotechnol Prog, 2012. **28**(4): p. 1045-54.
26. Podichetty, J.T. and S.V. Madihally, *Modeling of porous scaffold deformation induced by medium perfusion.* J Biomed Mater Res B Appl Biomater, 2013.
27. Pok, S., D.V. Dhane, and S.V. Madihally, *Computational simulation modelling of bioreactor configurations for regenerating human bladder.* Comput Methods Biomech Biomed Engin, 2013. **16**(8): p. 840-51.
28. Polo, M.L., et al., *Responsiveness to PI3K and MEK inhibitors in breast cancer. Use of a 3D culture system to study pathways related to hormone independence in mice.* PLoS One, 2010. **5**(5): p. e10786.
29. Raja Bhaskar, P., *Design of an axial flow bioreactor for tissue regeneration*. 2012, Oklahoma State University: Ann Arbor. p. 100.
30. Roy, P., et al., *Effect of flow on the detoxification function of rat hepatocytes in a bioartificial liver reactor.* Cell Transplant, 2001. **10**(7): p. 609-14.
31. Smith, M.L., A.M. Brown, and C. Gross, *Note on the nitrogen content of certain proteins.* Biochem J, 1932. **26**(5): p. 1473-6.
32. St-Denis, C.E. and C.J.D. Fell, *Diffusivity of oxygen in water.* The Canadian Journal of Chemical Engineering, 1971. **49**(6): p. 885-885.
33. Tarrant, A.M., M.J. Atkinson, and S. Atkinson, *Uptake of estrone from the water column by a coral community.* Marine Biology, 2001. **139**(2): p. 321-325.
34. Weise, F., et al., *Analysis and comparison of oxygen consumption of HepG2 cells in a monolayer and three-dimensional high density cell culture by use of a matrigrid(R).* Biotechnology and Bioengineering, 2013. **110**(9): p. 2504-12.
35. Wilkening, S., F. Stahl, and A. Bader, *COMPARISON OF PRIMARY HUMAN HEPATOCYTES AND HEPATOMA CELL LINE HEPG2 WITH REGARD TO THEIR BIOTRANSFORMATION PROPERTIES.* Drug Metabolism and Disposition, 2003. **31**(8): p. 1035-1042.
36. Yetter, D.R., *PDUFA Activities in Drug Development*, U.S.F.a.D. Administration, Editor. 2012.
37. Young, V.R., et al., *Rates of Urea Production and Hydrolysis and Leucine Oxidation Change Linearly over Widely Varying Protein Intakes in Healthy Adults.* The Journal of Nutrition, 2000. **130**(4): p. 761-766.

APPENDIX A. –Calculations for Kinetic Constants of Oxygen

1. Initial concentration
   Using Henry's Law @ 37° C
   H_{O2} and P_{O2} were obtained from Principles of Biomedical Engineering – Madihally 2010

$$x_{O2} = \frac{P_{O2}}{H_{O2}} = \frac{0.20948 \text{ atm}}{51118 \text{ atm}} = 4.098\text{E}-6$$

For 1 liter of water at 37° C = 991.27 g

$$n_{H2O} = \frac{991.27\text{g}}{18.02 \text{ g/mol}} = 55.0094 \text{ mol H2O/Liter}$$

Molar concentration O_2 from mole fraction definition

$$C_{O2} = \frac{n_{O2}}{n_{O2} + n_{H2O}} = 4.098\text{E}-6$$

$$n_{O2} = \frac{-x_{O2} * n_{H2O}}{x_{O2} - 1}$$

$$= \frac{-4.098\text{E}-6 \ * 55.0094 \text{ mol/Liter}}{4.098\text{E}-6 \ -1} * \frac{1000 \text{ Liter}}{1 \text{ m}^3} = 0.225 \text{ mol/m}^3$$

2. K_m Value
   Use a cell density ratio to calculate K_m in mol/m^3
   Literature values from Devarapalli 2009 [6].

$$K_{m,O2} = \frac{Cell\ Density}{Cell\ Density_{Literature}} * K_{m,O2,\text{Literature}}$$

$$= \frac{1.29\text{E}12 \text{ cells}/m^3}{1.2\text{E}12 \text{ cells}/m^3} * \ 0.263 \frac{\text{mol}}{m^3} = 0.0283 \text{ mol/m}^3$$

3. Vm Value
   Use a cell density ratio to calculate K_m in mol/m^3
   Literature values from Devarapalli 2009 [6].

$$V_{m,O2} = \frac{Cell\ Density}{Cell\ Density_{Literature}} * V_{m,O2,\text{Literature}}$$

$$V_{m,O2} = \frac{1.29\text{E}12 \text{ cells}/m^3}{1.2\text{E}12 \text{ cells}/m^3} * 41.1\text{E}-6 \ \frac{\text{mol}}{\text{m}^3 * s} = 4.42\text{E}-5 \frac{\text{mol}}{\text{m}^3 * \text{s}}$$

4. Free Diffusivity at 37 °C
   Value obtained from [31].

$$D_\infty = \frac{3.0\text{E}-5 \text{ cm}^2}{\text{Second}} * \frac{1 \text{ m}^2}{10000 \text{ cm}^2} = 3.0\text{E}-9 \frac{\text{m}^2}{\text{Second}}$$

5. Effective Diffusivity
   Use the Mackie-Meares relation to determine the effective diffusivity through the scaffold

$$D_{eff} = D_{\infty} \left(\frac{\phi}{2 - \phi} \right)^2$$

   A. 85% porosity - $\varphi = .85$

$$D_{eff} = 3.0E-9 \frac{m^2}{second} * \left(\frac{.85}{2 - .85} \right)^2 = 1.639E-9 \frac{m^2}{second}$$

   B. 25% porosity - $\varphi = .25$

$$D_{eff} = 3.0E-9 \frac{m^2}{second} * \left(\frac{.25}{2 - .25} \right)^2 = 6.122E-11 \frac{m^2}{second}$$

APPENDIX B. – Calculations for Kinetic Constants of Estrogen

1. Initial concentration of Estrogen.
   Physiological concentration of estrogen in the body is 10E -9 mol/Liter

   $$\text{Volume of Media in Bioreactor} = \pi * r^2 * h$$

   $$= \pi * \ 16.5 \text{ mm}^{\ 2} * 2.34 \text{ mm} * \frac{1 \text{ m}^3}{1000 \text{ mm}^{\ 3}} * \frac{1000 \text{ Liter}}{1 \text{ m}^3}$$

   $$= 2.0\text{E} - 3 \text{ Liters}$$

   $$\#\text{ moles of Estrogen in Media}$$

   $$= \text{ Physiological concentration}$$

   $$* \text{ volume of media in Bioreactor}$$

   $$= \ 10\text{E} - 9 \ \frac{\text{mol}}{\text{Liter}} \ * \ 2\text{E} - 3 \text{ Liter} \ = 2.0\text{E} - 11 \text{ mols}$$

   $$\text{Initial concentration of Estrogen } \ C_{\text{Estrogen}}$$

   $$= \frac{\#\text{ moles of Estrogen in Media}}{\text{Volume of Media in Bioreactor}}$$

   $$= \frac{2\text{E} - 11 \text{ mols}}{2\text{E} - 3 \text{ Liters}} * \frac{1000 \text{ Liters}}{1 \text{ m}^3} = 1.0\text{E} - 5 \ \frac{\text{mols}}{\text{m}^3}$$

2. K_m Value
   K_m = 0.006E -3 mol/Liter was obtained from [8]

   $$K_m = 0.006\text{E} - 3 \ \frac{\text{mol}}{\text{Liter}} * \frac{1000 \text{ Liter}}{1 \text{ m}^3} = \ 6.0\text{E} - 3 \ \frac{\text{mol}}{\text{m}^3}$$

3. V_m Value
   V_m = 0.32E -9 mol/mg protein/minute was obtained from [8]. Because of the units a value as to the amount of protein preset number of cells was needed. This value of 5.5E -6 g protein/10^6 cells was obtained from [16].

   $$V_m = V_{m,\text{Literature}} * \frac{\text{amount of protein}}{\#\text{ of cells}}$$

   $$V_m = 0.32\text{E} - 9 \ \frac{\text{mol}}{\text{mg protein} * \text{minute}} * \frac{1 \text{ minute}}{60 \text{ seconds}} \ *$$

   $$5.5\text{E} - 6 \ \frac{\text{g protein}}{10^6 \text{ cells}} * \frac{1000 \text{ mg protein}}{1 \text{ g protein}} * 3.25\text{E } 11 \ \frac{\text{cells}}{\text{m}^3}$$

$$= 9.53E-9 \ \frac{mol}{m^3 * second}$$

4. Free Diffusivity of Estrogen at 37 °C
   Free diffusivity of Estrogen in water was obtained from [33].

$$D_\infty = 4.0E-10 \ \frac{m^2}{second}$$

5. Effective Diffusivity of Urea at 37 °C
   Use the Mackie-Meares relation to determine the effective diffusivity through the scaffold

$$D_{eff} = D_\infty \left(\frac{\phi}{2-\phi}\right)^2$$

   A. 85% porosity - $\varphi = .85$

$$D_{eff} = 4.0E-10 \ \frac{m^2}{second} * \left(\frac{.85}{2-.85}\right)^2 = 2.19E-10 \frac{m^2}{second}$$

   B. 25% porosity - $\varphi = .25$

$$D_{eff} = 3.0E-9 \frac{m^2}{second} * \left(\frac{.25}{2-.25}\right)^2 = 8.16E-12 \ \frac{m^2}{second}$$

APPENDIX C. – Calculations for Kinetic Constants of Urea

1. Zero order rate law constant for urea production.

$$k = \frac{0.65}{15.9}\frac{mmol}{L * hour} * \frac{\#\ of\ Cells}{\#\ \text{cells}_{Literature}} * \frac{1\ hour}{3600\ seconds} * \frac{1000\ mol * L}{1000\ mmol * m^3}$$

A. 2mm scaffold – 400,000 cells

$$k = \frac{0.65 * 400{,}000\ cells}{15.9 * 270{,}000\ cells * 3600\ seconds} = 16.8\ \frac{\mu mol}{m^3 * s}$$

B. 1mm scaffold – 200,000 cells

$$k = \frac{0.65 * 200{,}000\ cells}{15.9 * 270{,}000\ cells * 3600\ seconds} = 8.41\ \frac{\mu mol}{m^3 * s}$$

C. 0.75mm scaffold – 150,000 cells

$$k = \frac{0.65 * 150{,}000\ cells}{15.9 * 270{,}000\ cells * 3600\ seconds} = 6.31\ \frac{\mu mol}{m^3 * s}$$

D. 0.5mm scaffold – 100,000 cells

$$k = \frac{0.65 * 100{,}000\ cells}{15.9 * 270{,}000\ cells * 3600\ seconds} = 4.21\ \frac{\mu mol}{m^3 * s}$$

E. 0.25mm scaffold – 50,000 cells

$$k = \frac{0.65 * 50{,}000\ cells}{15.9 * 270{,}000\ cells * 3600\ seconds} = 2.10\ \frac{\mu mol}{m^3 * s}$$

2. Free Diffusivity of Urea at 37 °C
   Free diffusivity of urea in blood was obtained from [5].

$$D_\infty = 0.925E-3\frac{cm^2}{second} * \frac{1\ m^2}{10000\ cm^2} = 9.25E-8\ \frac{m^2}{s}$$

3. Effective Diffusivity of Urea at 37 °C
   Use the Mackie-Meares relation to determine the effective diffusivity through the scaffold

$$D_{eff} = D_{\infty} \left(\frac{\phi}{2-\phi} \right)^2$$

A. 85% porosity - $\varphi = 0.85$

$$D_{eff} = 9.25E-8 \frac{m^2}{s} * \left(\frac{.85}{2-.85} \right)^2 = 5.05E-8 \frac{m^2}{s}$$

B. 25% porosity - $\varphi = 0.25$

$$D_{eff} = 3.0E-9 \frac{m^2}{s} * \left(\frac{.25}{2-.25} \right)^2 = 1.03E-9 \frac{m^2}{s}$$

APPENDIX D. – COMSOL Simulation Procedures

D.1 Start Up

1. Open Comsol 4.3a by double clicking on the icon

2. Select the 3D spatial dimension and then click the blue arrow pointing to the right to go on to the next page of the set up

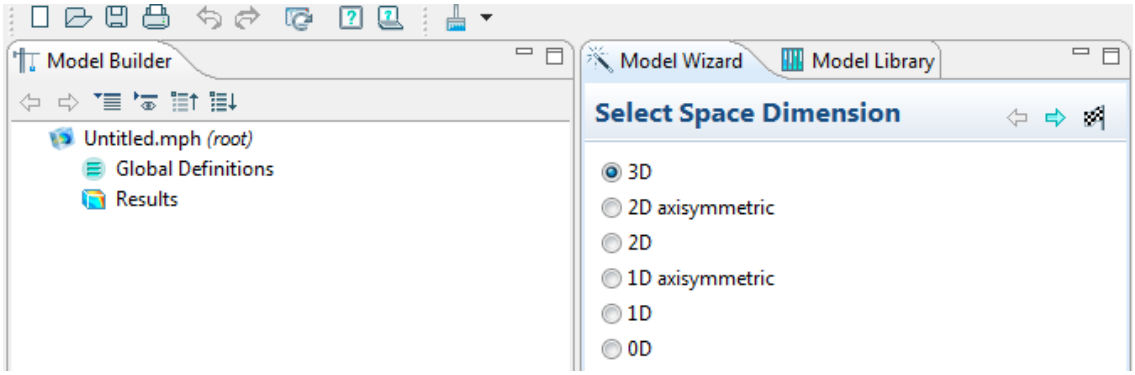

3. Select the physics module that applies to your simulation. For the static bioreactor *Transport of a Diluted Species* was used. You can also rename your dependent variables here so that they are easier to pick out later. Notice you can pick out more than one

physics module for a single simulation. Once selections have been made, click on the right facing arrow to go to the next set up page.

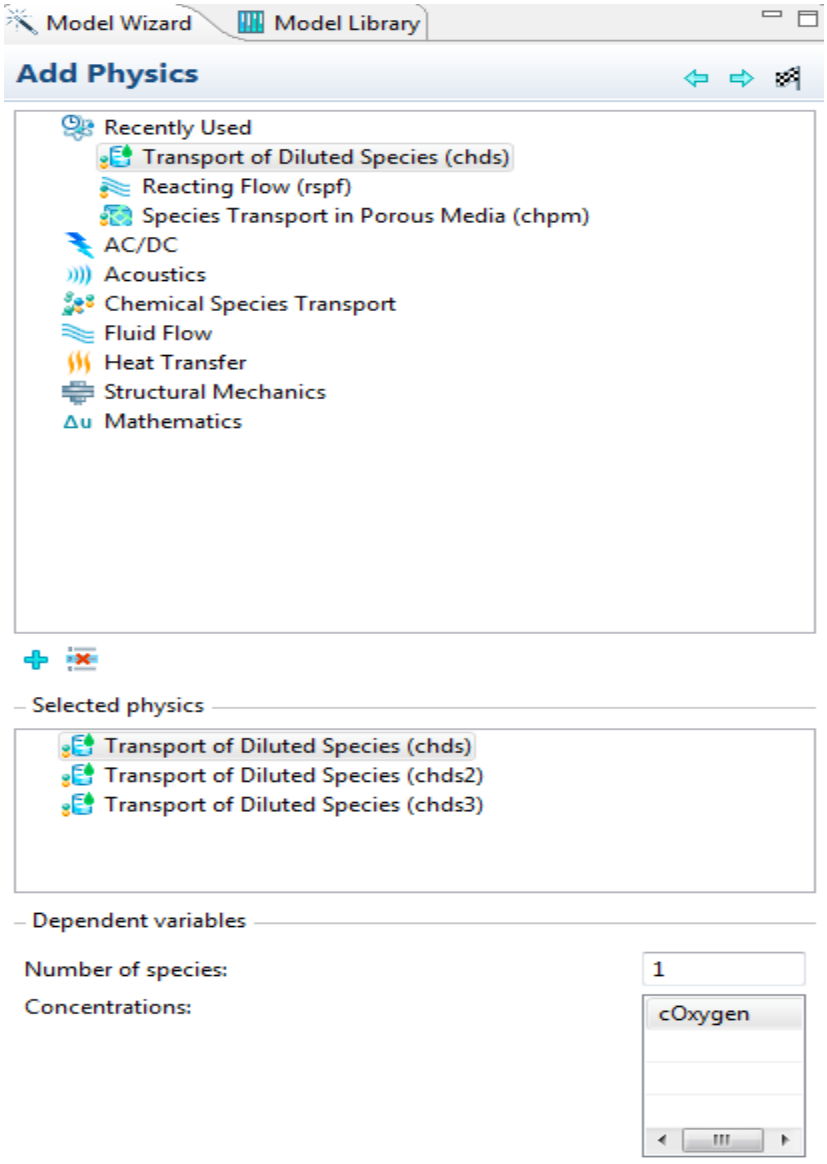

4. Next select the type of study. A time dependent study was chosen for the static bioreactor. All physics do not have to be selected for this study. A green check mark means they will be solved for in the study. It is possible to have more than one study. Click on the checkered flag to finish set up once all selections have been made.

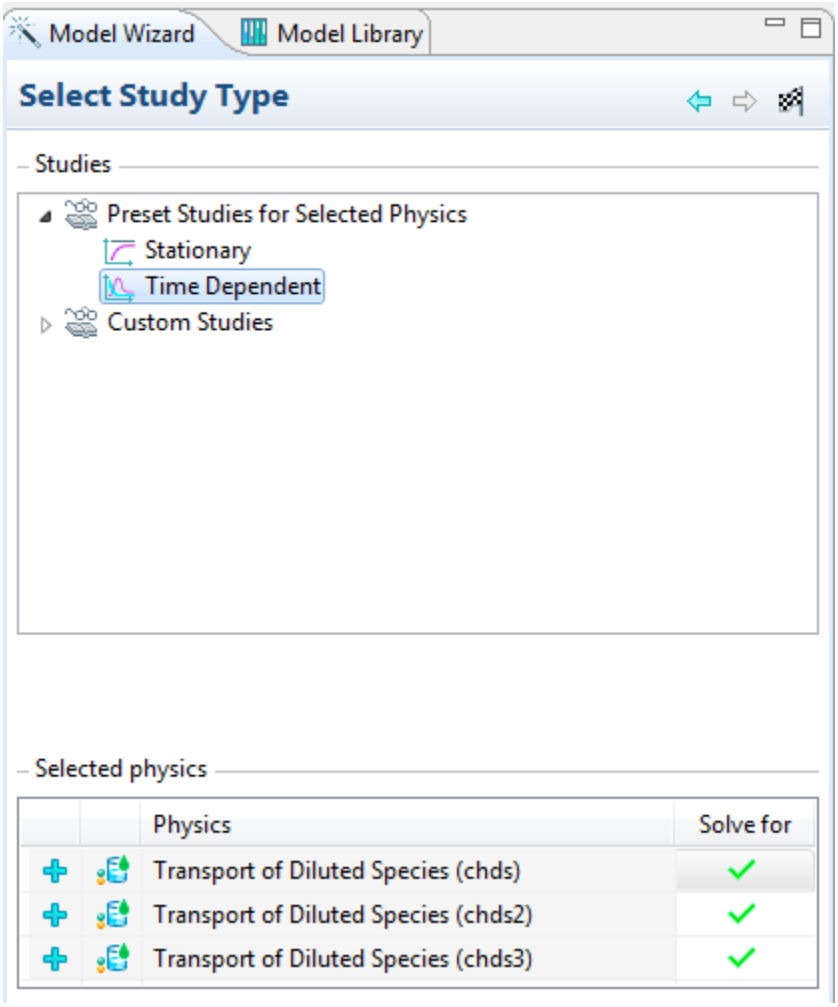

5. Set up is now complete and the input of information into the model builder can begin.

D.2 Static Bioreactor Geometry

Creating the Static Bioreactor Shell

1. The screen that pops up after finishing the set up will have a model builder frame, geometry frame, and graphics frame. In the geometry frame change the length unit setting from meters (m) to millimeters (mm).

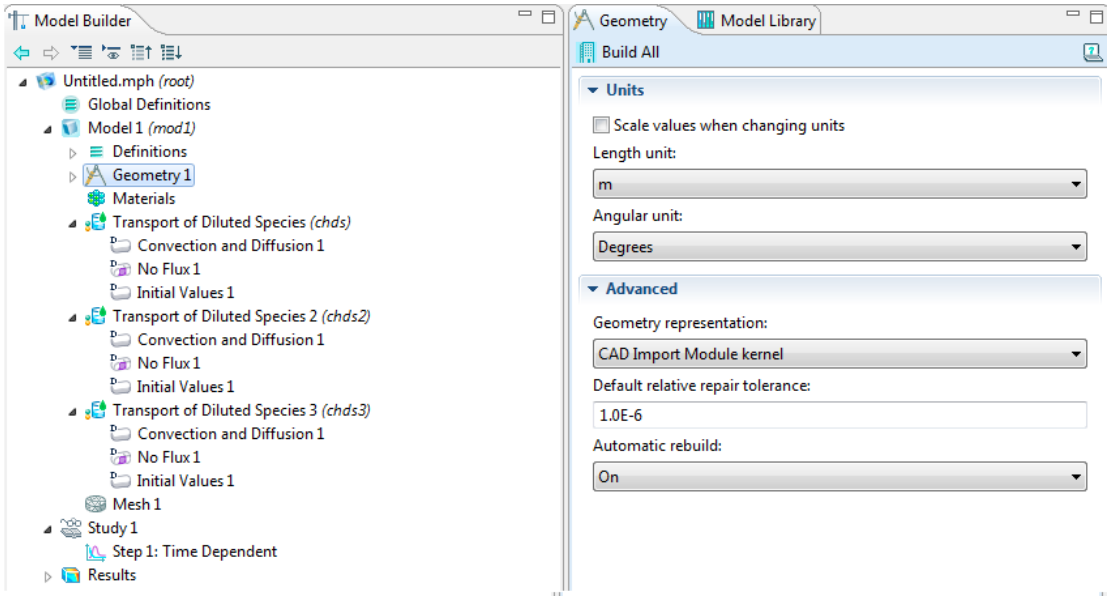

2. Locate the geometry tab in the model builder frame and expand it by clicking on the triangle to the left of it .Right click geometry and select “Work Plane.” A work plane will appear in the graphics window and “Work Plane1” will appear under “Geometry1” in the model builder frame.

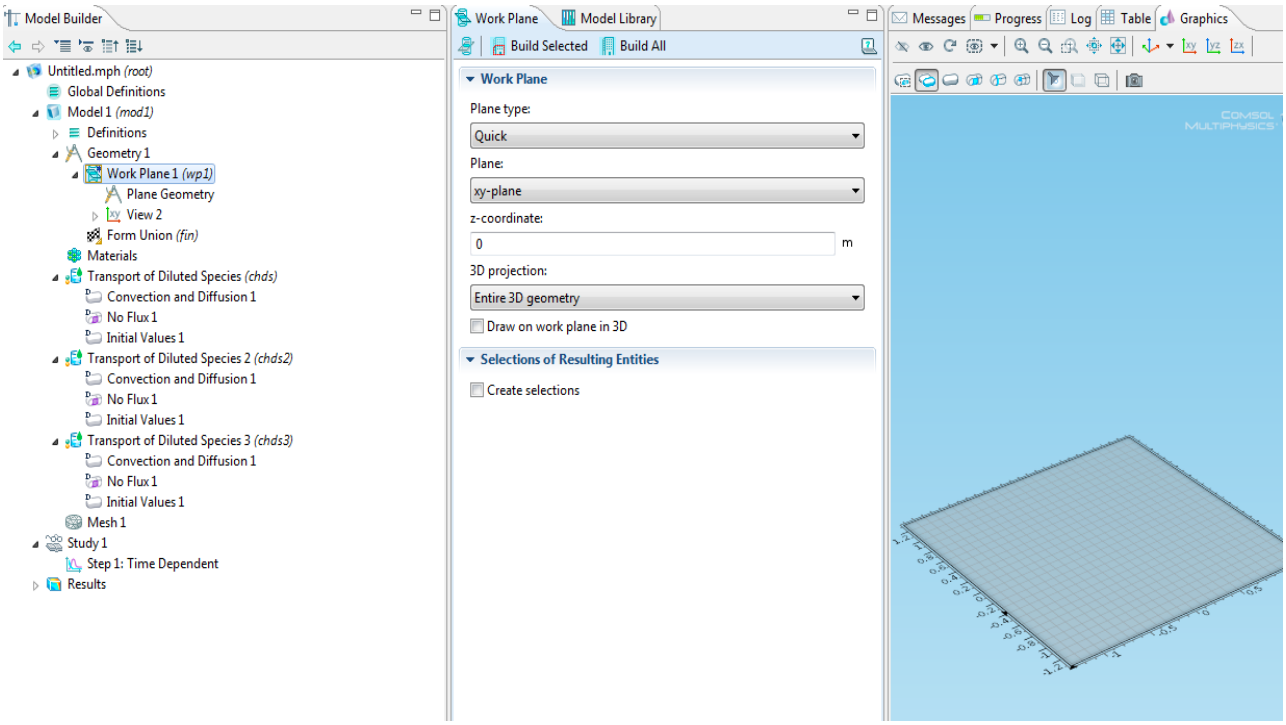

The work plane can be renamed by right clicking on the work plane tab and selecting rename. In this simulation "Work Plane 1" will be renamed "Shell" because it will become the outside shell of the bioreactor. Notice that the height of the work plane can be set in the work plane window under the z-coordinate section. Leave the z-coordinate set to zero for this work plane.

3. Right click on the "Plane Geometry" tab and select circle. The bioreactor shell is hollow cylinder. The radius of the circle should be changed to 16.5mm. Then click "Build All" under the circle tab and the circle will appear in the graphics window.

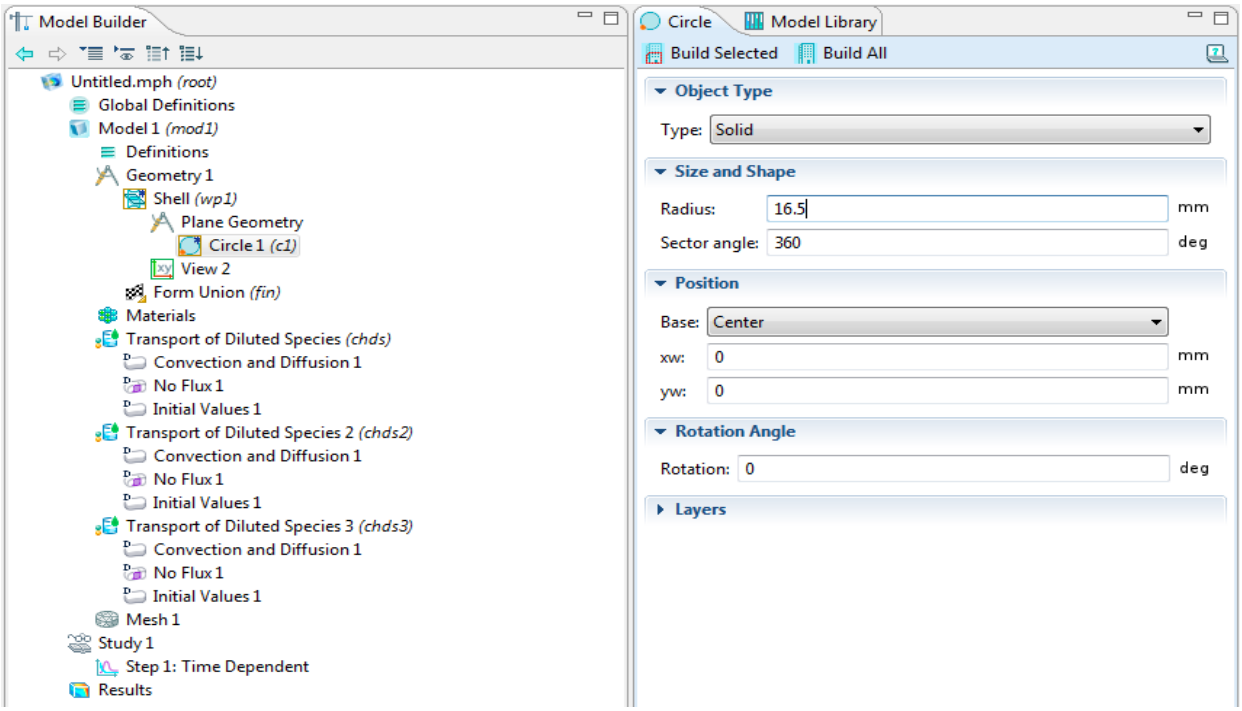

4. In order to give the bioreactor shell height use the extrude function. Right click on "Shell (work plane1)" and select extrude. Under "Distances from Plane" input 2.34mm as this is the height of the bioreactor. Click on "Build All" and your cylinder will appear in the graphics window.

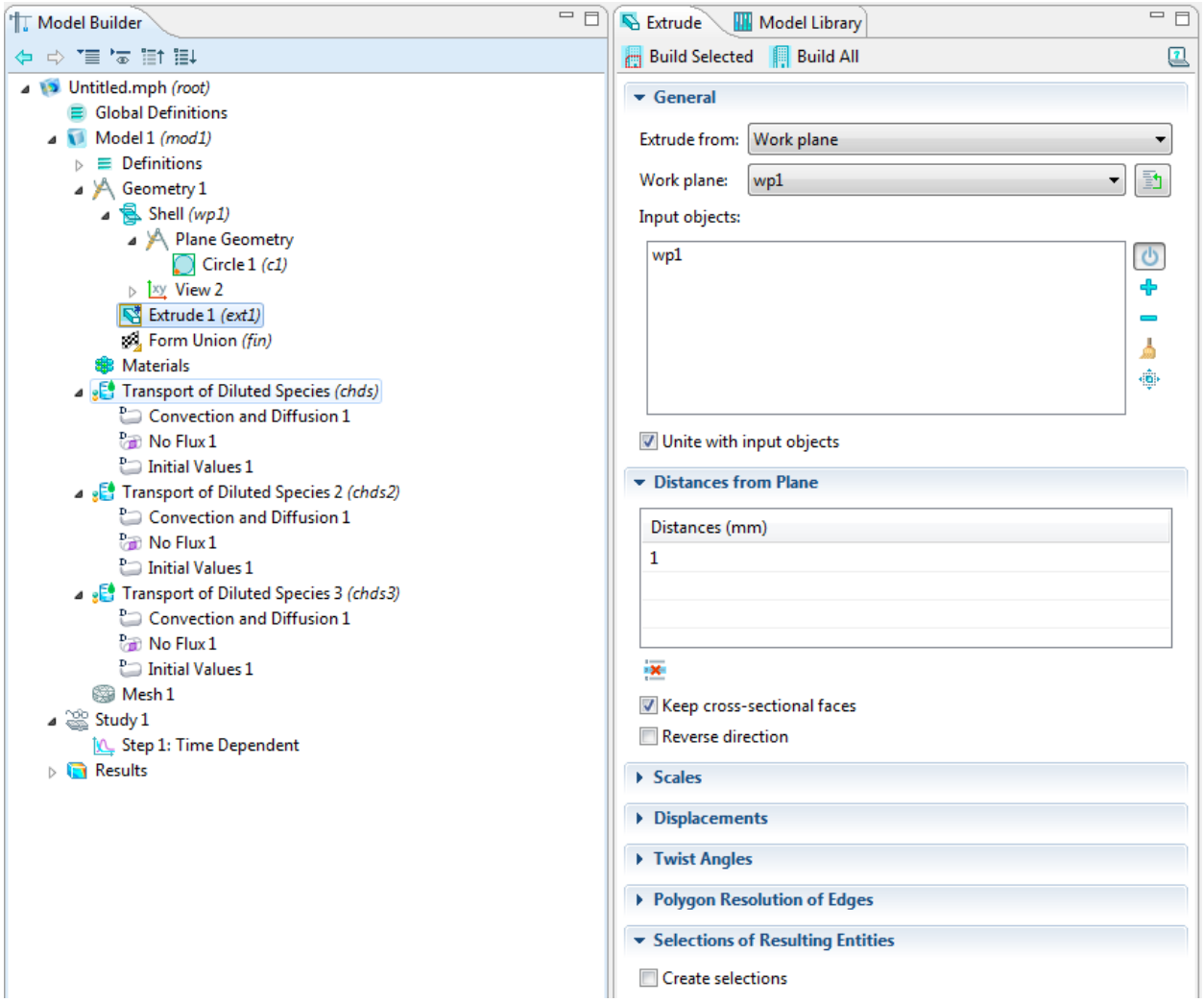

5. The outside shell of the static bioreactor is now complete.

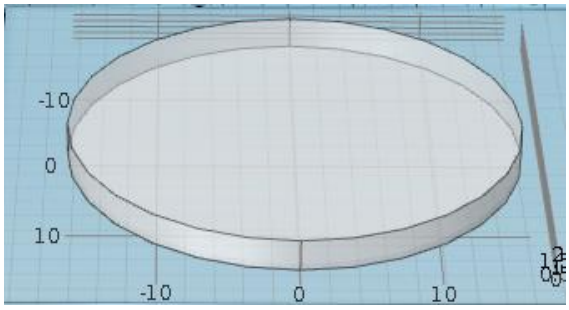

Creating the Scaffold Region

1. A new work plane is needed to create the scaffold region inside of the bioreactor. Once again, right click on "Geometry1" and select Work Plane. This work plane was renamed "Scaffold." In this simulation scaffold height was 0.5mm from the bottom of the bioreactor, so the z-coordinate must be changed to 0.5mm.

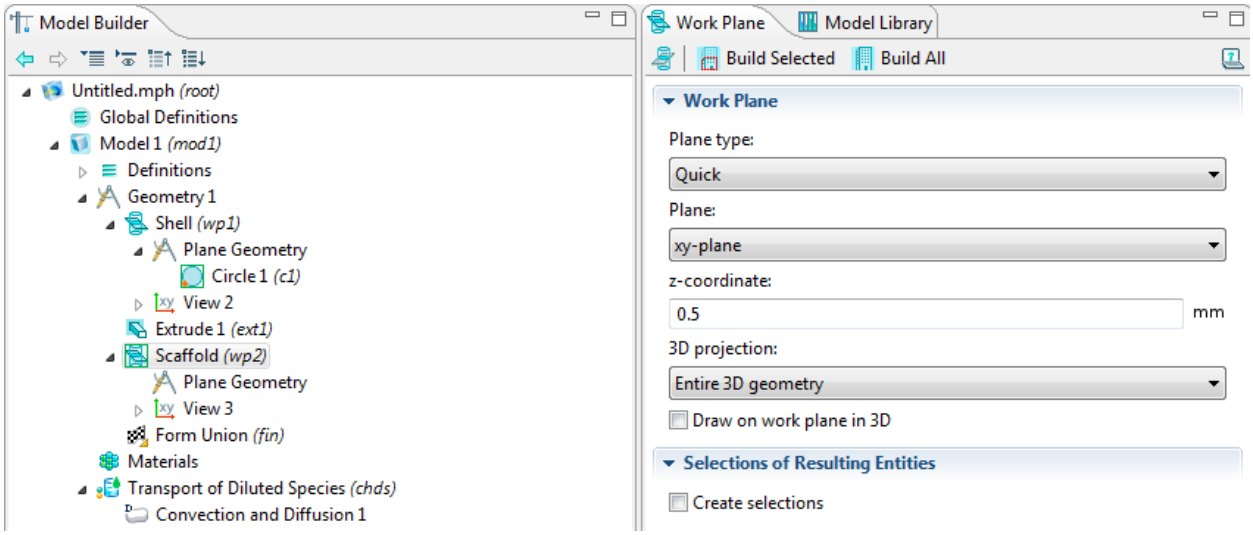

2. The scaffold is also a cylinder, so begin with a circle. Under the "Scaffold" tab, right click "Plane Geometry" and select circle. Change the radius to 7mm. Click on "Build All."

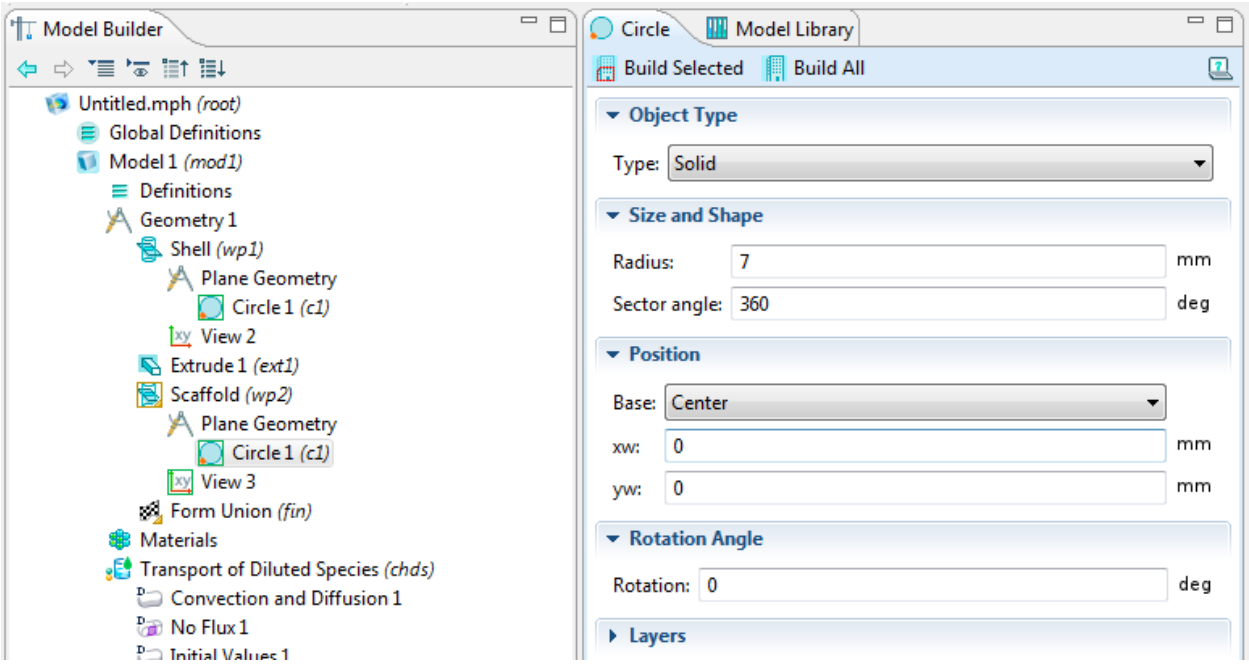

3. The height of the scaffold varied in this study. This example will be done with a 1mm thick scaffold. Right click on "Scaffold" and select extrude. Change the "Distances from Plane" to 1mm. Click on "Build All"

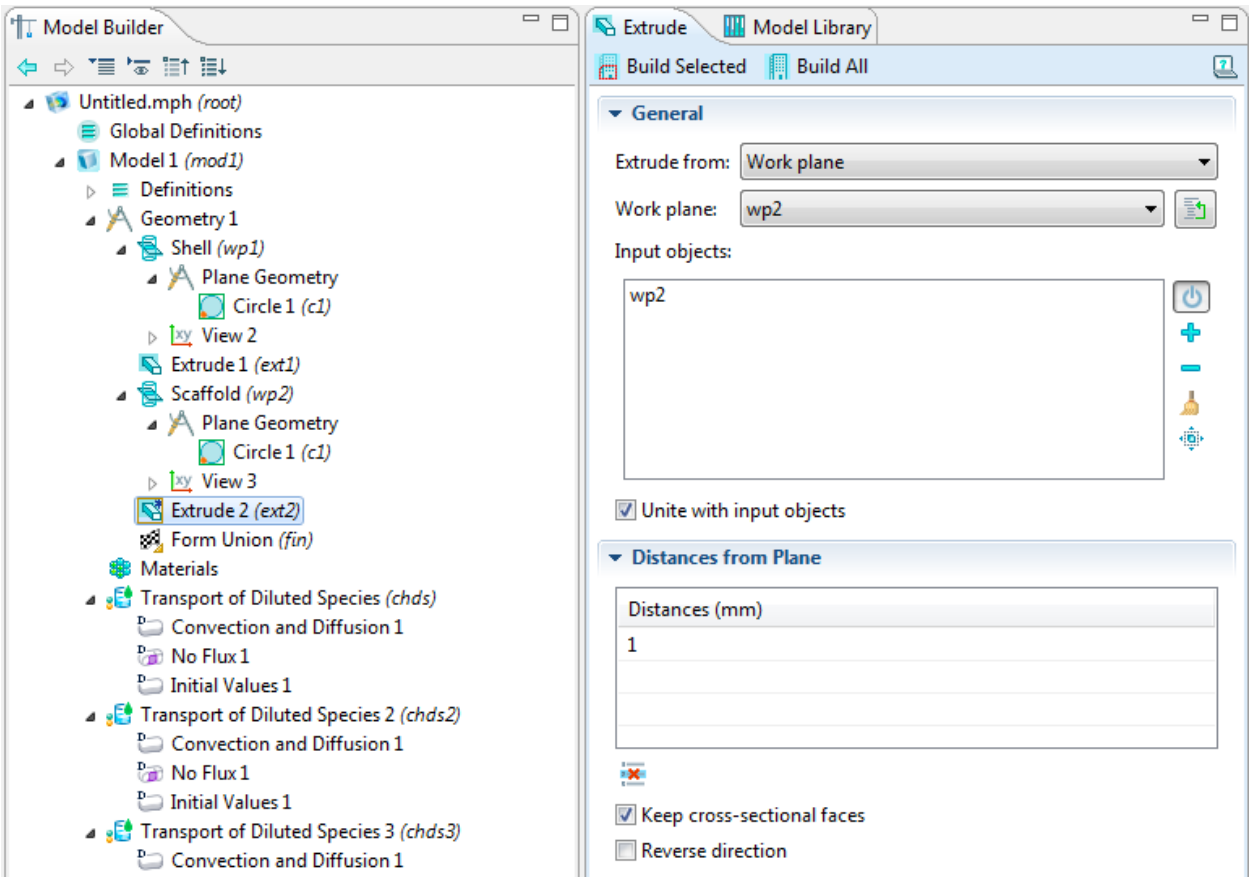

4. The scaffold region is now complete. The graphics section will show the static bioreactor with the scaffold inside.

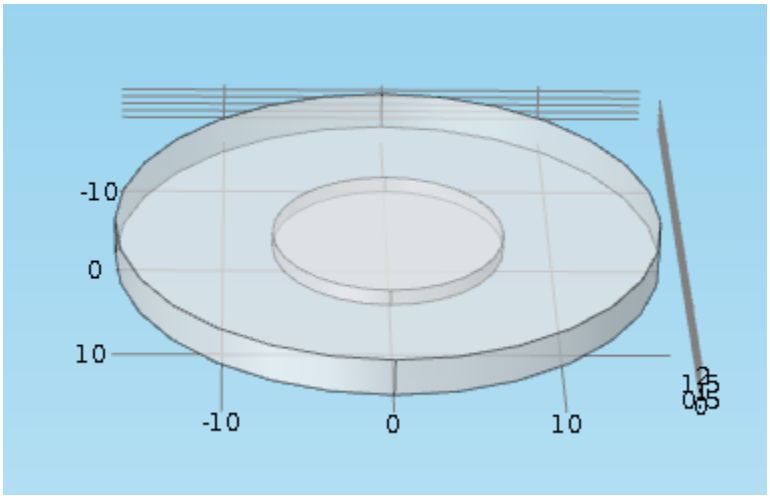

D.3 Constants/Initial Conditions Input

1. All constants and initial conditions can be input as parameters. Expand the "Global Definitions" tab and click on the "Parameters" tab.

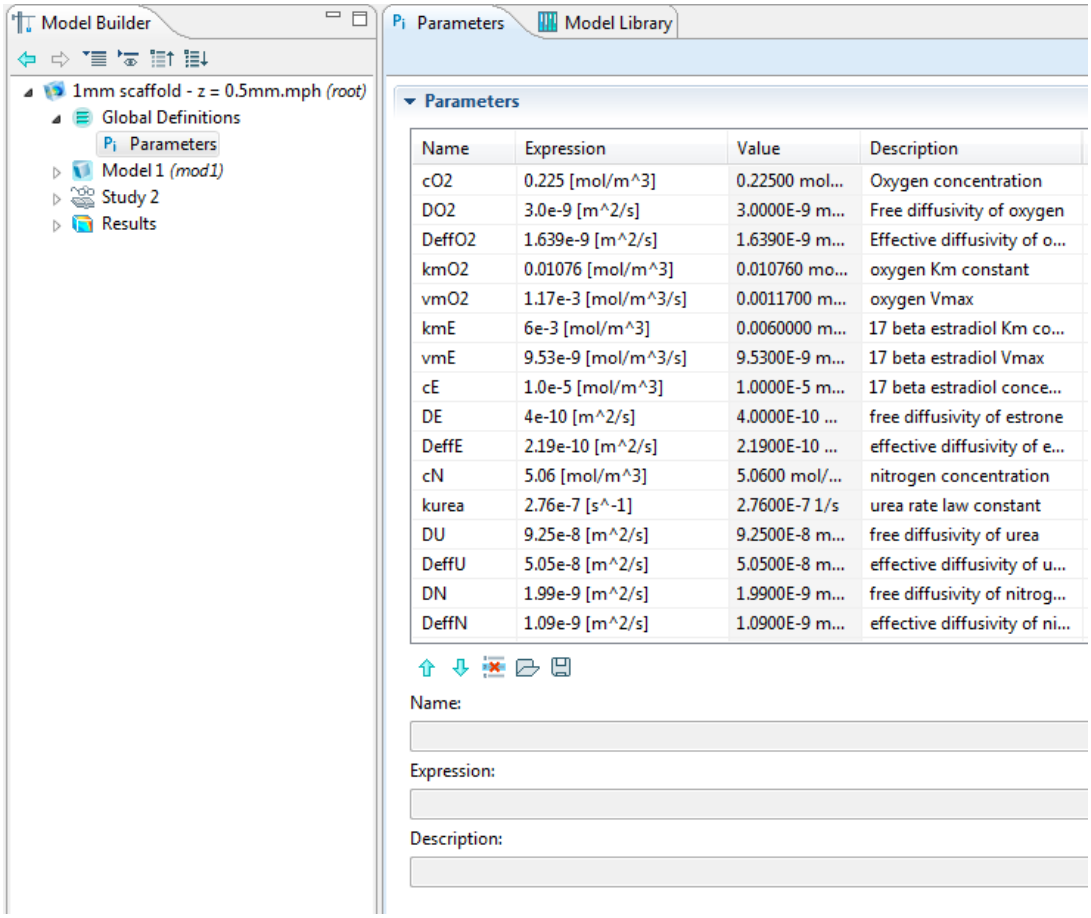

2. Enter a name for the constant or initial value in the name box.

3. Enter a value and units for the constant or initial value in the expression box

4. Enter a description of the variable in the description box (optional)

5. Find the section that the constant or initial value should be input into. For example, the effective diffusivity of oxygen, DeffO2, will be input into a diffusion section for *Transport of a Diluted Species (Oxygen)*. Notice that the domain must be selected so that the program understands which sections these parameters belong to.

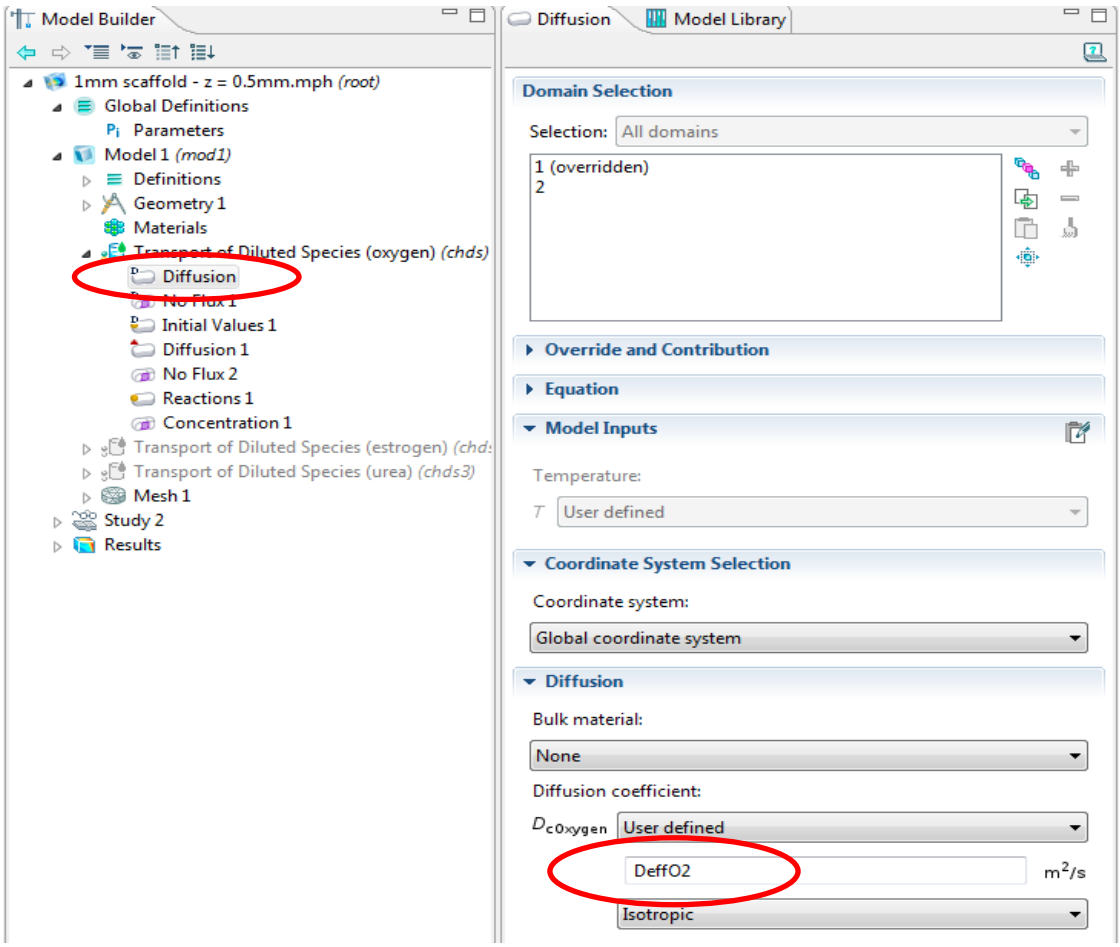

6. This is also done in the initial values section with the initial concentration of a species.
7. The second diffusion section is for the free diffusivity of a species in the non-porous region.

*Note, to add a diffusion, reactions, initial values, flux, etc. section, right click on the *Transport of a Diluted Species (Oxygen)* tab and select the section needed.

D.4 Equations Input

1. Equations for the concentration change can either be put into the reactions section directly or input into the variables section.

2. To input the equation into the variables section, expand the "Model" tab, then expand the "Definitions" tab, and finally right click on the "Variables" tab.

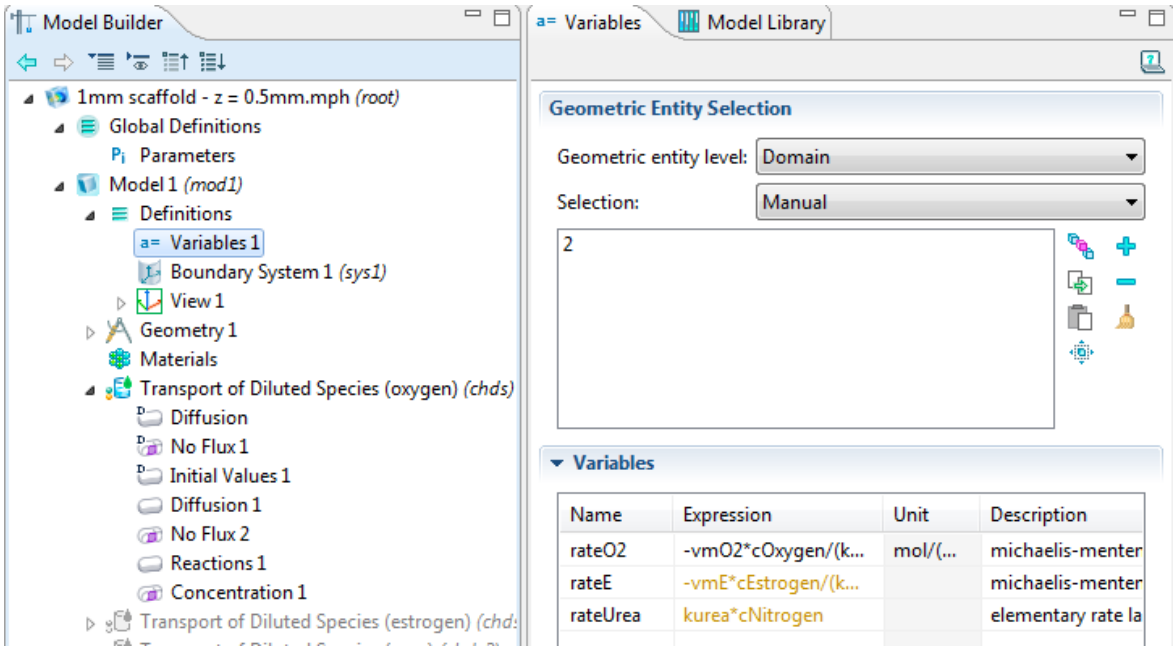

3. Write the equation name in the name box

4. Input the expression to be calculated at each node. Notice that parameters and variables can be input into equations

5. Input a description into the description box (optional)

6. Next, expand the *Transport of a Diluted Species (Oxygen)* tab and click on the reactions section.

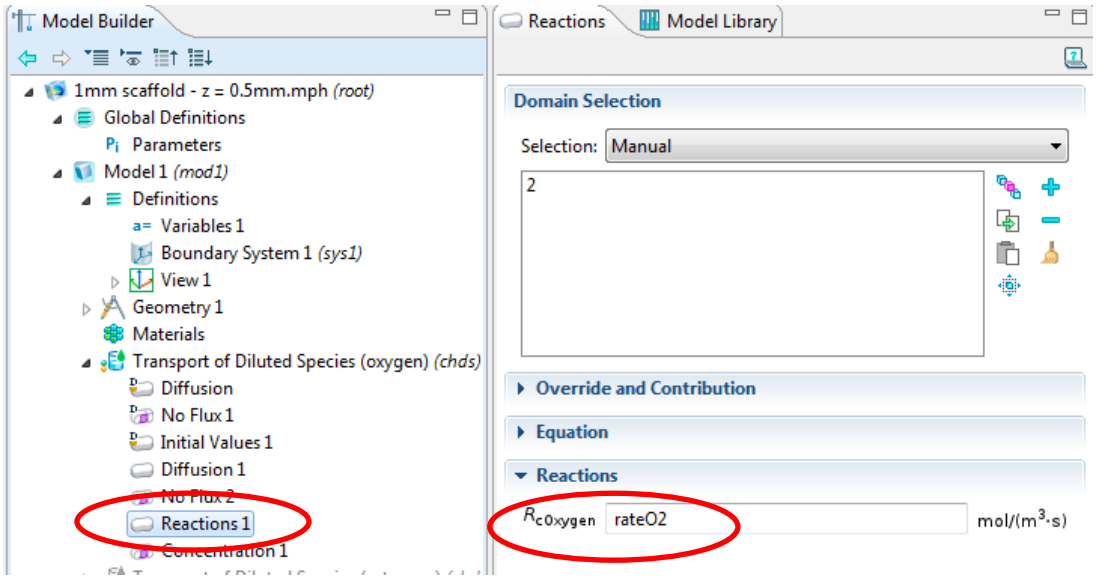

7. Input the name of the expression into the reactions box

D.5 Profiles and Derived Values

1. Profiles for shear rate, concentration, velocity and a variety of other variables can be obtained once the simulation has been run.

2. Expand the “Results” tab.

3. Right click on the “Results” tab to select the type of plot you want. For this example we will choose a 3D plot

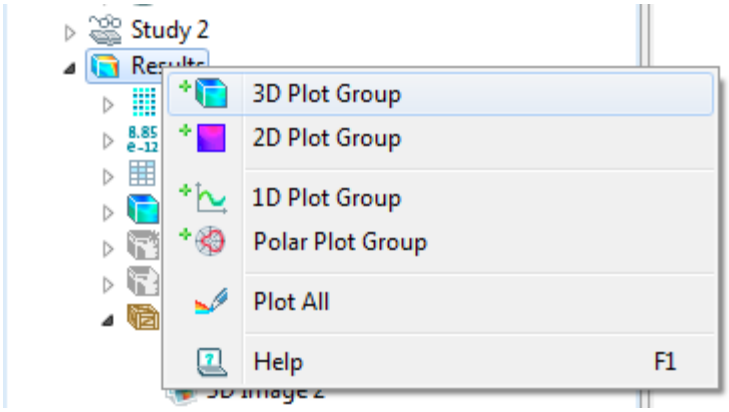

4. A new 3D plot section will appear

5. Right click on the new plot and you can rename the section so that profile identification is easy. This profile will be renamed Oxygen Concentration.

6. Again right click and choose the type of profile you want to see. For this example we will choose a slice

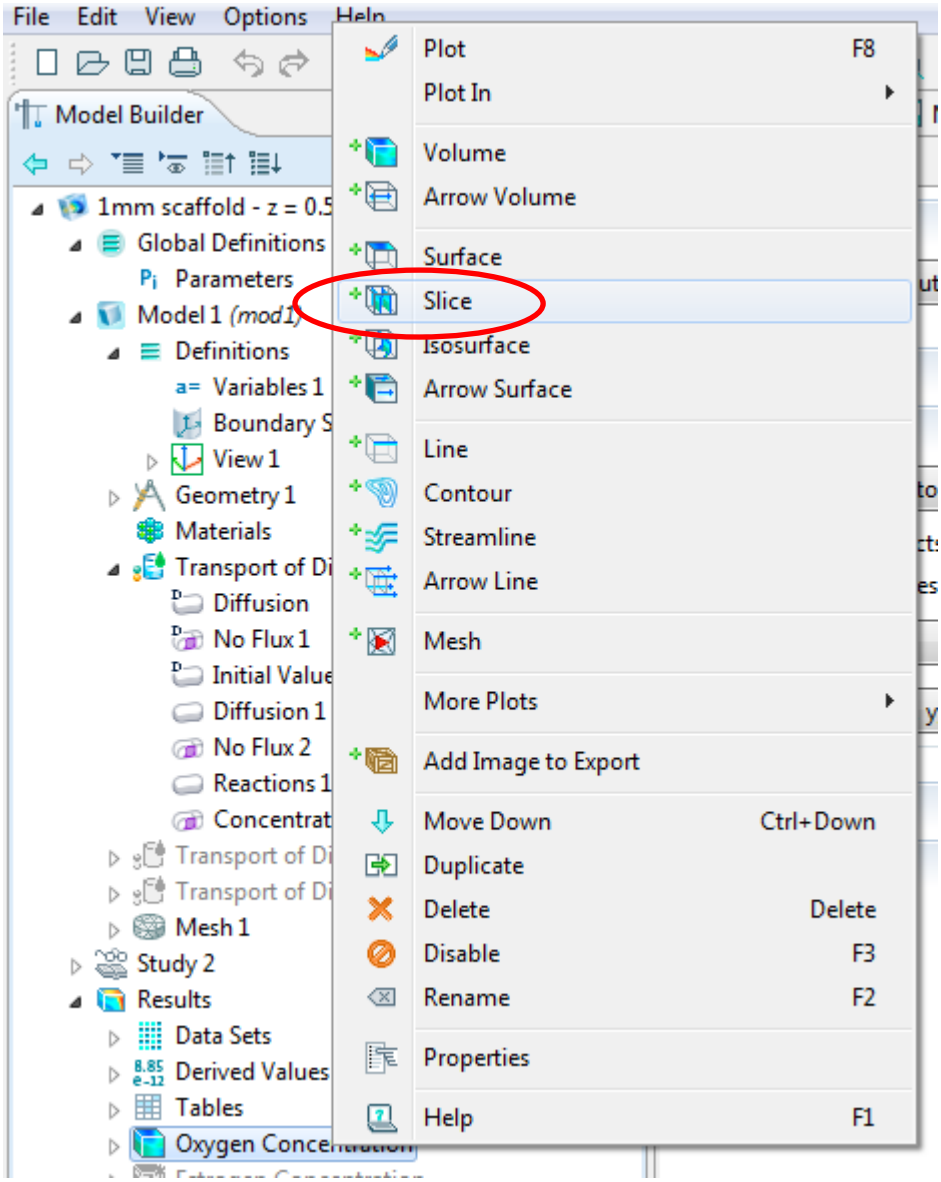

7. A new section will appear under the Oxygen Concentration section

8. Here you can choose the expression you want to plot by clicking on the green and orange arrow icon

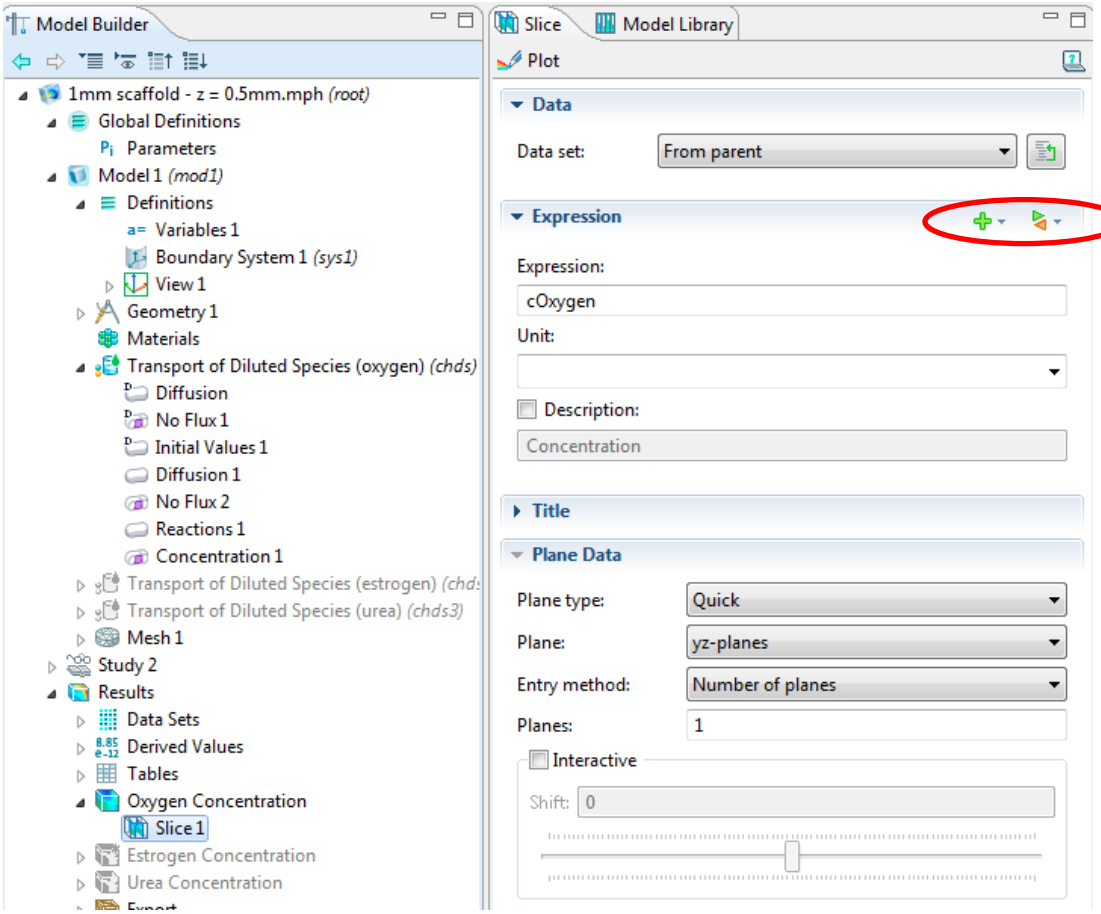

9. We will choose oxygen concentration for this example

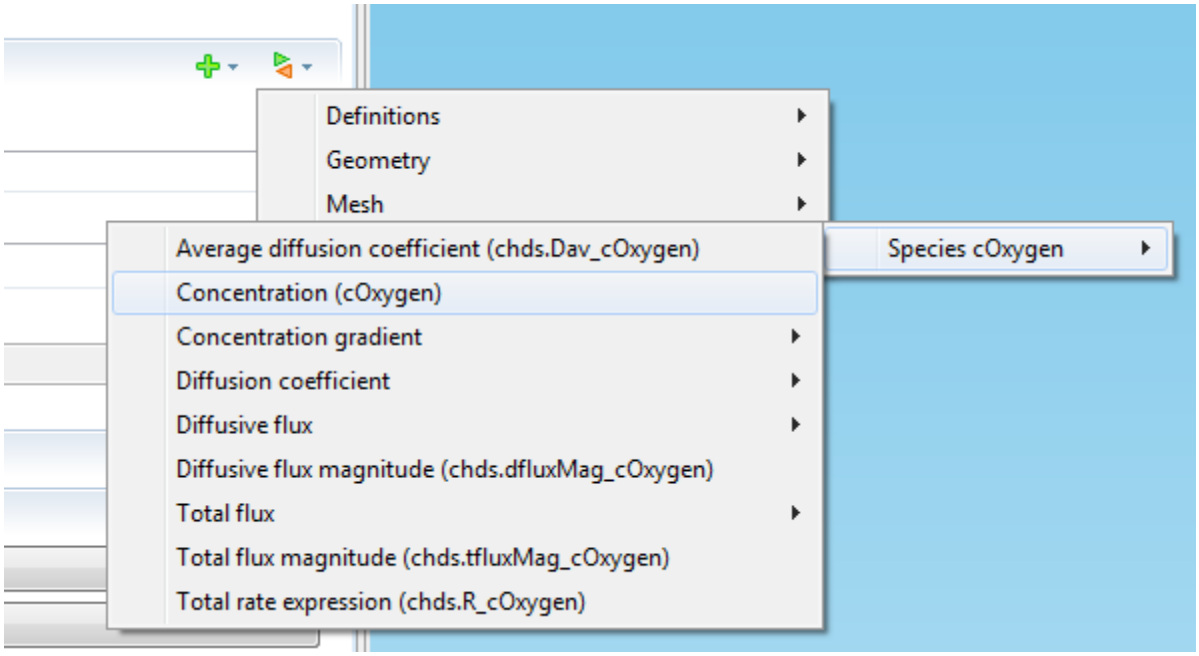

10. The number of slices or coordinates of a slice can be selected in the Plane Data section, and the color range can be set for easy comparison of profiles in the Range section

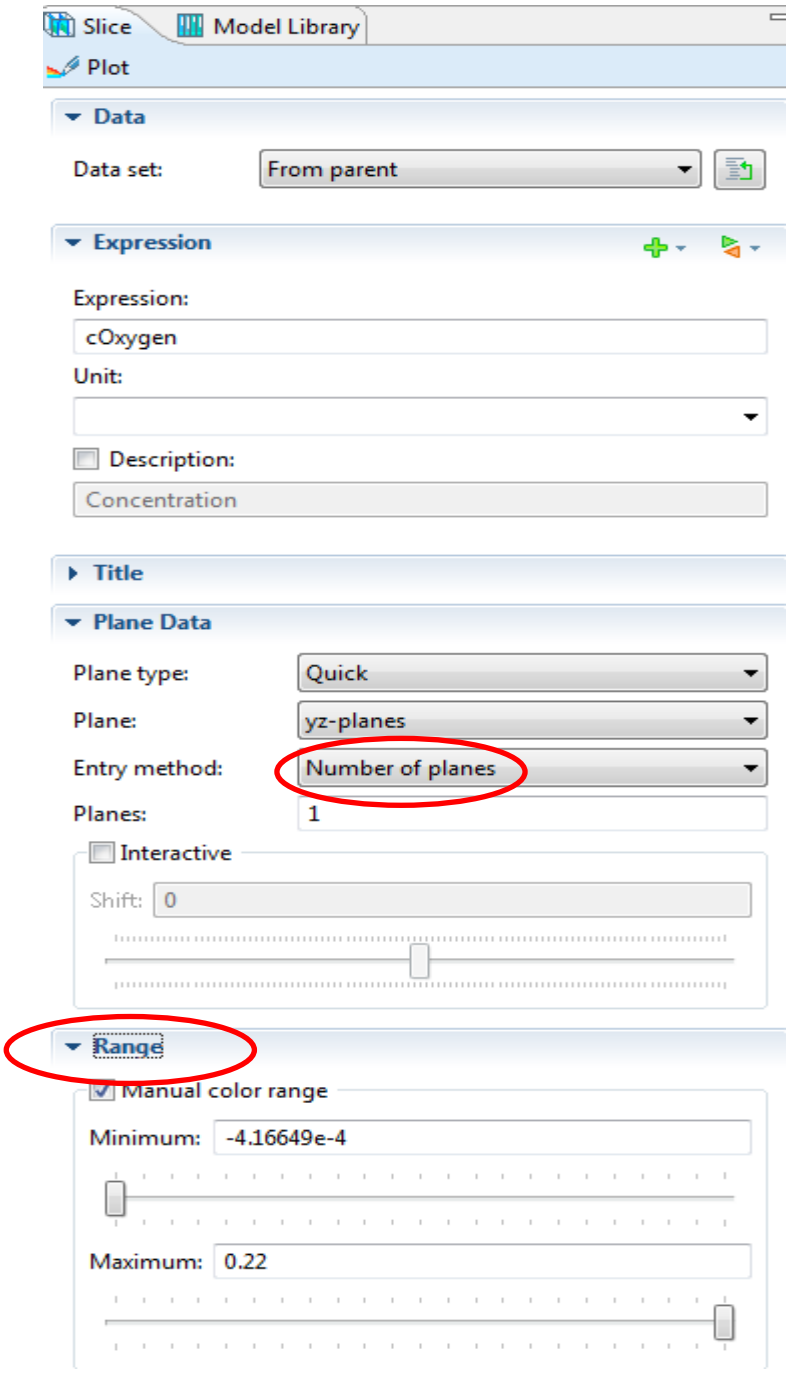

11. Volume and Surface averages/maximums can be obtained from the Derived Values section under the "Results" tab.

12. Right click on the Derived Values section and select Average, then select Volume Average

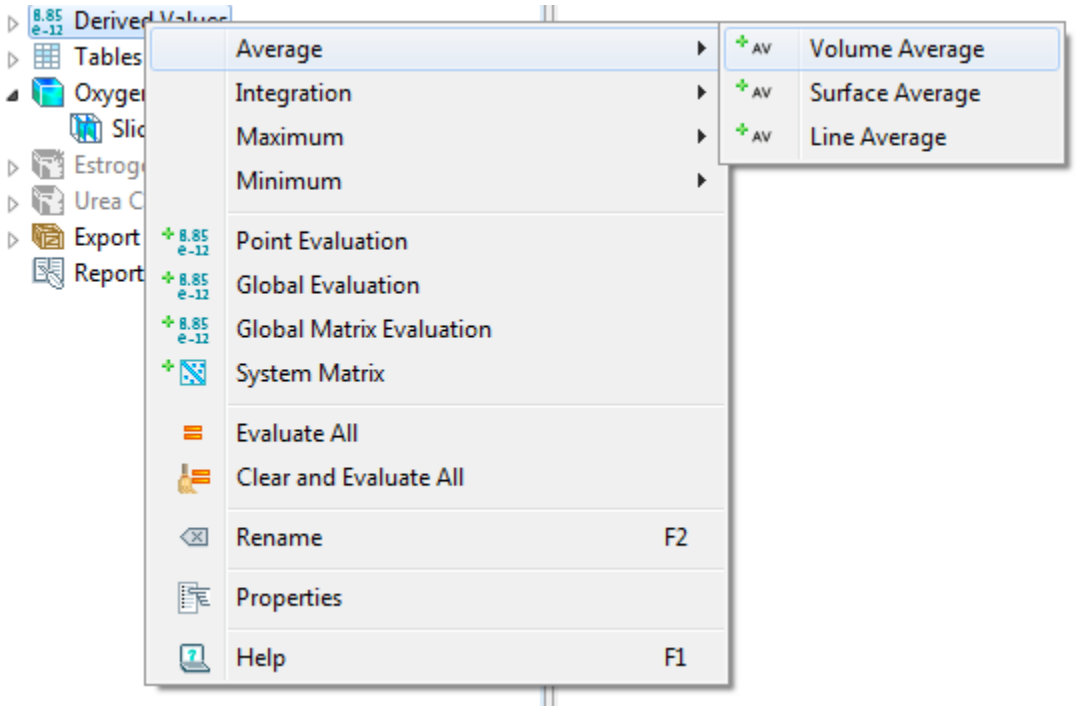

13. A box will new section will appear that allows you to select the volume(s) for which you want to find the average. We will find the average volume concentration of oxygen throughout the entire reactor for this example.

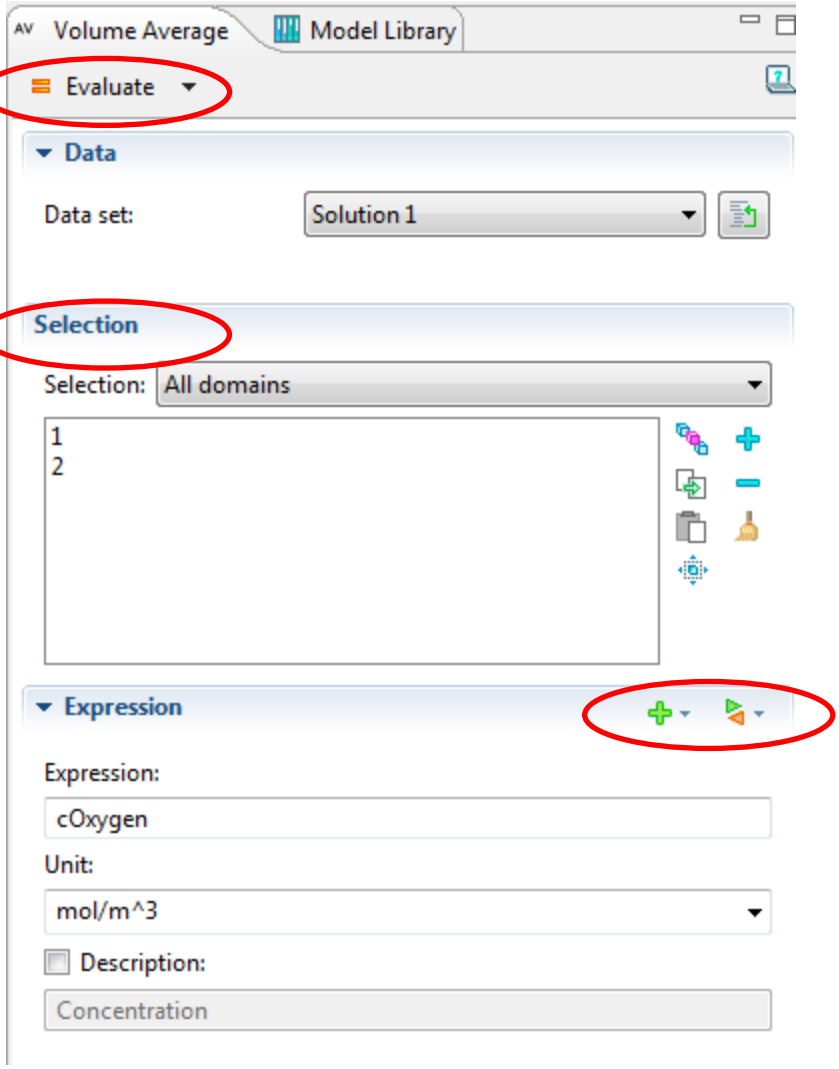

14. Notice that both domains are chosen so that the entire volume is included

15. Oxygen concentration has been selected for the expression, similarly to how we choose it for the concentration profile.

16. Finally, click Evaluate and the value will appear in a table to the far right of your screen

APPENDIX E. – Reynolds Number Analysis

	Case 1		
Volumetric Flow Rate (mL/min)	10	5	1
Volume Average Velocity	2.20E-04	6.882E-05	9.79E-06
Volume Maximum Velocity	7.42E-04	1.48E-04	2.25E-05
Average Reynolds Number	0.02338	0.00730	0.00104
Maximum Reynolds Number	0.07868	0.01565	0.00239

	Case 2 (1mm)			
Volumetric Flow Rate (mL/min)	10	5	1	0.1
Volume Average Velocity	0.00103	5.13E-04	1.00E-04	1.00E-05
Volume Maximum Velocity	0.00131	6.55E-04	1.14E-04	1.30E-05
Average Reynolds Number	0.10923	0.05444	0.01064	0.00106
Maximum Reynolds Number	0.13893	0.06948	0.01210	0.00138

	Case 2 (2mm)		
Volumetric Flow Rate (mL/min)	10	5	0.1
Volume Average Velocity	9.72E-04	1.00E-04	1.00E-05
Volume Maximum Velocity	0.00128	1.10E-04	1.50E-05
Average Reynolds Number	0.10307	0.01064	0.00106
Maximum Reynolds Number	0.13574	0.01171	0.00159

APPENDIX F. – RTD Data/Analysis

Spectrophotometer Data

aw	0.032667									
ac	0.039									
a0	1.661									
		Time(s)	a	a0	a-aw-ac	a0-aw-ac	(a-aw-ac)/(a0-aw-ac)	c/co	new Time(s)	
	0	0	0.039	1.661	-0.032666667	1.58933333	-0.020553691	0		
	4	240	0.055	1.661	-0.016666667	1.58933333	-0.010486577	0	0	0
	8	480	0.14	1.661	0.068333333	1.58933333	0.042994966	0.042994966	240	0.042995
	12	720	0.33	1.661	0.258333333	1.58933333	0.162541946	0.162541946	480	0.162542
	16	960	0.629	1.661	0.557333333	1.58933333	0.350671141	0.350671141	720	0.350671
	20	1200	0.434	1.661	0.362333333	1.58933333	0.227978188	0.227978188	960	0.227978
	24	1440	0.714	1.661	0.642333333	1.58933333	0.404152685	0.404152685	1200	0.404153
	28	1680	0.949	1.661	0.877333333	1.58933333	0.552013423	0.552013423	1440	0.552013
	32	1920	0.93	1.661	0.858333333	1.58933333	0.540058725	0.540058725	1680	0.540059
	36	2160	1.011	1.661	0.939333333	1.58933333	0.59102349	0.59102349	1920	0.591023
	40	2400	0.831	1.661	0.759333333	1.58933333	0.477768456	0.477768456	2160	0.477768
	50	3000	0.796	1.661	0.724333333	1.58933333	0.455746644	0.455746644	2400	0.455747
	60	3600	1.102	1.661	1.030333333	1.58933333	0.648280201	0.648280201	3000	0.64828
	70	4200	1.214	1.661	1.142333333	1.58933333	0.71875	0.71875	3600	0.71875

Eliminating negative values from (a-aw-ac)/(a0-aw-ac) gives the values to be plotted and new time values

Time(s)	Time(min)	c/c0
0	0	0
240	4	0.04299497
480	8	0.16254195
720	12	0.35067114
960	16	0.22797819
1200	20	0.40415268
1440	24	0.55201342
1680	28	0.54005872
1920	32	0.59102349
2160	36	0.47776846
2400	40	0.45574664
3000	50	0.6482802
3600	60	0.71875

Chapman 3 parameter fit data obtained from Sigma Plot

Parameter	Value	StdErr	CV(%)	Dependencies
a	6.94E-01	1.17E-01	1.69E+01	0.912945

b	5.32E-02	3.44E-02	6.46E+01	0.975609
c	1.30E+00	6.88E-01	5.31E+01	0.937929

0.694*(1-Exp(-0.0532*x))^1.3

$$\frac{d}{dx}\left(0.694\,(1-\exp(-0.0532\,x))^{1.3}\right) = 0.047997\,e^{-0.0532\,x}\left(1-e^{-0.0532\,x}\right)^{0.3}$$

$$\int_0^{200} 0.047997\exp(-0.0532\,x)\,(1-\exp(-0.0532\,x))^{0.3}\,dx = 0.693978$$

$$\int_0^{200} (x\,0.047997)\exp(-0.0532\,x)\,(1-\exp(-0.0532\,x))^{0.3}\,dx = 15.3527$$

VITA

Carrie Lynn German

Candidate for the Degree of

Master of Science

Thesis: MODELING LIVER METABOLISM FOR DRUG DEVELOPMENT

Major Field: Chemical Engineering

Biographical:

Education:

Completed the requirements for the Master of Science in Chemical Engineering at Oklahoma State University, Stillwater, Oklahoma in July, 2014.

Completed the requirements for the Bachelor of Science in Secondary Education at Oklahoma State University, Stillwater, Oklahoma in May, 2006.

Experience:
Research and Teaching Assistant, Oklahoma State University, Stillwater, OK.

Professional Memberships:
Chemical Engineering Graduate Student Association – member and officer
American Institute of Chemical Engineers – member